7-2008

COMPUTATIONAL ANALYSIS OF FEASIBILITY AND UTILITY OF DIRECT-ADHESION POLYMER-TO-METAL HYBRID TECHNOLOGIES FOR USE IN LOAD BEARING BODY-IN-WHITE AUTOMOTIVE COMPONENTS

Vijay Sellappan
Clemson University, vijaysellappan@yahoo.com

COMPUTATIONAL ANALYSIS OF FEASIBILITY AND UTILITY OF DIRECT-ADHESION POLYMER-TO-METAL HYBRID TECHNOLOGIES FOR USE IN LOAD BEARING BODY-IN-WHITE AUTOMOTIVE COMPONENTS

A Thesis
Presented to
the Graduate School of
Clemson University

In Partial Fulfillment
of the Requirements for the Degree
Master of Science
Mechanical Engineering

---

by
Vijay Sellappan
August 2008

Accepted by:
Dr. Mica Grujicic, Committee Chair
Dr. Mohammed Omar
Dr. Laine Mears

ABSTRACT

Traditionally, metals and plastics are fierce competitors in many automotive engineering applications. This paradigm is gradually being abolished as the polymer-metal-hybrid (PMH) technologies, developed over the last decade, are finding ways to take full advantage of the two classes of materials by combining them into a singular component/sub-assembly. By employing one of the several patented PMH technologies, automotive original equipment manufacturers (OEMs) have succeeded in engaging flexible assembly strategies, decreasing capital expenditures and reducing labor required for vehicle manufacture. The basic concept utilized in all PMH technologies is based on the fact that while an open-channel thin-wall sheet-metal component can readily buckle under compressive load, with very little lateral support, provided by a thin-wall rib-like injection-molded plastic subcomponent, the buckling resistance (and the stiffness) of the component can be greatly increased (while the accompanied weight increase is relatively small).

In the present work, the potential of direct-adhesion PMH technologies for use in load-bearing structural automotive components is explored computationally. Within the direct adhesion PMH technology, load transfer between stamped sheet-metal and injection-molded rib-like plastic subcomponent is accomplished through a variety of nanometer-to-micron scale chemical and mechanical phenomena which enable direct adhesion between the two materials. Multi-disciplinary computations are carried out ranging from: (a) computational investigation of the sheet-metal stamping process including determination of the residual stresses and the extent of stamped-component warping; (b) computational fluid mechanics of the filling, packing and cooling stages of the injection-molding process including determination of flow-induced fiber orientation in the molded plastic and the extent of residual stresses and warping in the injection-molded sub-component: and (c) structural-mechanics computational investigation of the effect of injection-molded component residual stresses and warping on their ability to withstand thermal

loading encountered in the paint shop and mechanical in-service loading. The results obtained revealed that a minimal level of the polymer-to-metal adhesion strength (5-10MPa) must be attained in order for the direct-adhesion PMH technologies to be a viable alternative in the load-bearing body-in-white (BIW) components.

In the present work, also various PMH approaches used to promote direct (adhesive-free) adhesion between metal and injection-molded thermoplastics are reviewed and critiqued. The approaches are categorized as: (a) micro-scale polymer-to-metal mechanical interlocking; (b) in-coil or stamped-part pre-coating for enhanced adhesion; and (c) chemical modifications of the injection-molded thermoplastics for enhanced polymer-to-metal adhesion. For each of these approaches their suitability for use in load-bearing BIW components is discussed. In particular, the compatibility of these approaches with the BIW manufacturing process chain (i.e. (pre-coated) metal component stamping, BIW construction via different joining technologies, BIW pre-treated and painting operations) is presented. It has been found that while considerable amount of research has been done in the PMH direct-adhesion area, many aspects of these technologies which are critical from the standpoint of their use in the BIW structural applications have not been addressed (or addressed properly). Among the PMH technologies identified, the one based on micro-scale mechanical interlocking between the injection-molded thermoplastic polymer and stamped-metal structural component was found to be most promising.

Lastly, the suitability and the potential of various polymer-powder spraying technologies for coating metal stampings and, thus, for enhancing the polymer-to-metal adhesion strength in direct-adhesion PMH load-bearing automotive-component applications is considered. The suitability of the spraying technologies is assessed with respect to a need for metal-stamping surface preparation/treatment, their ability to deposit the polymeric material without significant material degradation, the ability to selectively overcoat the metal-stamping, the resulting

magnitude of the polymer-to-metal adhesion strength, durability of the polymer/metal bond with respect to prolonged exposure to high-temperature/high-humidity and mechanical/thermal fatigue service conditions, and compatibility with the automotive BIW manufacturing process chain. The analysis revealed that while each of the spraying technologies has some limitations, the cold-gas dynamic-spray process appears to be the leading candidate technology for the indicated applications.

Keywords: Polymer Metal Hybrid; Polymer-to-metal Adhesion; Automotive Structural Components; Polymer Coating Processes

DEDICATION

For my family, who offered me unconditional love and support throughout the course of this thesis.

ACKNOWLEDGEMENTS

I would like to express my deep and sincere gratitude to my research advisor, Dr. Mica Grujicic for helping me out in completing this thesis and funding me throughout my graduate study. His wide knowledge and logical way of thinking have been of great value to me. His understanding, encouragement and personal guidance have provided a good basis for the present thesis. I would also like to thank Dr. Mohammed Omar for helpful discussions on Vehicle Manufacturing Processes and Dr. Laine Mears for being in my committee, and giving me some useful inputs.

The material presented in this thesis is based on work conducted as a part of the project "*Lightweight Engineering: Hybrid Structures: Application of Metal/Polymer Hybrid Materials in Load-bearing Automotive Structures*" supported by BMW AG, München, Germany. I am indebted to Dr. David Angstadt, Dr. Greg Moco, Dr. Joshua Summers and Dr. Lonny Thompson for stimulating discussions.

I would like to thank the staff of the Mechanical Engineering Department who have helped me at various times: Ms. Gwen Dockins, Ms. Lindsey Mahaffey, Ms. Tameka Boyce, Ms. Kathryn Poole, Ms. Linda Cocke.

I warmly thank Mr. Bhaskar Pandurangan, Mr. Guruprasad Arakere, Mr. W. Cameron Bell and Mr. Balajee Ananthasayanam for their valuable advice and friendly help. Their extensive discussions have been very helpful for this study.

Finally, I would like to thank my parents, for their guidance throughout my life.

TABLE OF CONTENTS

Page

Table of Contents (Continued)

Page

Table of Contents (Continued)

Page

LIST OF TABLES

LIST OF FIGURES

List of Figures (Continued)

List of Figures (Continued)

Figure Page

CHAPTER 1

INTRODUCTION

1.1. Introduction

Lightweight engineering for automobiles is progressively gaining in importance in view of rising environmental demands and ever-tougher emissions standards. As displayed in Figure 1-1, current efforts in the automotive lightweight engineering involve at least the following five distinct approaches: (a) Requirement lightweight engineering which includes efforts to reduce the vehicle weight through reductions in component/subsystem requirements (e.g. a reduced required size of the fuel tank); (b) Conceptual lightweight engineering which includes the development and implementation of new concepts and strategies with potential weight savings such as the use of a self-supporting cockpit, a straight engine carrier, etc.; (c) Design lightweight engineering which focuses on design optimization of the existing components and sub-systems such as the use of ribs and complex cross-sections for enhanced component stiffness at a reduced weight; (d) Manufacturing lightweight engineering which utilizes novel manufacturing approaches to reduce the component weight while retaining its performance (e.g. a combined application of spot welding and adhesive bonding to maintain the stiffness of the joined sheet-metal components with reduced wall thickness); and (e) Material lightweight engineering which is based on the use of materials with a high specific stiffness and/or strength such as aluminum alloys and polymer-matrix composites or a synergistic use of metallic and polymeric materials in a hybrid architecture (referred to as polymer metal hybrids, PMHs, in the remainder of this thesis). Within the present work, suitability of the PMHs for use in load-bearing body-in-white (BIW) automotive components and a compatibility of the PMH technologies with a current BIW manufacturing process chain are investigated.

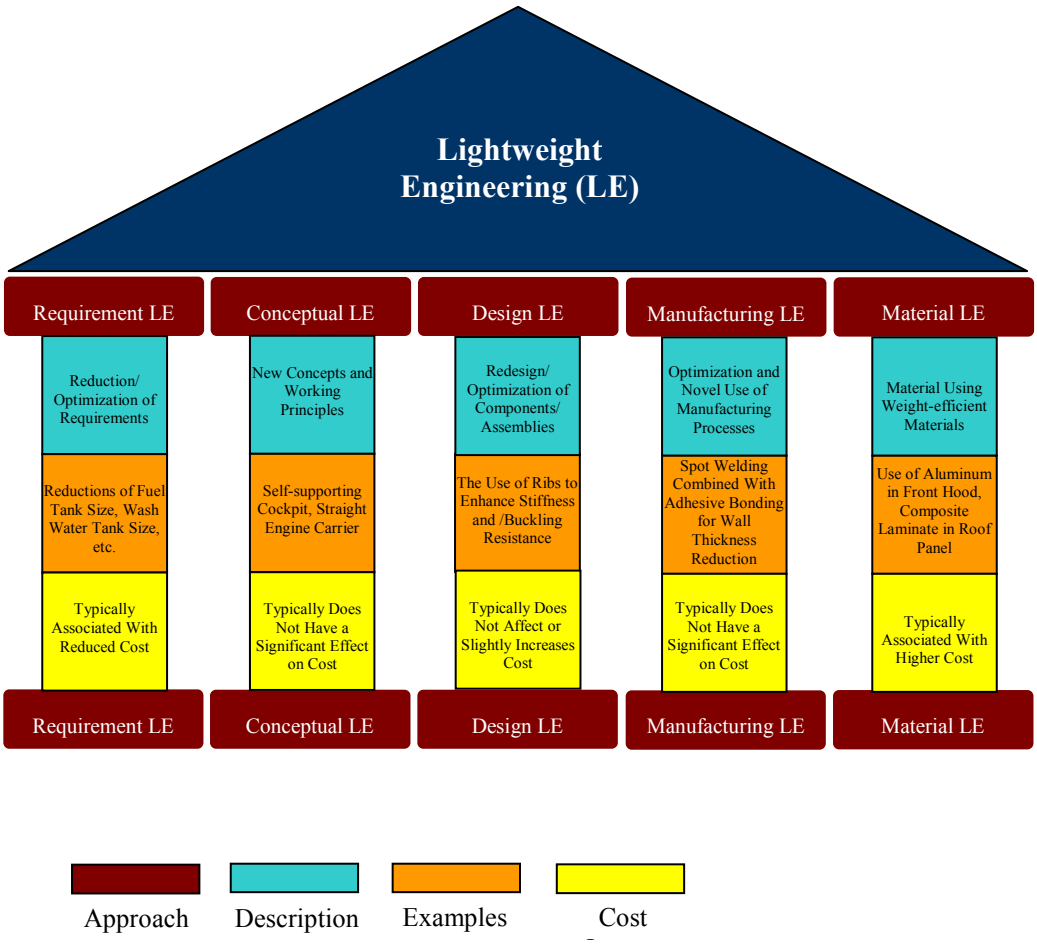

Figure 1-1: Five Major Approaches to Lightweight Automotive Engineering

1.2. Literature Review

The relevant literature survey for each of the sub-topics covered in the present work is provided in Chapters 2-5.

1.3. Thesis Objective and Outline

The initial objective of the present work was to examine computationally the potential of injection over-molding and adhesively bonded PMH technologies for use in load-bearing BIW automotive components. However, at the half-mark of this project, the sponsor decided to re-

direct the focus of the present work towards the investigation of direct-adhesion PMH technology. More specifically, a computational investigation was requested pertaining to the assessment of suitability of the direct-adhesion PMH technology for use in High-strength steel load-bearing BIW automotive components. In addition to assessing the potential of this technology with respect to meeting functional requirements of the components in question, compatibility of the direct-adhesion PMH technology with a current BIW manufacturing process chain had to be determined. The organization of the present work is as follows:

In Chapter 2, a comprehensive computational investigation is carried out to determine the required level of polymer-to-metal adhesion strength for the load-bearing automotive components hybridized using direct-adhesion PMH technology.

In Chapter 3, an overview and detailed examination is provided for the main phenomena/mechanisms responsible for polymer-to-metal adhesion .The investigation carried out in Chapter 3 suggested a potential need for the use of a polymer spraying technology as a way of achieving the necessary level of polymer-to-metal adhesion strength.

Consequently, in Chapter 4, an overview is provided of the current polymer spraying technologies and a procedure for the selection of the optimal spraying technology was developed.

In Chapter 5, a comprehensive investigation of the suitability of a direct-adhesion PMH technology for use in load-bearing BIW automotive components based on high-strength steels is provided.

Lastly, in Chapter 6, a brief summary and few suggestions for the future work are presented.

It should be noted that there are several aspects of the present work which are currently under Invention Disclosure Procedure and hence, cannot be discussed in the present work. Among these portions of the work are the so-called *"clinch-lock direct-adhesion PMH concept"*,

a novel total-life-cycle material selection procedure and a new method for the assessment of residual stresses in the direct-adhesion PMH components.

CHAPTER 2

COMPUTATIONAL FEASIBILITY ANALYSIS OF DIRECT-ADHESION POLYMER-TO-METAL HYBRID TECHNOLOGY FOR LOAD-BEARING BODY-IN-WHITE STRUCTURAL COMPONENTS

2.1. Abstract

The potential of direct-adhesion polymer-metal-hybrid (PMH) technology for use in load-bearing structural automotive components is explored computationally. Multi-disciplinary computations are carried out ranging from computational fluid mechanics of injection-mold filling and packing processes, flow-induced fiber orientation analysis, visco-elastic analysis of in-cavity residual stress developments and structural-mechanics computation of injection-molded part warping (under the effect of residual stresses) and deflection under simulated thermal loading encountered in the paint shop and under mechanical in-service loading. The results obtained helped identify the minimum level of polymer-to-metal adhesion strength and an optimal PMH-component architecture which are required in order for the direct-adhesion PMH technology to be considered a viable (weight-saving, parts-consolidation, manufacturing process-chain compatible) alternative to the currently used PMH technologies.

2.2. Introduction

In conventional automotive manufacturing practice, metals and plastics are fierce competitors. The polymer metal hybrid technologies, in contrast, aspire to take full advantage of the two classes of materials by combining them in a single component/sub-assembly. The first example of a successful implementation of this technological innovation in practice was reported at the end of 1996, when the front end of the Audi A6 (made by Ecia, Audincourt/France) was produced as a hybrid structure, combining sheet steel with elastomer-modified polyamide PA 6 -

GF 30 (type: Durethan BKV 130 from Bayer). A key feature of hybrid structures is that the materials employed complement each other so that the resulting hybrid material can offer structural performance which is not present in either of the two constituent materials independently.

Currently, polymer metal hybrids (PMHs) are replacing all-steel structures in automotive front-end modules at an accelerated rate. Moreover, new PMH technologies are being introduced as alternatives to the over-molding method first established by Bayer. In addition to their aforementioned use in the front-end modules, PMHs are currently being used in instrument-panel and bumper cross-beams, door modules, and tailgates applications as well as in non-automotive applications, ranging from appliance housings to bicycle frames.

The main PMH technologies currently being employed in the automotive industry can be grouped into three major categories: (a) Injection over-molding technologies; (b) Metal over-molding technologies combined with secondary joining operations; and (c) Adhesively-bonded PMHs. In the following, a brief description is provided for each of these groups of PMH manufacturing technologies.

In the injection over-molding process (originally developed and patented by Bayer [2.1]), metal inserts with flared through-holes are stamped, put in an injection mold and over-molded with 30% short glass fiber-reinforced nylon 6 to create a cross-ribbed supporting structure. The metal and nylon are joined by nylon melt penetrating through-holes to form rivets that provide mechanical interlocks. Because an injection molding press opens in one direction, cross-rib geometry was initially limited to just two dimensions. Recently, multi-directional ribbing was produced using this process by adding side motion to the tooling. Significant boosts in the load-bearing capability of U-shaped steel stampings were observed.

In the metal over-molding PMH technology, which was developed and patented by Rhodia [2.2] and adopted for the front-end module used on a 2004 light truck in South America, a steel stamping is placed in an injection mold, where its underside is coated with a thin layer of reinforced nylon. In a secondary operation, the plastics-coated surface of the metal insert is ultrasonically welded to an injection molded nylon sub-component. In this process, a closed-section structure with continuous bond lines is produced which offers a high load-bearing capability. The hollow core of the part permits functional integration like cable housings and air or water channels. Additionally, gas or water injection-molding can be employed to produce a stiffer, thinner coating for enhanced load-bearing capabilities and increased functional integration. A lower-cost variation of the metal over-molding PMH technology is Rhodia's so called Plastic-Metal Assembling process. A U-shaped steel stamping with punched holes and a nylon injection molded component, which contains columns or heat stakes that can lock into the stamping holes, are produced separately. The two sub-components are subsequently joined by riveting the ends of the plastic columns using ultrasonic welding or heat staking.

Adhesively-bonded PMHs were developed and patented by Dow Automotive [2.3] and were introduced in 2003 in prototype form for a Volkswagen front-end module. In this PMH technology, glass-fiber reinforced poly-propylene is joined to a metal stamping using Dow's proprietary low-energy surface adhesive (LESA). The acrylic-epoxy adhesive does not require pre-treating of the low surface-energy poly-propylene and is applied by high-speed robots. Adhesive bonding creates continuous bond lines, minimizes stress concentrations and acts as a buffer which absorbs contact stresses between the metal and polymer sub-components. The latest LESA grade, grade 74030, provides a good compromise between stiffness and toughness as well as improved adhesion and faster cure. To help maintain alignment of the sub-components during curing of the adhesive, snap features are designed into the sub-components. Adhesively-bonded

PMHs enable the creation of closed-section structures which offer high load-bearing capabilities and the possibility for enhanced functionality of hybrid parts (e.g. direct mounting of air bags in instrument-panel beams or incorporation of air or water circulation inside door modules).

While the aforementioned PMH technologies have demonstrated their potential and are being widely used in various non-structural and load-bearing automotive components, they nevertheless display some significant shortcomings. For example, in many applications, to maintain the structural integrity of the part hole punching needed for polymer-to-metal interlocking in the injection over-molding process may not be allowed. Similarly, stamped-edges over-molding may be restricted. In the case of adhesively bonded PMHs, the adhesive cost, long curing time and the ability of the adhesive to withstand aggressive chemical and thermal environments encountered in the paint-shop during body-in-white (BIW) pretreatment and E-coat curing may be an issue. Consequently, alternative lower-cost PMH technologies for structural load-bearing BIW component which are compatible with the BIW manufacturing process chain are being sought. One of such technologies, which is the subject of the present work, is the so called direct-adhesion PMH technology in which the joining between the metal and thermo-plastic sub-components is attained through direct adhesion of injection-molded thermo-plastics to the metal without the use of interlocking rivets/over-molded edges or structural adhesives. There are several potential advantages offered by this technology over the ones discussed above: (a) Polymer-to-metal adhesion strengths (ca. 35MPa) comparable with those obtained in the case of thermo-setting adhesives are feasible but only at a small fraction of the manufacturing cycle time; (b) The shorter cycle time and the lack of use of an adhesive allow for more economical PMH-component production; (c) Unlike the adhesive-bonding technology, joining is not limited to simple and non-interfering contact surfaces; (d) Reduced possibility for entrapping air in undercuts of a complex surface; (e) No holes for the formation of interlocking rivets are required

and, hence, structural integrity of the part is not compromised; and (f) Overall reduction in the constraints placed upon the design complexity of the PMH component.

In this chapter, a comprehensive multi-disciplinary computational analysis is carried out in order to assess the potential of the direct-adhesion PMH technology for use in load-bearing BIW structural components. The analysis included: (a) detailed numerical simulation of the filling (including flow-induced fiber orientation), packing, and cooling stages of the injection molding process; (b) an anisotropic thermo-visco-elastic computation of the thermally and pressure-induced (in-mold residual) stresses in an injection molded fiber-reinforced polymer-matrix composite insert; (c) structural mechanics analysis (based on the use of multi-layer shell elements) of shrinkage and warping caused by the relaxation of the stresses after part ejection; and (d) structural mechanics analysis (including the effect of adhesion-based load transfer between the metal stamping and plastic injection molded insert) of the component stiffness and strength under several simple monotonic loading modes and under creep.

The organization of the chapter is as follows: An overview of the geometrical, material and structural models and the computational procedures is presented in Section 2.3. The results obtained in the present work are presented and discussed in Section 2.4. The main conclusions resulting from the present work are summarized in Section 2.5.

2.3. Problem Formulation and Computational Analysis

2.3.1. Geometrical and Structural-Mechanics Modeling of Control BIW Structural Component

Structural components in the BIW generally consist of two (flanged) metal stampings (shells) which are subsequently spot welded along the length of the flanges. Typically one of the stampings has a (flanged) U-shape while the other is either a U-shape or a "*cover plate*". The resultant closed-box configuration generally provides a good combination of (compressive,

bending and torsional) stiffnesses and strengths but, in the case of the all-steel construction, the weight of the components is relatively high.

To assess the potential of the direct adhesion PMH technology in load-bearing BIW structural components, a simple geometrical model for the generic BIW structural component is used in the present work, Figure 2-1(a). The sheet metal thickness is set to 1mm, while the other dimensions of the part are indicated in Figure 2-1(a). Both parts are made of a dual-phase steel with the Young's modulus E=210GPa, Poisson's ratio ν=0.3 and the yield strength σ_y=350MPa. The U-shape and the cover plate are joined using 5mm-diameter 25mm-spaced spot welds and a provision is made for the matching flanges of the U-shape and the cover plate to contact each other during loading. The resulting box-shape component is used as a control during a finite-element structural-mechanics investigation in order to assess the mass-based load-bearing efficiency of the corresponding PMH component (discussed in next section). In such analysis, 4400 and 2800 triangular shell elements are used for the U-shape and the cover plate, respectively. The U-shape and the cover plate are joined using 200 spot welds and a hard-contact (with friction) algorithm is used for modeling the potential contact between the two parts along the flange surfaces of the U-shape. Spot welds are modeled as fasteners in which the coupling constraint is distributed to a group of nodes on the joined surfaces in the immediate neighborhood of the attachment point called "*a region of influence*". The structural-mechanics analysis is carried out using ABAQUS/Standard 6.6, a general purpose finite element (FE) package [2.4]. During the FE analysis, all the nodes on one end of the box-shape component are fixed while the corresponding nodes on the other end are displaced in accordance with the basic loading modes: (a) axial compression in the x-direction; (b) bending in the y-direction; (c) bending in the z-direction and (d) twisting about the x-axis. The resulting load-displacement and torque v/s twist angle curves are presented and discussed in Section 2.4.1. A standard mesh sensitivity analysis is

carried out to ensure that the results obtained are essentially invariant to further mesh-size refinements.

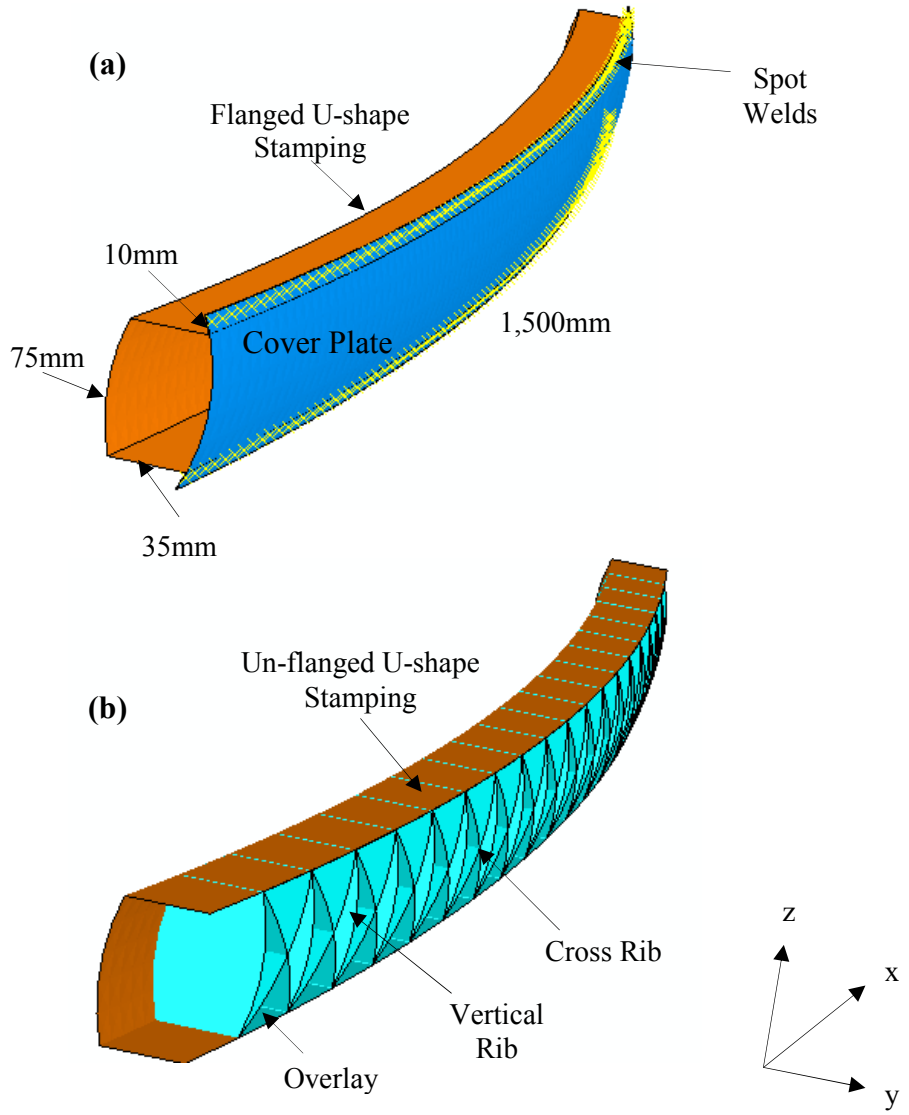

Figure 2-1: Geometrical Models (with dimensions) for: (a) the Control All-steel BIW Structural Component and (b) the Corresponding Direct-adhesion PMH component

2.3.2. Geometrical and Structural-mechanics Modeling of BIW Polymer Metal Hybrid Structural Component

To assess the potential of the direct adhesion PMH technology in BIW structural components, the control BIW structural component described in the previous section is modified in the following way: (a) the flanges are removed from the U-shape channel; (b) the cover plate is eliminated; and (c) a plastic insert consisting of an overlay (mates with the interior of the U-shape channel) and a series of "*vertical*" and "*cross*" ribs is added. To ensure that the plastic insert will not be affected by welding of the U-shape channel ends to the BIW structure, the length of the insert is set to 90% of the U-shape channel length and it is center relative to it lengthwise. A set of 19 (or 16 or 13) vertical and 18 (or 15 or 12) cross ribs is used, Figure 2-1(b). As in the case of the control component, four basic loading modes are applied to the hybrid component to carry out a structural-mechanics analysis using ABAQUS/Standard. The (un-flanged) U-shape steel channel was represented using 3600 triangular (single layer) shell elements. The plastic insert, on the other hand, is made of Durethan BKV 130 H2.0 (a 30wt. % glass-fiber filled Nylon 6, elastomer modified with enhanced heat-age resistance). The insert is represented using 6160 (20-layer) shell triangular elements. The (planar isotropic) thermo-mechanical properties of each layer of the material are obtained as a result of the mold filling analysis (discussed in next section). The hybrid component is assumed to be processed by placing the U-shape channel into the mold as an insert and injection molding the plastic insert against it. Since in many applications the structural integrity of the U-shape channel cannot be compromised by punching-out holes (used in the injection over-molding technology to join the plastic and the metal via formation of a plastic rivet), such holes were not used in the present work. Likewise, since over-molding of the stamping edges may be restricted, no edge over-molding was considered. In other words, joining of the metal and the plastic is considered to rely completely on their mutual adhesion. The

adhesion between the metal and the polymer is treated, in the FE structural analysis, using specialized cohesive elements. Through the use of a traction-separation relation, such elements allow modeling of the initial loading, the initiation of damage, damage-induced adhesion stiffness/strength degradation and the propagation of damage leading to eventual decohesion of the adhering surfaces under different normal and shear loading modes. The load vs. displacement and torque vs. twist angle results obtained in the present structural-mechanics analysis are overviewed and discussed in Section 2.4.4.

2.3.3. Modeling of Injection-molding Fabrication of BIW Polymer Metal Hybrid Structural Component

Thermoplastics injection molding is a widely used manufacturing process for producing parts/components with a high degree of geometrical complexity. A typical injection molding process involves four distinct stages: (a) filling of the mold with molten thermoplastics; (b) packing – injection of additional material into the mold under high pressure to compensate for the cooling-induced volumetric shrinkage of the material; (c) cooling which gives rise to the solidification of the material residing in the mold; (d) ejection of the solidified part/component from the mold. During the filling, packing and cooling stages of the injection molding process, the material is subjected to complex thermo-mechanical loading which gives rise to the changes in local specific volume (density), part shape as well as to the development over the residual stresses in the part. In other words, while the (thin-wall) part resides in the mold, it is constrained within its mid-plane causing the (residual, built-in) stresses to develop in the part during solidification of the melt. Upon ejection, these stresses relax causing distortion/warping and further shrinkage of molded part. Further warping and shrinkage of the part may occur during cooling of the ejected molded part.

To take into account the fact that the plastic insert was injection molded and made of glass-fiber filled thermo-plastics, and hence, may possess residual stresses at the moment of component ejection from the mold and possess a heterogeneous, non-isotropic material, the following analyses were conducted: (a) identification of the optimal placement and the number of polymer injection points; (b) mold filling analysis which yielded the filling time, the through-the-shell-thickness fiber orientation in the material and in-cavity residual stresses; (c) plastic insert shrinkage and warping analyses after part ejection from the mold under constraints imposed by the U-shape channel; and (d) structural-mechanics analysis of the PMH component for comparison with the all-steel control component (discussed in the previous section). The analyses (a) and (b) were carried out using Moldflow Plastics Insight 6.0 [2.5] while the analysis (c) and (d) was determined using ABAQUS/Standard [2.4].

In the injection molding analysis carried out in the present work, it was assumed that a Netstal commercial injection molding machine Model 4200H-2150 is used with the following specifications: (a) The injection unit - maximum machine injection stroke = 248mm, maximum machine injection rate = 5024 cm^3/s, machine screw diameter = 80 mm; (b) The hydraulic unit - maximum machine hydraulic pressure = 17.5MPa, intensification ratio = 10.0, machine hydraulic response time = 0.2s; and (c) The clamping unit - maximum machine clamp force = 3800 ton. Also the injection molding is assumed to be done under the following process parameters: Filling stage- melt temperature=563K, injection rate=400 cm^3/s, velocity/pressure switchover at 99% volume filled; Packing stage - time=10s, pressure=80MPa; Cooling stage - mold surface temperature=363K, ejection temperature=458K, fraction of solid phase at ejection=1.0; Mold material – tool steel P20; Thermoplastics material - Durethan BKV 130 H2.0 (an elastomer-modified Nylon 6 filled with 30wt.% of glass fibers and heat-age stabilized).

2.3.3.1. Optimal Placement and Number of Injection Points

Before simulations of the injection molding process can be carried out, the optimal placement and the number of injection points has to be determined. The gate location analysis employed in the present work uses the part geometry, the selected material and the specified process settings and relies on the following criteria: molding feasibility and the achievement of balanced flow, so that areas furthest away from the gate(s) (i.e. injection point(s)) are filled at approximately the same time [2.5]. To ensure that small enough plastics-wall-thicknesses can be injection molded, two gates (one attached to the first and the other to the last vertical rib) are utilized in the present work.

2.3.3.2. Mold Filling/Packing, Fiber Distribution and In-cavity Residual Stress Analyses

In this section, a brief description is given of the mold filling/packing, fiber orientation and in-mold residual stress computational analyses carried out in the present work.

Initial computational efforts reported in the literature were focused on predicting pressure and temperature distributions and melt-front advancement during mold filling [2.6-2.11]. Over the last several years, however, post-filling phenomena such as part in-mold stresses, fiber orientation distribution, shrinkage and warping received more attention [2.12,2.13]. While the early efforts were mainly empirical [e.g. 2.13], subsequent work was more fundamental and relied on more realistic materials models [e.g. 2.14].

Mold-filling Analysis

The mold filling process is governed by the following conservation equations:

Momentum Conservation:

$$\sigma_{ij,j} = 0 \tag{2.1}$$

Mass Conservation:

$$\frac{D\rho}{Dt} + \rho v_{i,i} = 0 \tag{2.2}$$

Energy Conservation:

$$\rho c_p \frac{DT}{Dt} = kT_{,i} + \sigma_{ij} D_{ij} - \frac{T}{\rho}\frac{\partial \rho}{\partial T}\frac{Dp}{Dt} + \rho_c H_c \frac{\partial \chi}{\partial t} \tag{2.3}$$

where the Cartesian index notation is used in Eqs. (2.1)-(2.3), the repeated indices imply summation, and a comma denotes partial differentiation with respect to the coordinate, D/Dt is the material derivative, σ_{ij} denotes the total stress tensor, $\rho = \rho(T, p)$ represents the fluid density at local temperature, T and pressure, p, v_i is the velocity vector, c_p is the constant-pressure specific heat, k is the thermal conductivity, ρ_c is the solid-material density, H_c is the latent heat of solidification, χ is the extent of crystallinity and D_{ij} is the strain-rate tensor defined as $D_{ij} = (v_{i,j} + v_{j,i})/2$. For semi-crystalline materials, an additional governing equation, the rate of crystallization equation, has to be specified in addition to Eqs. (2.1)-(2.3).

When injection molding of thermo-plastics filled with fibers is considered, as is the present case, the flow field is generally assumed to be independent of the orientation distribution of the fibers. In other words, the mold-filling and packing analyses are de-coupled from the fibers orientation analysis. This assumption is strictly justified only in the case of injection molding of the thin-walled parts, as is the present case, in which the fibers are oriented nearly parallel to the mid-plane and, hence, their interaction with the melt flow is limited [2.15-2.20]. The conditions which have to be satisfied in order for the influence of the fibers on the fluid motion to be neglected can be found in Ref. [2.21].

When the mold filling of thin-wall parts is analyzed, as is the present case, the following two "*lubrication*" approximations are generally made: (a) Through-the-thickness-variations in pressure are neglected; and (b) The pressure field is taken to satisfy Hele-Shaw (elliptic) equation of the form:

$$\nabla \cdot \left(S \nabla p \right) = \int_{-h/2}^{h/2} \frac{1}{\rho} \frac{Dp}{Dt} dx_3 \tag{2.4}$$

where ∇ denotes the gradient operator with respect to the mid-plane, S the flow conductance factor which depends on melt viscosity and the cavity thickness, h, and x_3, the local thickness coordinate. The shear-rate, pressure and temperature dependencies of the material viscosity are accounted for through the use of a Cross model [2.14].

Eq. (2.4) was subjected in the present work to the following boundary conditions: (a) Either the inlet-flow rate or the pressure boundary condition is defined at the injection points (gates); (b) A zero-pressure condition is defined on the advancing flow front; and (c) A zero-normal-pressure gradient $\partial p / \partial n = 0$ is specified over the mold-cavity-surface. These conditions do not ensure a no-slip condition over the mold-cavity-surface, which may allow the fluid to "*slip*". The resulting inaccuracies in the velocity-field predictions, however, were found not to be significant [2.22]. Since Eq. (2.4) considers only the flow parallel with the local mid-plane, it cannot be used to model the fountain flow. The resulting inaccuracies in the temperature and fiber-orientation predictions in the outermost layers of an injection molded part were corrected using one of the local approximations [2.10].

To obtain temporal and spatial evolutions of the pressure during filling, Eq. (2.4) is solved numerically using the conventional Galerkin finite element method (within a local coordinate system in which the x_1 axis coincides with a line connecting the first two nodes of a given element and the x_1 and x_2 axes define the mid-plane). Three-node triangular elements are

used to discretize the mid-plane of the part while two-node beam elements to model the runner system. Before element-based equations are assembled, a local-to-global coordinate transformation is applied to obtain a full three-dimensional computational model.

The flow front is tracked using the standard node-centered control-volume approach [2.5]. After the governing equation for pressure is solved, the flow rate into each node located on the flow front is calculated. This is used in conjunction with a given time step to determine if the control volume associated with the node in question is filled. If the control volume is filled, the flow front is advanced to the node in question.

To obtain spatial and temporal evolutions of temperature during mold filling (and packing). Eq. (2.3) is solved numerically in such a way that the convection and viscous dissipation terms from a previous time step are treated as source terms during the current time step. Fast heat conduction over the steel U-shape and mold surfaces is accounted for using a cycle-averaged (constant and uniform) temperature boundary condition at the U-shape/polymer and mold/polymer interfaces. The cycle-averaged temperature of the U-shape and mold surfaces is obtained by solving a three-dimensional steady-state heat conduction equation using a boundary element method [2.23]. Due to a lack of reliable data, no effect of thermal contact resistance (which may lead to a temperature discontinuity) at the U-shape/polymer and mold/polymer interfaces is considered. Likewise, no assumption that the flow and temperature fields are symmetrical about the mid-plane is employed since this may lead to incorrect predictions in the part warping upon ejection (e.g. [2.24,2.25]).

Fiber Orientation Analysis

For accurate predictions of the shrinkage and warping of an injection-molded part made of fiber-filled thermo-plastics, knowledge of the (flow-induced) fiber-orientation distribution throughout the part is critical [e.g. 2.26-2.28]. Since most commercial fiber-filled thermo-plastics

commonly used for injection molding can be classified as semi- or highly-concentrated suspensions, fiber/fiber interactions and spatial constraints to the fiber motion may significantly affect the final fiber-orientation distribution in the part.

Fiber/fiber interactions are accounted for, in the present work, using Folgar and Tucker model [2.26]. In this model, a suspension-specific isotropic parameter, C_I, called the "*Interaction Coefficient*" is introduced in the diffusion term of the equation of motion for an isolated fiber in a Newtonian fluid originally proposed by Jeffery [2.29]. The value for C_I is assessed using direct numerical–simulations of fiber/fiber interactions within simple-shear flow [2.27] in which short-range interactions are quantified using a lubrication model [2.30] while long-range interactions were calculated using a boundary element method.

The orientation of a fiber is typically defined using the unit vector p which is collinear with the fiber axis. The fiber-orientation probability-distribution function is then defined using the second, $-a_{ij} = \langle pp \rangle$, and the fourth, $a_{ijkl} = \langle pppp \rangle$, order orientation tensors, where the angular brackets denote the ensemble average. The Folgar-Tucker model is then defined by the following equation [2.31]:

$$\frac{Da_{ij}}{Dt} = \omega_{ik}a_{kj} - a_{ik}\omega_{kj} + \lambda\left(D_{ik}a_{kj} + a_{ik}D_{kj} - 2D_{kl}a_{ijkl}\right) + 2C_I\dot{\gamma}\left(\delta_{ij} - \alpha a_{ij}\right) \tag{2.5}$$

where $\lambda = (a_R^2 - 1)/(a_R^2 + 1)$ is a function of the fiber aspect ratio a_R, $\omega_{ij} = (v_{i,j} - v_{j,i})/2$ is the local vorticity, $\dot{\gamma}$ is the generalized shear rate defined as $\dot{\gamma}^2 = 2D_{ij}D_{ij}$, δ_{ij} the Kronecker delta and α a constant (=3 for three-dimensional and =2 for planar-orientation distribution of fibers) introduced in order to satisfy the condition trace$\langle pp \rangle = 1$. Before Eq. (2.5) can be solved, the fourth-order tensor needs to be expressed in terms of the second-order tensor using a "*closure*

approximation". There are a number of such approximations proposed in the literature [e.g. 2.32-2.35].

Direct simulations of simple-shear flow yields the final fibers orientation unit normal, p, (as a function of the initial fiber orientation, aspect ratio, the number density in the suspension and the shear-strain magnitude) and, in turn, the components of the second- and fourth-order orientation tensors a_{ij} and a_{ijkl}. These are next used in the following anisotropic rotary diffusion equation:

$$\frac{Da_{ij}}{Dt} = \omega_{ik}a_{kj} - a_{ik}\omega_{kj} + \lambda\left(D_{ik}a_{kj} + a_{ik}D_{kj} - 2D_{kl}a_{ijkl}\right) \_ 3\dot{\gamma}\left(C_{jk}a_{kj} + C_{jk}a_{ik}\right) + 6\dot{\gamma}C_{kl}a_{ijkl} + 2\dot{\gamma}\left(C_{ij} - C_{kk}a_{ij}\right) \tag{2.6}$$

to determine the interaction coefficient C_I. In Eq. (2.6), the original Folgar-Tucker isotropic diffusion coefficient $C_I\delta_{ij}$ has been replaced by a symmetric second-order tensor C_{ij} to account for the material anisotropy. The differences in values of the three eigen-values of this tensor reflect the extent of material anisotropy. The tensor C_{ij} determined in this way is next used in simulations of the fibers-orientation evolution during the filling stage of the injection molding process. In the present work, the largest eigen-value is found to be more than 25 times larger than the smallest eigen-value suggesting that, for an accurate determination of the fibers orientation, the use of the anisotropic rotary diffusion equation, Eq. (2.6), is critical. Eq. (2.6) is solved numerically using the explicit Euler time-differencing scheme with a time step which is smaller than that used for the flow front advancement analysis and which satisfy the following Courant stability criterion:

$$\Delta t_f < \frac{\Delta x}{|v|} \tag{2.7}$$

where Δx represents the size of an element and $|v|$ the magnitude of the velocity. For triangular elements, Δx is defined as the minimum of the distances between the centroid and each of the three nodes, while v is generally taken as the flow speed at the mid-plane. For the initial value problem defined by Eq. (2.6), initial values of the fiber-orientation tensors in the elements which are associated with the gates have to be specified. While the exact fibers orientations at the gates locations are usually unknown, the choice of the initial condition has been found to have little impact on the final orientation distribution of the fibers [e.g. 2.55].

As mentioned earlier, the Hele-Shaw approximation does not include the effect of the lateral mold-walls on the advancement of flow field which, in turn, can lead to incorrect predictions of the fibers orientation in the outermost layers of an injection-molded part. This, in turn, may lead to incorrect prediction of the part warping. To overcome these shortcomings, two ad-hoc remedies are used in the present work: (a) a vanishing tangential velocity along the mold walls is imposed during fiber-orientation calculations when computing velocity gradients from the velocity field; and (b) an "*infinite-aspect-ratio*" assumption is used for the fibers near the mold walls [2.15].

Mold-packing Analysis

While the packing phase of the injection molding process is governed by the same conservation equations as the filling phase, an additional equation, the equation of state (also known as the P-V-T relation), must be defined in order to include the effect of melt compressibility. The P-V-T relation defines a functional relationship between the specific volume, $\hat{V}$, temperature, pressure, and cooling rate as:

$$\hat{V} = \hat{V}(p, T, \frac{\partial T}{\partial t}) \tag{2.8}$$

The type of the P-V-T relation used in the present work is discussed in Appendix A. It should be noted that the cooling rate dependence of the specific volume, as indicated by Eq. (2.8), is generally considered only in the case of semi-crystalline polymers. It should be further noted that a number of material properties (such as volume thermal expansion coefficients and compressibility) and their temperature and pressure dependencies can be derived from the equation of state. Also, the P-V-T relation is used to represent various phase transformations such as freezing/melting, crystallization, and ductile-to- glass-transition.

In-mold Stress Analysis

There are two main sources for residual stresses in injection molded parts: (a) Visco-elastic deformations of the thermoplastic material during filling/packing can give rise to the development of the so called "*flow-induced*" residual stresses; and (b) When the (inhomogeneous) cooling- and solidification-induced shrinkage of the polymer is restricted by the mold and the applied packing pressure, the so-called "*thermally and pressure-induced*" stresses are generated. Following the general practice, the flow-induced residual stresses are neglected in the present work, since these are readily relieved while the part resides in the mold at high temperatures prior to ejection. There are numerous reports of numerical investigations of the pressure and thermally-induced stresses in injection molded parts in the literature [e.g. 2.36-2.45]. These investigations clearly revealed the effects of mold constraints and thermo-plastics material models on the extent and distribution of the residual stresses.

As the injected material begin to cool inside the mold, its relaxation time starts to increase and to approach the in-mold resident time. Hence, an accurate prediction of the thermal stresses entails the knowledge of the visco-elastic material properties. In the range of small strains, as is the present case, the visco-elastic behavior of an injection-molded fiber-filled

thermo-plastics can be described using the anisotropic linear thermo-visco-elasticity [2.46,2.47] in the form:

$$\sigma_{ij} = \int_0^t c_{ijkl}\left(\xi(t) - \xi(t')\left(\frac{\partial \varepsilon_{kl}}{\partial t'} - \alpha_{kl}\frac{\partial T}{\partial t}\right)dt' \right. \tag{2.9}$$

where $c_{ijkl}(t)$ is the forth-order visco-elastic relaxation tensor and $\xi(t)$ denotes the so-called "*pseudo-time scale*" defined by:

$$\xi(t) = \int_0^t \frac{1}{a_T} dt' \tag{2.10}$$

where a_T is the time-temperature shift factor that reflects the inter-changeable effects of time and temperature on the material response. For amorphous polymers, the time-temperature shift factor in a temperature range between T_g and $T_g + 100K$ (where T_g is the glass transition temperature) is generally defined by the so-called WLF equation [2.48] in the form:

$$\log_{10} a_T = -\frac{C_1(T - T_r)}{C_2 + (T - T_r)} \tag{2.11}$$

where C_1 and C_2 are constants and T_r is a reference temperature. When the relevant experimental data are lacking for a given material and the values for constants C_1, C_2 and T_r, cannot be assessed, the so-called "*universal values*" $C_1 = 17.44$, $C_2 = 51.6$, $T_r = T_g$ are used. For temperatures outside the above range or for semi-crystalline materials, the following Arrhenius-type expression is generally used to assess the time-temperature shift factor:

$$\ln a_T = \frac{E_a}{R}\left(\frac{1}{T} - \frac{1}{T_r}\right) \tag{2.12}$$

where E_a is the activation energy and R the universal gas constant.

Materials obeying the time-temperature superposition principle are generally referred to as thermo-rheologically simple materials. In such materials, visco-elastic material functions determined at one temperature and plotted against the logarithmic time remain essentially unaltered when the temperature is changed. While fiber-filled thermo-plastics generally behave as rheologically-complex materials, the material used in the present work is treated as being rheologically simple due to a lack of experimental data needed to evaluate the necessary parameters. To compute the in-mold stresses, the following procedure is utilized. First, the total-stress second-order tensor in Eq. (2.9) is decomposed into the hydrostatic stress and the deviatoric stress as:

$$\sigma = -p_h I + \tau \tag{2.13}$$

where p_h is the hydrostatic pressure, I the second-order identity tensor and τ the deviatoric stress tensor. While residing in the mold, the part is considered to be fully constrained within the local element-based 1-2 mid-plane. The resulting hydrostatic pressure is then defined as:

$$p_h = -\frac{1}{3}\sigma_{ii} = \int_0^t \left(\beta \frac{\partial T}{\partial t'} - KTr\,\dot{\varepsilon} \right) \tag{2.14}$$

where β and K are given in terms of the elastic constants c_{ij} and thermal α_i material properties (using the contracted notation) as:

$$\beta = \frac{1}{3}\left[\left(c_{11}^{(e)} + c_{12}^{(e)} + c_{13}^{(e)} \right)\alpha_1 + \left(c_{12}^{(e)} + c_{22}^{(e)} + c_{23}^{(e)} \right)\alpha_2 + \left(c_{13}^{(e)} + c_{23}^{(e)} + c_{33}^{(e)} \right)\alpha_3 \right] \tag{2.15}$$

and

$$K = \frac{1}{3}\left(c_{13}^{(e)} + c_{23}^{(e)} + c_{33}^{(e)} \right) \tag{2.16}$$

Since, in injection molded parts, the fibers generally lie in the (flow) mid-plane, the fiber direction is chosen as the material 1-direction while the material 3-direction is aligned with the corresponding through-the-thickness direction.

The normal components of the deviatoric stress are given as:

$$\tau_{ii}(t) = 2\int_0^t G_i(\xi(t)-\xi(t'))\frac{\partial \varepsilon_{ij}^d}{\partial t}dt' - \int_0^t \beta_i(\xi(t)-\xi(t'))\frac{\partial T}{\partial t}dt' \tag{2.17}$$

where ii = 11, 22, 33, i=1, 2, 3, ε_{ij}^d is the deviatoric strain defined as:

$$\varepsilon_{ij}^d = \varepsilon_{ij} - \frac{1}{3}Tr\varepsilon\delta_{ij} \tag{2.18}$$

$$G_i(t) = G_i(0)F(t) \qquad (i=1,2,3) \tag{2.19}$$

and

$$\beta_i(t) = \beta_i(0)F(t) \qquad (i=1,2,3) \tag{2.20}$$

with

$$G_1(0) = \frac{1}{2}\left(c_{23}^{(e)} - c_{13}^{(e)} + c_{33}^{(e)}\right) \tag{2.21}$$

$$\beta_1(0) = \frac{1}{3}\left[\left(2c_{11}^{(e)} - c_{12}^{(e)} - c_{13}^{(e)}\right)\alpha_1 + \left(2c_{12}^{(e)} - c_{22}^{(e)} - c_{23}^{(e)}\right)\alpha_2 + \left(2c_{13}^{(e)} - c_{23}^{(e)} - c_{33}^{(e)}\right)\alpha_3\right] \tag{2.22}$$

and $G_2(0)$, $G_3(0)$, $\beta_1(0)$ and $\beta_2(0)$ are defined using analogous expressions and it is assumed that all $G_i(t)$ and $\beta_i(t)$ depend on the same relaxation function $F(t)$. The relaxation function is approximated as a sum of weighted exponential functions as:

$$F(t) = \sum_{k=1}^{N} g_k \exp\left(-\frac{t}{\lambda_k}\right) \tag{2.23}$$

with $\sum_{k=1}^{N} g_k = 1$. The current model for $F(t)$ requires the knowledge of $N(g_k, \lambda_k)$ pairs of values.

Computations of the pressure and thermally-induced in-mold stresses via Eqs. (2.14) and (2.17) are carried out under the following assumptions and boundary conditions:

Assumptions:

1. The shear strains $\varepsilon_{13} = \varepsilon_{23} = 0$ with respect to the local coordinate system in which x_3-direction is normal to the mid-plane;

2. The normal stress σ_{33} is constant across the element thickness;

3. As long as $\sigma_{33} < 0$, the injected polymer is considered to be in contact with the U-shape/mold;

4. Before ejection, the part is fully constrained within the mid-plane so that the only non-zero component of the strain is ε_{33}.

5. The U-shape and the mold are assumed to be rigid.

Boundary Conditions:

When specifying the boundary conditions for the normal stress σ_{33}, the following three cases are considered:

1. When the part resides in the mold and the injected material contains both a solid outer-layer and a liquid core, the normal stress σ_{33} is set equal to the negative fluid pressure, $\sigma_{33} = -p$. In addition, all strain components except for ε_{33} are set to zero.

2. When the part resides in the mold and the injected material has completely solidified, the part may either be in contact with the U-shape/mold or be detached from it. In the first case,

σ_{33} is determined using the condition: $\int_{-h/2}^{h/2} \varepsilon_{33} dx_3 = 0$. In the latter case, $\sigma_{33} = 0$. Again, all strain components except for ε_{33} are set to zero.

3. After the part is ejected from the mold, no external loads are applied to it and, hence, σ_{33} is determined from the following zero-surface-traction boundary condition: $\sigma_{ij} n_j = 0$, where n_j is j[th] component of the plastic-insert unit outward surface normal except for the insert surfaces which adhere to the U-shape. It should be noted that the residual stresses (present in the plastic insert just prior to ejection) are used as the initial-stress conditions in the subsequent post-ejection shrinkage and warping analysis of the PMH component.

The pressure and thermally-induced stresses at time t_{n+1} are computed using a numerical scheme based on the known stress state at time t_n. Toward that end, Eq. (14) is first re-written as:

$$p_h(t_{n+1}) = p_h(t_n) + \beta \Delta T - KTr\Delta\varepsilon \tag{2.24}$$

where ΔT and $\Delta\varepsilon$ are the changes in T and ε, respectively, during time step $\Delta t = t_{n+1} - t_n$.

Next, a discrete formulation of Eq. (2.17) for the τ_{11} normal deviatoric stress is developed by substituting Eqs. (2.19), (2.20) and (2.23) into Eq. (2.17) to get:

$$\tau_{11}(t) = \sum_{k=1}^{N} \left[s_{11}^{(k)}(t) - \Theta_1^{(k)}(t) \right] \tag{2.25}$$

where

$$s_{11}^{(k)}(t) = 2G_1(0) g_k \int_0^t \exp\left(- \frac{\xi(t) - \xi(t')}{\lambda_k} \right) d\varepsilon_{11}^d(t') \tag{2.26}$$

and

$$\Theta_1^{(k)}(t) = \beta_1(0) g_k \int_0^t \exp\left(-\frac{\xi(t) - \xi(t')}{\lambda_k} \right) d\varepsilon_{11}^d(t') \tag{2.27}$$

Differentiation of Eq. (26) with respect to t then yields:

$$\frac{ds_{11}}{dt} + \frac{1}{\lambda}\frac{d\xi}{dt} s_{11} = 2G_1(0) g_k \frac{d\varepsilon_{11}^d}{dt} \tag{2.28}$$

The differential equation, Eq. (28), is next discretized as:

$$\frac{s_{11}(t_{n+1}) - s_{11}(t_n)}{\Delta t} + \frac{1}{\lambda}\frac{d\xi}{dt} s_{11}(t_{n+1}) = 2G_1(0) g_k \frac{\Delta\varepsilon}{\Delta t} \tag{2.29}$$

so that

$$s_{11}^{(k)}(t_{n+1}) = \xi_k \left[s_{11}^{(k)}(t_n) + 2G_1(0) g_k \Delta\varepsilon_{11}^d \right] \tag{2.30}$$

where $\xi_k = \left(1 + \frac{\Delta\xi}{\lambda_k} \right)^{-1}$ and $\Delta\xi$ is approximated by: $\Delta\xi = \frac{\Delta t}{a_T}$.

A similar procedure applied to Eq. (2.27) yields:

$$\Theta_1^{(k)}(t_{n+1}) = \xi_k \left[\Theta_1^{(k)}(t_n) + \beta_1(0) g_k \Delta T \right] \tag{2.31}$$

The procedure presented above yields a formula for updating τ_{11}. The same procedure is next applied to obtain the analogous formulae for τ_{22} and τ_{33}. Since the chosen coordinate system coincides with the fiber-reinforced material principal coordinate system and the fibers are assumed to lie parallel to the mid-plane, the in-plane shear stress τ_{12} is zero. However, after the coordinate system is transformed to the local element-base coordinate system, the in-plane shear stresses take on no-zero values.

Next, a procedure for the calculation of the incremental strain $\Delta\varepsilon_{33}$ is discussed. According to the assumption 4 presented above, the following relations are implied:

$$Tr(\Delta\varepsilon) = \Delta\varepsilon_{33} \tag{2.32}$$

$$\Delta\varepsilon_{11}^{d} = \Delta\varepsilon_{22}^{d} = -\frac{1}{3}\Delta\varepsilon_{33} \tag{2.33}$$

$$\Delta\varepsilon_{33}^{d} = \frac{2}{3}\Delta\varepsilon_{33} \tag{2.34}$$

Since the stress σ_{33} is given as a boundary condition, the incremental strain component $\Delta\varepsilon_{33}$ at the time interval (t_n, t_{n+1}) can be calculated using $\sigma_{33}(t_{n+1})$ and its value at the previous time step t_n. The stress component $\sigma_{33}(t_{n+1})$ can be expressed as:

$$\sigma_{33}(t_{n+1}) = \sigma_{33}^{*} + \left(K + \frac{4}{3} G_3(0) \sum_{k=1}^{N} \xi_k g_k \right) \Delta\varepsilon_{33} \tag{2.35}$$

where σ_{33}^{*} is given by:

$$\sigma_{33}^{*} = -\left\{ p_h(t_n) + \beta\Delta T + \sum_{K=1}^{N} \xi_k \left[\Theta_3^{(k)}(t_n) + \beta_3(0) g_k \Delta T \right] \right\} + \sum_{K=1}^{N} \xi_k s_{33}^{(k)}(t_n) \tag{2.36}$$

Thus,

$$\Delta\varepsilon_{33} = \frac{\sigma_{33}(t_{n+1}) - \sigma_{33}^{*}}{K + \frac{4}{3} G_3(0) \sum_{k=1}^{N} \xi_k g_k} \tag{2.37}$$

To summarize, under the assumption that material state is known at time t_n, the computational procedure for the determination of pressure and thermally-induced stresses at time t_{n+1} involves the following steps:

1. The pressure, velocity, temperature and fibers orientation fields at t_{n+1} as well as $\Delta T = T(t_{n+1}) - T(t_n)$ are calculated first;

2. The updated fibers orientation tensors are next used to update thermo-mechanical materials properties;

3. Next, the time-temperature shift factor a_T, the pseudo-time step $\Delta\xi$ and ξ_k $(k = 1,2,....,N)$ based on Eqs. (2.11)-(2.12) and the two relations following Eq. (2.30) are all calculated.

4. σ_{33} is next determined while identifying whether the part contains a molten core or not;

5. Eqs. (2.36) and (2.37) are then used to calculate σ_{33}^* and $\Delta\varepsilon_{33}$, respectively;

6. p_h, τ_{11}, τ_{22} and τ_{33} are after that calculated using Eqs. (2.24) and (2.25); and

7. Finally, Eq. (2.13) is used to calculate σ_{11} and σ_{22}.

The calculations presented above are carried out for each layer of each of the elements.

Micro-mechanics Analysis of the Effective Materials Properties

As mentioned earlier, for injection molded thermo-plastics filled with fibers isotropic material models are generally not valid, unless the embedded fibers are randomly oriented. Typically, fibers-induced material anisotropy can have a profound influence on the extent and distribution of shrinkage and warping in the injection molded part. In the section entitled Fiber

Orientation Analysis, it was demonstrated how non-random orientation-distributions of the fibers are induced by the melt-flow kinematics during filling and, to a lesser extent during packing. In this section, the development/utilization of a micromechanical model which can be used to estimate anisotropic elastic and thermal properties of a fiber-filled/thermo-plastic-matrix composite from the properties of the constituent fiber and matrix materials and the known fiber-orientation distribution are discussed [2.49].

Materials processed using injection molding are generally considered to be transversely isotropic, i.e. their properties are equal in two directions (the transverse direction and through-the-thickness direction). The elastic response of such materials is defined by five (temperature-dependent) elastic moduli: the longitudinal Young's modulus E_{11}, the transverse Young's modulus E_{22}, the in-plane shear modulus G_{12}, the out-plane shear modulus G_{23}, and the plane-strain bulk modulus K_{23}. The Poisson ratios ν_{12}, ν_{21} and ν_{23} can then be determined from these elastic moduli using standard relations [e.g. 2.55]. These properties are defined with respect to a local coordinate system in which the 1-direction is taken to coincide with the fiber axis and to be normal to the plane of isotropy (defined by the 2 and 3 directions).

The elastic and thermal properties of fiber filled thermoplastics are typically assessed using a two-step micro-mechanics procedure. First, the properties of the material in which the fibers are fully aligned are assessed. Next, an orientation averaging procedure is applied to include the effect of the fiber-orientation distribution at hand.

Step 1:

Derivations of the properties of materials in which the fibers are fully aligned can be found in many sources [e.g. 2.49]. Thermo-elastic properties of injection-molded fiber-filled polymers are typically specified as longitudinal, α_1, and transverse, α_2, thermal expansion

coefficients and are defined in terms of the thermal expansion coefficients for the fiber and the matrix as [2.50]:

$$\alpha_1 = \frac{E_f \alpha_f \phi + E_m \alpha_m (1-\phi)}{E_f \phi + E_m (1-\phi)} \tag{2.38}$$

and

$$\alpha_2 = (1+\nu_m)\alpha_m (1-\phi) + (1+\nu_f)\alpha_f \phi - \alpha_1 \nu_{12} \tag{2.39}$$

where subscripts *f* and *m* denote fiber and matrix, respectively, ϕ fiber volume fraction, E the Young's modulus and ν the Poisson ratio.

Step 2:

For a transversely isotropic material with the isotropy-plane normal coinciding with the 1-direction, the following form of Hooke's law holds:

$$\begin{pmatrix} \sigma_1 \\ \sigma_2 \\ \sigma_3 \\ \sigma_4 \\ \sigma_5 \\ \sigma_6 \end{pmatrix} = \begin{pmatrix} c_{11}^{(e)} & c_{12}^{(e)} & c_{12}^{(e)} & 0 & 0 & 0 \\ c_{12}^{(e)} & c_{22}^{(e)} & c_{23}^{(e)} & 0 & 0 & 0 \\ c_{12}^{(e)} & c_{23}^{(e)} & c_{22}^{(e)} & 0 & 0 & 0 \\ 0 & 0 & 0 & c_{44}^{(e)} & 0 & 0 \\ 0 & 0 & 0 & 0 & c_{55}^{(e)} & 0 \\ 0 & 0 & 0 & 0 & 0 & c_{66}^{(e)} \end{pmatrix} \begin{pmatrix} \varepsilon_1 \\ \varepsilon_2 \\ \varepsilon_3 \\ \varepsilon_4 \\ \varepsilon_5 \\ \varepsilon_6 \end{pmatrix} \tag{2.40}$$

in which $c_{44}^{(e)} = \frac{1}{2}(c_{22}^{(e)} - c_{23}^{(e)})$, $c_{55}^{(e)} = c_{66}^{(e)}$ and the contracted notation (1=11, 2=22, 3=33, 4=23, 5=13 and 6=12) is used.

The components of the elastic-stiffness matrix are defined in terms of the elastic moduli as [2.51]:

$$c_{11}^{(e)} = \frac{(1-\nu_{23})E_{11}}{1-\nu_{23}-2\nu_{12}\nu_{21}} \tag{2.41}$$

$$c_{12}^{(e)} = \frac{\nu_{23} E_{11}}{1 - \nu_{23} - 2\nu_{12}\nu_{21}} \tag{2.42}$$

$$c_{22}^{(e)} = \frac{E_{22}}{2(1 - \nu_{23} - 2\nu_{12}\nu_{21})} + G_{23} \tag{2.43}$$

$$c_{23}^{(e)} = \frac{E_{22}}{2(1 - \nu_{23} - 2\nu_{12}\nu_{21})} - G_{23} \tag{2.44}$$

$$c_{55}^{(e)} = G_{12} \tag{2.45}$$

Once the properties of short-fiber uni-directionally reinforced polymers are determined, an orientation averaging procedure is used in conjunction with the known fibers orientation tensors to determine the corresponding assembly-average elastic and thermo-elastic material properties as [2.31]:

$$\begin{aligned} \left\langle c_{ijkl}^{(e)} \right\rangle = {} & B_1 a_{ijkl} + B_2(a_{ij}\delta_{kl} + a_{kl}\delta_{ij}) + B_3(a_{ik}\delta_{jl} + a_{il}\delta_{jk} + a_{jl}\delta_{ik} + a_{jk}\delta_{il}) + B_4\delta_{ij}\delta_{kl} \\ & + B_5(\delta_{ik}\delta_{jl} + \delta_{il}\delta_{jk}) \end{aligned} \tag{2.46}$$

and

$$\left\langle \alpha_{ij} \right\rangle = (\alpha_1 - \alpha_2) a_{ij} + \alpha_2 \delta_{ij} \tag{2.47}$$

where $B'_i s$ denote the five invariants of the stiffness tensor of the uni-directionally reinforced polymers [2.31]. It should be noted that the expressions given in Eq. (2.46) and Eq. (2.47) are specific examples of the so called "*effective material-properties averaging schemes*". Within such schemes, a composite material is considered as an aggregate of discrete constituent materials and different averaging schemes are based on different assumptions. For example, the thermal expansion coefficient defined by Eq. (2.47) is obtained under the assumption of a uniform stress and temperature gradient throughout the fiber/matrix aggregate [2.52,2.53].

2.3.4. Post-ejection Shrinkage and Warping Analyses

While the injection-molded material resides in the mold, it is constrained and can not distort. However, after ejection, the part can undergo shrinkage and warping. In the present case, the thermo-plastics insert remains somewhat constrained by its adhesion to the steel stamping. Shrinkage and warping analyses were carried out here using the ABAQUS/Standard finite element method described in Section 2.3.2. The same finite element mesh is utilized as that used in the filling and packing analyses. The in-mold residual stresses and element-based through-the-thickness variations in thermo-mechanical properties of the injected thermoplastic material are exported from Moldflow Plastics Insight to ABAQUS/Standard. The exported in-plane residual stresses and material properties are defined with respect to two (mid-plane) principal directions for the elastic stiffness matrix. The exported residual stresses are considered as initial-stress conditions in the thermo-plastic insert right after part ejection and are used to construct the loading term in the finite element equations. Next, a boundary condition is applied by constraining all six degrees of freedom for a single node of the steel U-shape channel in order to prevent the part from undergoing a rigid body motion. Since the ejected part spends relatively short amount of time at the temperature at which thermoplastics exhibits viscous behavior, only linear thermo-elastic shrinkage and warping FE analysis is performed in the present work.

2.4. Results and Discussion

2.4.1. Structural Response of the All-steel Control Component

As discussed in Sections 2.3.1 and 2.3.2, both the all-steel control and the PMH component are tested in (longitudinal) x-compression, y- and z-bending and torsion around the x-axis. These four deformation modes in the case of the control component are depicted in Figures 2-2(a)-(d).

The load vs. displacement and the torque vs. twist angle results of these analyses for the control component are displayed in Figures 2-3(a)-(b), respectively. These results should be considered as structural requirements for the PMH component. In other words, as the weight of the PMH component is reduced by eliminating the U-shape flanges and the cover plate, and by reducing the plastic-insert wall thickness and the number of ribs, the structural load-bearing capability of the PMH component should not fall below that depicted in Figures 2-3(a)-(b).

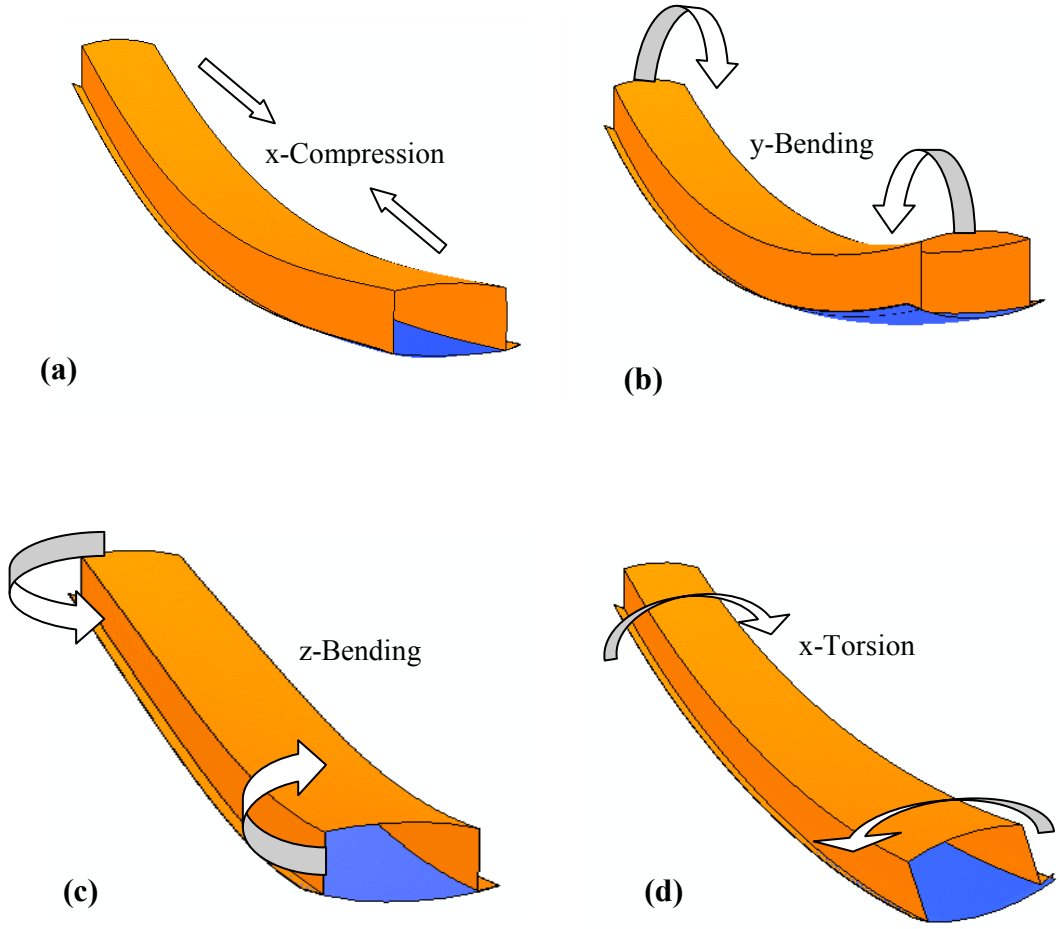

Figure 2-2: Four Loading Modes Used to Establish the Load-bearing Capacity of the All-steel and the PMH Components

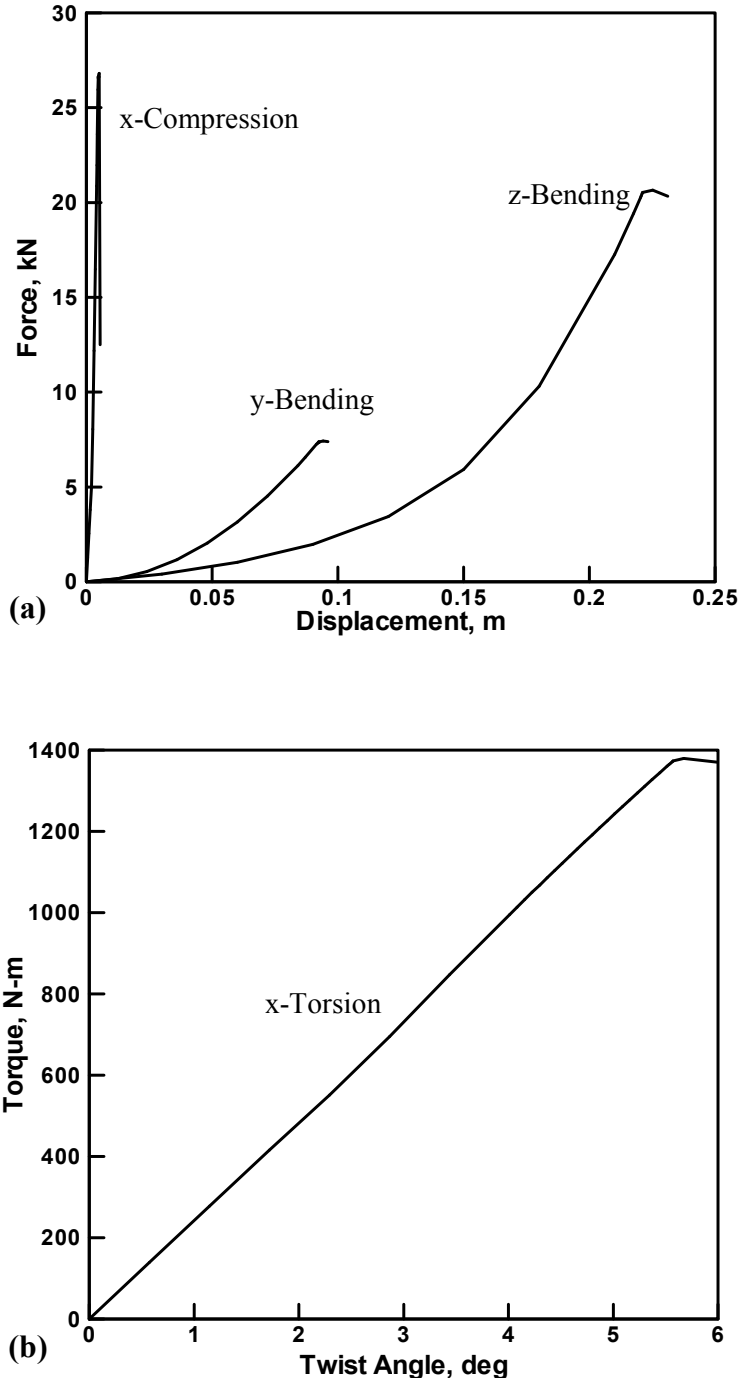

Figure 2-3: Load vs. Displacement and (b) Torque vs. Twist Angle Curves for the All-steel Control Component

2.4.2. Manufacturability of the PMH Component by Injection Molding

To ensure manufacturability of the PMH component by injection molding, the following measures are implemented: (a) A 0.5^{o} draft angle is applied to all plastic-insert walls in the direction of mold motion; (b) The un-flanged U-shape is placed in the fixed part of the mold, the part which contains the sprue; (c) The parting plane is chosen to coincide with the inner bottom surface of the U-shape; and (d) Since no holes are allowed in the U-shape, two side-injection points (gates) to the mold cavity (one attached to the first and the other to the last vertical rib) are considered. The location of one of the gates is indicated in Figure2-4(a), while the other resides at the corresponding location on the other end of the component.

As discussed in Section 2.3.2, the PMH component consists of an un-flanged U-shape, and a plastic insert (which, in turn consists of an overlay and vertical and cross ribs). The following three architectures of the plastic insert: 19/18, 16/15 and 13/12, are considered where the two numbers in each case represent the number of vertical and cross ribs, respectively. An example of the fill-time field plot obtained in the mold-filling analysis is displayed in Figure 2-4(a). The symmetric nature of the data displayed in Figure2-4(a) is an indication of the balanced flow resulting from the symmetric positioning of the gates. The variations of the fill time with the plastic-insert wall thickness, for the three PMH-component architectures, are displayed in Figure 2-5. The leftmost point for each of the three curves depicted in Figure 2-5 correspond to the lowest wall thickness which still ensure complete mold filling.

An example of the in-mold (in-plane) principal major and minor stresses is displayed in Figure 2-4(b)-(c), respectively. The in-mold stresses are exported to ABAQUS/Standard and used as initial conditions in the PMH-component shrinkage and warping analyses.

An example of the field plot showing fiber-orientation distribution (quantified by the angle between the fiber axis and the local element-based 1-direction) is displayed in Figure 2-

4(d). The fiber orientation results are used within a micro-mechanics model to compute through-the-shell-thickness variant thermo-mechanical properties of the injected fiber-filled thermoplastics. These were, in turn, exported to ABAQUS/Standard to define the (injection-molded) material properties for the shrinkage and warping as well as structural-mechanics analyses.

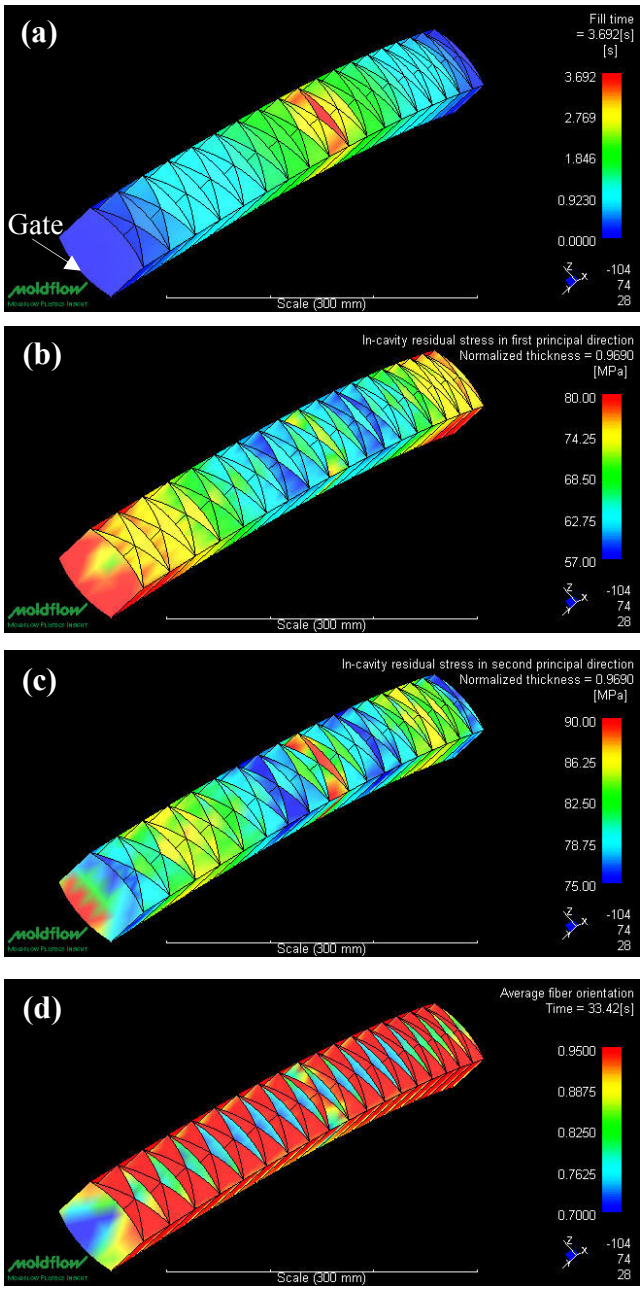

Figure 2-4: An Example of the: (a) Fill-time; (b) First In-plane Principal Stress; (c) Second In-plane Principal Stress; and (d) Fiber Orientation Parameter Field Plots Obtained in the Present Work

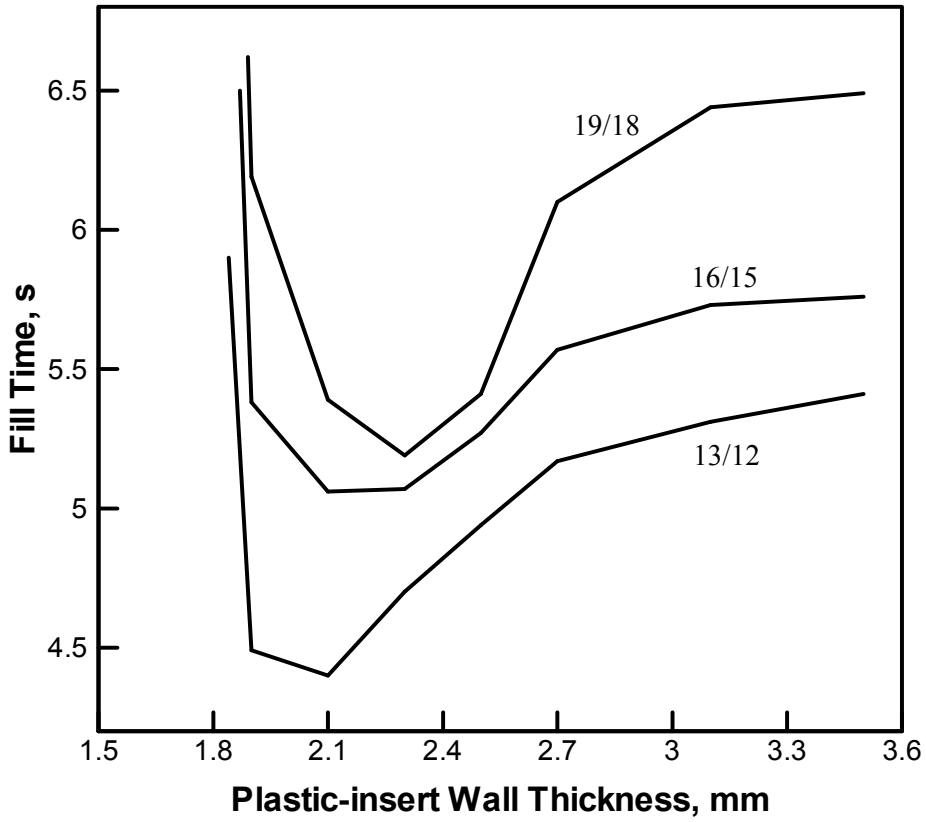

Figure 2-5: The Variations of the Fill Time with the Plastic-insert Wall Thickness, for the Three PMH-component Architectures

2.4.3. Shrinkage and Warping Analyses

Once the PMH component is ejected from the mold, shrinkage and warping thermo-mechanical analyses are carried out using ABAQUS/Standard. The transverse-isotropic thermo-mechanical properties of the fiber-filled polymer are as explained earlier, obtained using a micro-mechanics and the fiber-orientation distribution. Likewise, the initial temperature and stress distributions are set equal to those obtained using Moldflow at the end of packing (i.e. at the instant of part ejection). To prevent rigid-body motion of the PMH component, all six degrees of freedom of one of the U-shape nodes are fixed. Two levels of polymer-to-metal adhesion strength

(2 and 20 MPa) are considered. These are quite conservative estimates [e.g. 2.56] and were selected as the worse-case scenarios. The results of these analyses (not shown for brevity) revealed that:

(a) The maximum displacements of the U-shape (i.e. the maximum external displacements of the PMH component) are less than 0.45mm suggesting that post-ejection shrinkage and warping would not considerably affect dimensional tolerances of the component; and

(b) The maximum strains of the plastic-insert are less than 0.008 suggesting that only minor post-ejection distortions of the plastic-insert architectures take place.

2.4.4. Structural Performance of the PMH Component

The structural-mechanics analyses were carried out to determine the load-bearing capacity of the PMH component. The objective of these analyses was to determine which of the PMH -component architectures is most efficient structurally, i.e. can satisfy the structural requirements defined in Section 2.4.1 at a lowest weight. In the structural-mechanics analyses, several levels of polymer-to-metal adhesion strength in a 2-20MPa range were considered. The weight of each of the three PMH architectures as a function of the plastic-insert wall thickness is depicted in Figures 2-6(a)-(c). It should be recalled that in order to ensure PMH component manufacturability by injection molding, a 0.5^{o} draft angle was employed in the direction of injection-mold motion. Hence, the data displayed in Figures 2-6(a)-(c) pertains to the plastic-insert average wall thickness. For each of the three architectures, a lower-bound wall thickness is depicted in Figures 2-6(a)-(c) below which the mold-filling analysis revealed incomplete mold filling. Also, an upper-bound is indicated which corresponds to the plastic-insert wall thickness at which the PMH and the all steel control component have identical weights. Thus, the upper and lower-bounds of the plastic wall thickness define a thickness window within which both injection

molding and weight reductions of the PMH component are feasible. The subsequent analyses were used to identify a portion of this window within which the weight-based structural efficiency of the PMH component is maximal.

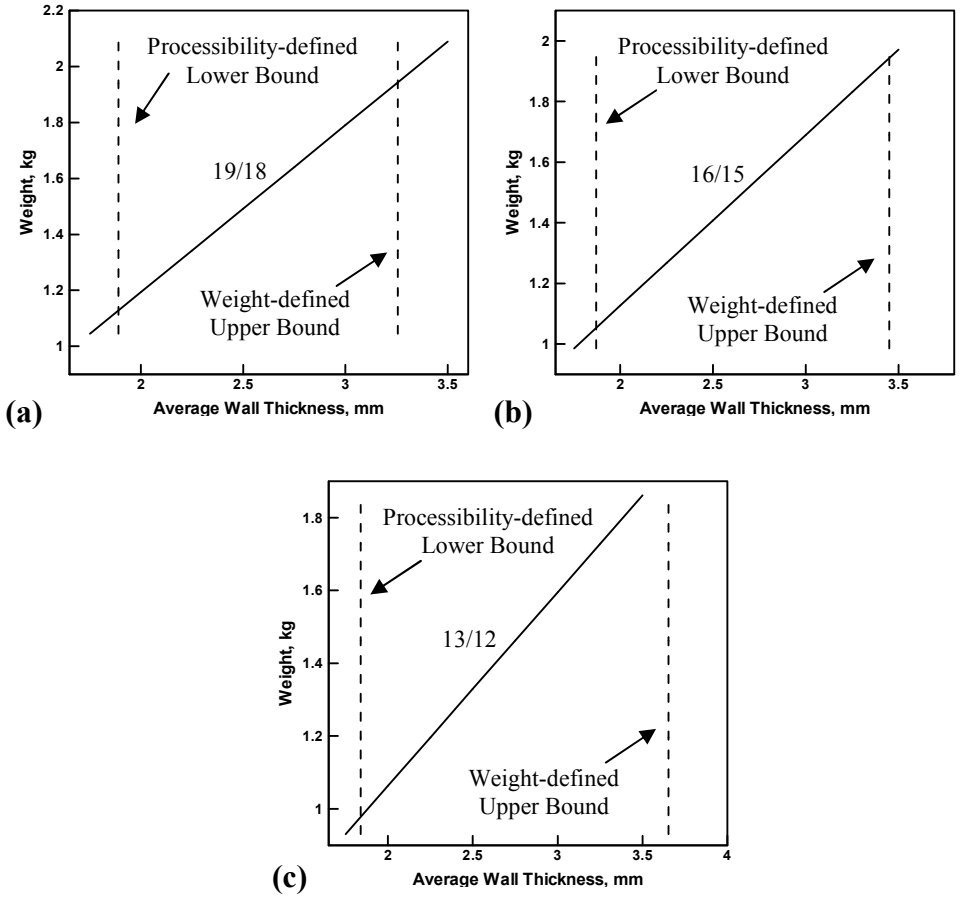

Figure 2-6: Weight vs. Plastic-insert Wall Thickness for the Three PMH-component Architectures Analyzed in the Present Work. Please See Text for Details

As mentioned earlier, the main purpose of the structural-mechanics analysis carried out in the present work is two-fold: (a) To identify, among the three PMH architectures considered here, the one which is structurally most efficient; and (b) To identify the level of polymer-to-metal adhesion strength needed in the PMH component. While a very extensive set of results was obtained in this section, only few representative and summary findings will be presented here due to space constraints. An example of such results is depicted in Figures 2-7(a)-(b) in which, for the cases of *x*-compression and adhesion strength levels of 2 MPa and 20 MPa, a variation in the PMH-component-strength and stiffness with the polymer-insert wall thickness is presented. The lower-bound strength and stiffness levels correspond to those obtained in Section 2.4.1 for the all-steel control component are indicated. Also, the numbers adjacent to the data points represent the three PMH architectures. The results like the ones displayed in Figures 2-7(a)-(b) are used to construct the plots like the one depicted in Figure 2-8. In Figure 2-8, the minimal PMH-to-control components weight ratios (named the "*Normalized PMH Component Weight"*) needed to obtain the required levels of strength or stiffness is plotted as a function of the polymer-to-metal adhesion strength. The results displayed in the Figure 2-8 reveal the following: (a) At adhesion strength levels exceeding ~10 MPa a further increase in the adhesion strength does not yield significant benefits; (b) At adhesion strength levels below ~10 MPa, lower weight reductions are obtained; and (c) Among the three PMH component architectures, the most efficient one is found to be the 16/15 one, suggesting that, perhaps, further weight reductions can be attained using a topology optimization procedure.

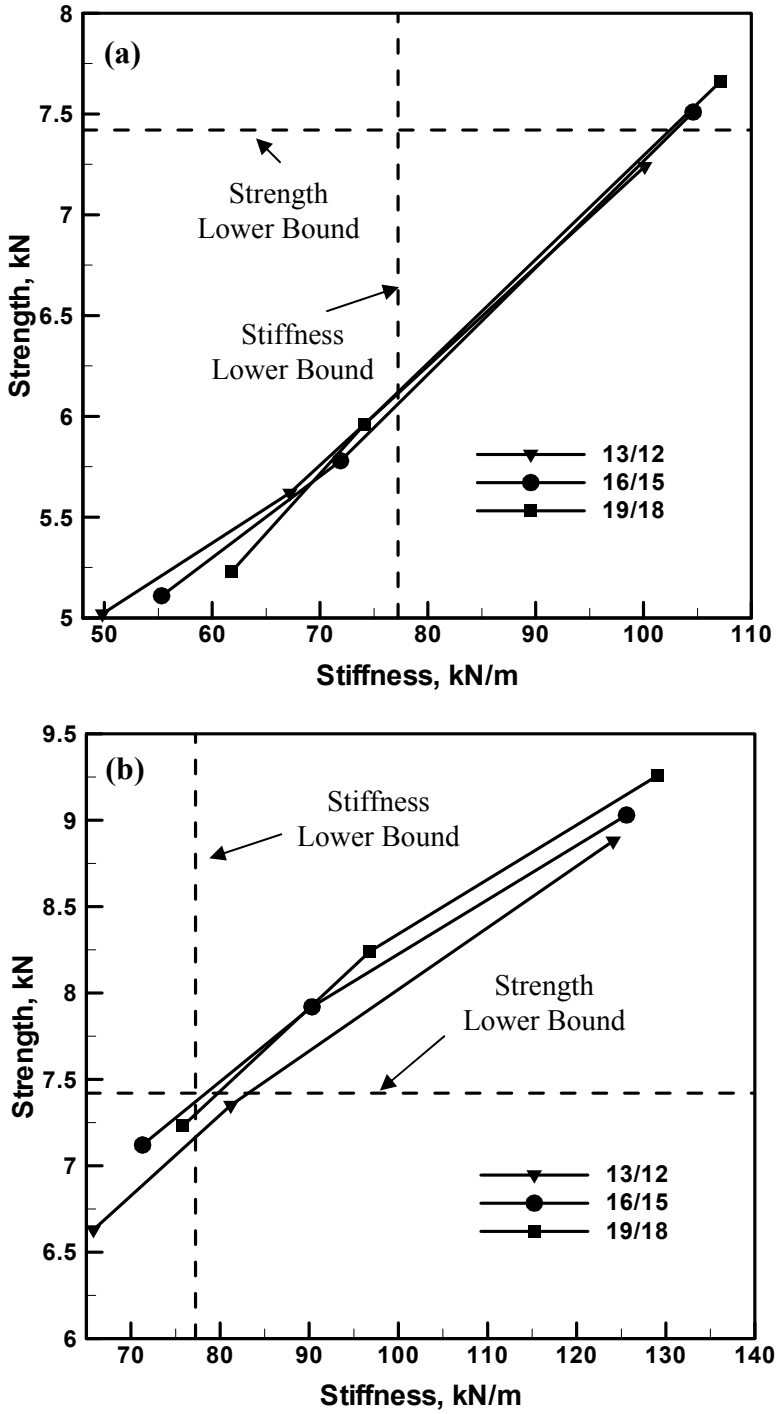

Figure 2-7: Variation of the PMH Component x-compression Stiffness and Strength with Plastic-Insert Wall-thickness at the Polymer-to-metal Adhesion Strength of: (a) 2MPa and (b) 20MPa

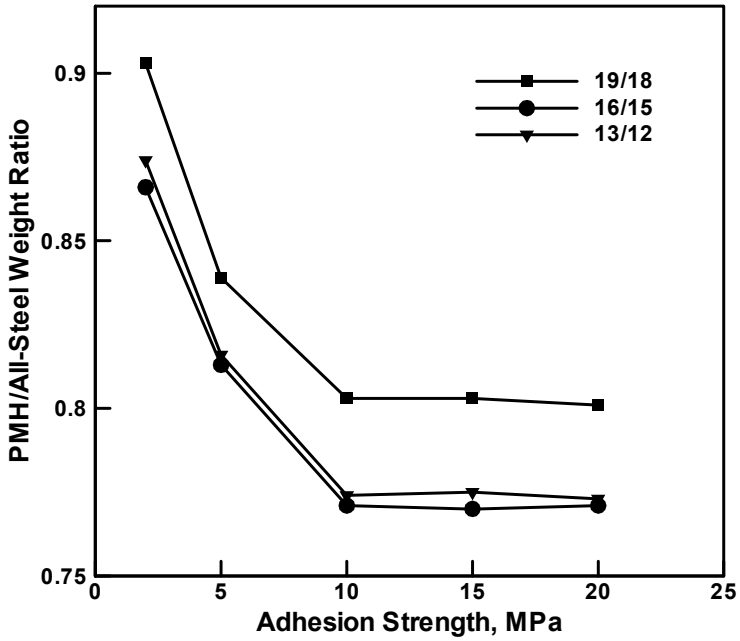

Figure 2-8: Potential Weight Reductions in PMH Component as a Function of the Polymer-to-metal Adhesion Strength

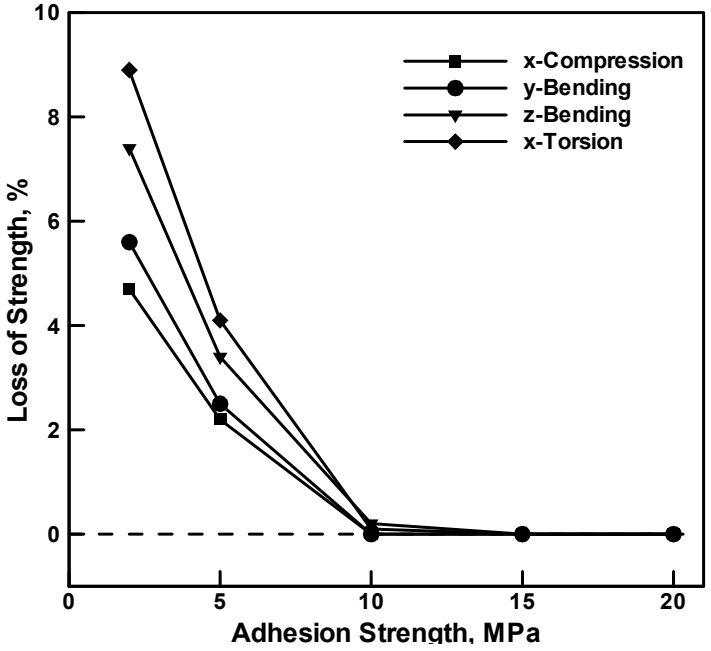

Figure 2-9: Potential Loss of the x-compression PMH-component Strength Due to its Exposure to a Simulated E-coat Curing Treatment

2.4.5. Creep Analysis during E-coat Curing Treatment

As explained earlier, one of the requirements the direct-adhesion PMH component has to satisfy is to survive a typical 190^{o}C/25min E-coat curing treatment that is typically applied to the BIW in the paint shop. It should be noted that previous investigations [e.g. 2.1] have shown that Durethan BKV 130 H2.0 does not undergo any noticeable chemical degradation during degreasing pre-treatment in the paint shop, does not release chemicals which may contaminate paint baths, and does not suffer from any thermal degradation after being exposed to the E-coat curing treatment. To what extent the fiber-filled thermo-plastic insert will creep under these conditions is assessed computationally by carrying out a standard creep analysis. Due to a potentially higher thermal inertia of the adjoining BIW structure, it is recognized that different sections of the PMH component may have different thermal histories in the E-coat curing oven. Consequently, the creep analysis is carried out under a fixed 50^{o}C temperature difference which was imposed between the (length-wise) ends (150^{o}C) and the middle section (200^{o}C) of the component. To assess the extent of a creep-induced loss of PMH-component strength, the structural-mechanics analyses described in Section 2.3.2 were repeated after the component was subjected to the simulated E-coat curing treatment. The results obtained revealed two important findings: (a) No significant creep-induced distortion of the PMH component takes place since the maximum creep strain is less than 0.003 and the maximum relative displacement of the two component ends is less than 0.6mm; and (b) As exemplified by the results displayed in Figure 2-9, no loss of component strength (due to decohesion at the polymer/metal interfaces) takes place when the adhesion strength is >~10MPa. In the case of 2MPa adhesion strength, a strength loss can be as high as 8%.

2.4.6. Feasibility of Direct-adhesion PMH Technology

The computational results obtained in the present work showed that the direct-adhesion PMH technology can be used to reduce the weight (and maintain the structural performance) of load-bearing BIW components provided polymer-to-metal adhesion strength exceeding 10MPa can be achieved. Such levels of adhesion strength are feasible [2.56] but may require preheating of the steel stamping prior to polymer-insert injection molding. In our future work, the problem of steel surface treatment and polymeric-material selection for durable high-strength polymer-to-metal adhesion will be addressed.

2.5. Summary and Conclusions

Based on the results obtained in the present work, the following main summary remarks and conclusions can be drawn:

1. A comprehensive multi-disciplinary computational analysis is developed to assess the potential use of a direct-adhesion polymer metal hybrid (PMH) technology in load-bearing BIW automotive structural components.

2. The analysis encompassed: (a) injection-molding process simulation and component manufacturability assess unit; (b) Determination of processing-induced residual stresses in the component, cooling and solidification induced shrinkage and warping, (c) Determination of the spatial distribution and the extent of material anisotropy; (d) Assessment of the ability of the PMH component to endure a typical. E-coat curing treatment; and (e) the extent of polymer-to-metal adhesion needed to attain a significant component-weight reduction.

3. Using a generic automotive BIW component, as a test structure, the present work showed that the direct-adhesion PMH technology may have a future in load-bearing BIW structural components provided a durable polymer-to-metal adhesion with a strength exceeding 10MPa can be achieved.

2.6. Appendix: Glass-filled Thermo-plastics Material Parameters

The plastic insert used in the present work is assumed to be made of Durethan BKV 130 H2.0 (an elastomer-modified Nylon 6 filled with 30wt.% of glass fibers and heat-age stabilized) produced by Bayer [2.1]. In this section, a brief summary is provided of the rheological, thermal and mechanical models and their parameterizations used for the material at hand.

Viscosity

The shear-rate, temperature and pressure dependent viscosity is modeled using the Cross–WLF model [2.5]:

$$\eta = \frac{\eta_0}{1 + \left(\frac{\eta_0 \dot{\gamma}}{\tau} \right)^{(1-n)}} \tag{A.2.1}$$

where $\eta_0 = D_1 \exp\left[\frac{-A_1 (T - T^*)}{A_2 + (T - T^*)} \right]$, $T^* = D2 + D3^*P$, $A_2 = A_{2\sim} + D_3^*P$ and the material parameters are listed in Table 2-1.

Table 2-1: Cross Model Viscosity Parameters for Durethan BKV 130 H2.0

Parameter	Unit	Value
n	N/A	0.3869
τ	Pa	137,000
D_1	Pa-s	$1.05 \cdot 10^{19}$
D_2	K	323.15
D_3	K/Pa	0.0
A_1	N/A	45.266
$A_{2\sim}$	K	51.6
T_{trans}	K	479.0

Thermal properties

The specific heat capacity, C_p and the thermal conductivity, *k*, are assigned single constant values and set equal in the melt and the solid thermo-plastics. The values for C_p and *k* as well as for the glass transition temperature at zero pressure are listed in Table 2-2.

Table 2-2: Thermal Properties for Durethan BKV 130 H2.0

Parameter	Symbol	Unit	Value
Specific Heat	C_p	J/kg·K	1,909
Glass Transition Temperature	T_{trans}	K	479.0
Thermal Conductivity	*k*	W/m·C	0.14

P-V-T Material Data

The quasi-equilibrium *P-V-T* behavior is modeled using a two-domain Tait *P-V-T* model as [2.5]:

$$V(T,p) = V_0(T)\left[1 - C\ln(1 + \frac{p}{B(T)})\right] + V_t(T,p) \qquad \text{(A.2.2)}$$

where V_0 is the specific volume at zero gauge pressure, C =0.0894 and B accounts for pressure sensitivity of the material. In the upper temperature region ($T > T_t$) the following relations are used: $V_0 = b_{1m} + b_{2m}\ (T - b_5)$; $B(T) = b_{3m}\ exp[-b_{4m}\ (T-b_5)]$; and $V_t(T,P) = 0$. In the lower temperature region ($T < T_t$) the following relations are used: $V_0 = b_{1s} + b_{2s}\ (T - b_5)$; $B(T) = b_{3s}\ exp[-b_{4s}\ (T-b_5)]$; and $V_t(T,P) = b_7\ exp((b_8(T-b_5)) - (b_9P))$.

The pressure dependence of the transition temperature T_t is described as: $T_t\ (P) = b_5 + b_6P$. Material parameters b_{1s}-b_{4s}, b_{1m}-b_{4m}, b_5, b_6, b_7, b_8, and b_9 are listed in Table 2-3.

Table 2-3: P-V-T Properties for Durethan BKV 130 H2.0

Parameter	Unit	Value
Melt Density	g/cm^3	1.1694
Solid Density	g/cm^3	1.3476
b_5	K	484.05
b_6	K/Pa	$4.94 \cdot 10^{-8}$
b_{1m}	m^3/kg	$81.79 \cdot 10^{-5}$
b_{2m}	$m^3/kg\text{-}K$	$4.7 \cdot 10^{-7}$
b_{3m}	Pa	$2.04403 \cdot 10^{8}$
b_{4m}	1/K	$407.4 \cdot 10^{-5}$
b_{1s}	m^3/kg	$78.61 \cdot 10^{-5}$
b_{2s}	$m^3/kg\text{-}K$	$2.37 \cdot 10^{-7}$
b_{3s}	Pa	$2.96551 \cdot 10^{+8}$
b_{4s}	1/K	$267.3 \cdot 10^{-5}$
b_7	m^3/kg	$1.95 \cdot 10^{-5}$
b_8	1/K	$32.3 \cdot 10^{-3}$
b_9	1/Pa	$1.38 \cdot 10^{-8}$

Mechanical and Thermo-mechanical Properties

The (planar-isotropic) mechanical and thermo-mechanical properties for the material under consideration (under a condition in which all the glass fibers are aligned in the first principal (i.e. melt flow) direction are listed in Table 2-4. It should be noted, however, that the actual (planar-isotropic) mechanical and thermo-mechanical properties and their through-the-shell-thickness variations used in the structural-mechanics analysis were obtained as a result of the mold filling/packing analysis.

Table 2-4: Planar-isotropic Mechanical and Thermo-mechanical Properties for Durethan BKV 130 H2.0 With Glass Fibers Fully Aligned in Direction 1

	Parameter	Symbol	Unit	Value
Mechanical Property	Elastic Modulus, 1st Principal Direction	E_1	MPa	9,087.49
	Elastic Modulus, 2nd Principal Direction	E_2	MPa	5,467.3
	Poissons Ratio	v_{12}	N/A	0.4039
	Poissons Ratio	v_{23}	N/A	0.4533
	Shear Modulus	G_{12}	MPa	2,344.79
Thermo-Mechanical Property	Coefficient of Thermal Expansion, 1st Principal Direction	α_1	1/C	$2.662 \cdot 10^{-5}$
	Coefficient of Thermal Expansion, 2nd Principal Direction	α_2	1/C	$5.658 \cdot 10^{-5}$

Relaxation Spectrum Data

The relaxation spectrum data which were used to construct the visco-elastic materials response are given in Table 2-5.

Table 2-5: Relaxation Spectrum Data for Durethan BKV 130 H2.0

k	α_k	g_k
1	$1.000 \cdot 10^{-6}$	$9.8884 \cdot 10^{-2}$
2	$8.3260 \cdot 10^{-4}$	$4.2487 \cdot 10^{-1}$
3	$6.9310 \cdot 10^{-1}$	$4.7554 \cdot 10^{-1}$
4	$5.7708 \cdot 10^{2}$	$7.2610 \cdot 10^{-5}$
5	$4.8040 \cdot 10^{5}$	$5.0610 \cdot 10^{-4}$
6	$4.0000 \cdot 10^{8}$	$1.3450 \cdot 10^{-4}$

Creep Properties

Creep data for the material at hand were obtained by applying a linear regression analysis to the experimental data reported in Ref. [2.54] and a power-law creep model:

$$\dot{\varepsilon}_{ij}^{d} = A_0 e^{-Q/RT} (\sigma^{eq})^{n-1} \tau_{ij} \qquad \text{(A.2.3)}$$

Where superscript eq denotes an equivalent quantity, R is the universal gas constant and A_0 $=3.88 \cdot 10^{-6} s^{-1}$, Q=40.1kJ/mole and n=0.4369.

2.7. References

2.1 O. J. Zoellner and J. A. Evans, "*Plastic-Metal Hybrid. A New Development in the Injection Molding Technology,*" ANTEC 2002 Annual Technical Conference, Sanfrancisco, CA, 2002, 1-4.

2.2 *Plastic-Metal Hybrid Material*, http://www.hbmedia.net/polymotive/polymotive/2003/01/articles/frontend1.shtml

2.3 D. Recktenwald, "*Advanced Adhesives Foster Hybrid Structures*," Machine Design, 77, 21, November 2005, 124-126.

2.4 ABAQUS, *Version 6.6*, *User Documentation*, ABAQUS Inc., Rising Sun Mills, Providence, RI, 2006.

2.5 Moldflow Plastics Insight, *Version 6.0*, *User Documentation*, Moldflow Corporation, Framingham, MA, 2006.

2.6 M. R. Kamal and S. Kenig, "*The Injection Molding of Thermoplastics Part I. Theoretical Model*," Polym. Eng. Sci., 12, 1972, 294-301.

2.7 C. A. Hieber and S. F. Shen, "*A Finite-element/Finite-difference Simulation of the Injection-molding Filling Process,*" J. Non-Newtonian Fluid Mech., 7, 1980, 1-32.

2.8 H. H. Chiang, C. A. Hieber and K. K. Wang, "*A Unified Simulation of the Filling and Postfilling Stages in Injection Molding Part 1. Formulation,*" Polym. Eng. Sci., 31, 1991, 116-124.

2.9 P. Kennedy, "*Flow Analysis of Injection Molds*," Hanser, Munich, 1995.

2.10 M. J. Crochet, F. Dupret and V. Verleye, *Flow and Rheology in Polymer Composites Manufacturing*, S. G. Advani (Ed.), Elsevier, Amsterdam, 1994, Ch. 11.

2.11 C. V. L. Kietzmann, J. P. Van Der Walt and Y. S. Morsi, "*A Free-front tracking algorithm for a control-volume Hele-Shaw method,*" Int. J. Num. Meth. Eng., 41, 1998, 253-269.

2.12 M. Gupta and K. K. Wang, "*Fibers orientation and Mechanical Properties of Short-fiber-reinforced Injection-molded Composites: Simulation and Experimental Results,*" Polym. Compos., 14, 1993, 367-381.

2.13 S. F. Walsh, "*Shrinkage and Warping Prediction for Injection Molded Components,*" J. Reinforced Plas. Compos., 12, 1993, 769-777.

2.14 R. C. Givler, M. J. Crochet and R. B. Pipes, "*Numerical Predictions of Fibers orientation in Dilute Suspensions,*" J. Compos. Mater., 17, 1983, 330-343.

2.15 G. G. Lipscomb II, M. M. Denn, D. U. Hur and D. V. Boger, "*The Flow of Fiber Suspensions in Complex Geometry,*" J. Non-Newtonian Fluid Mech., 26, 1988, 297-325.

2.16 J. Rosenberg, M. M. Denn and R. Keunings, "*Simulation of Non-recirculating Flows of Dilute Fiber Suspensions,*" J. Non-Newtonian Fluid Mech., 37, 1990, 317-345.

2.17 R. Zheng, *Boundary Element Methods for some Problems in Fluid Mechanics and Rheology*, Ph.D. Thesis, University of Sydney, 1991.

2.18 N. Phan-Thien, R. Zheng and A. L. Graham, "*The Flow of a Model Suspension Fluid Past a Sphere*," J. Statist. Phys., 62, 1991, 1173-1195.

2.19 N. Phan-Thien and A. L. Graham, "*A New Constitutive Model for Fiber Suspensions: Flow Past a Sphere*," J. Rheol., 30, 1991, 44-57.

2.20 M. C. Altan, S. I. GuÈceri and R. B. Pipes, "*Anisotropic Channel Flow of Fiber Suspensions*," J. Non-Newtonian Fluid Mech., 14, 1992, 65-83.

2.21 C.L. Tucker III, "*Flow Regimes for Fiber Suspensions in Narrow Gaps*," J. Non-Newtonian Fluid Mech., 39, 1991, 239-268.

2.22 D. Guell and M. Lovalenti, "*An examination of assumptions underlying the state of the art in injection molding modeling*," SPE ANTEC, 95 1, 1995, 728-732.

2.23 M. Rezayat and T. E. Burton, "*A Boundary-integral Formulation for Complex Three-Dimensional Geometries*," Int. J. Num. Meth. Eng., 29, 1990, 263-273.

2.24 A. Couniot, L. Dheur and F. Dupret, "*Numerical Simulation of Injection Molding: Nonisothermal Filling of Complex Thin Parts, Including Abrupt Changes of Thickness or Bifurcations of Midsurface*," in: M. Cross, J.F.T. Pittman, R.D. Wood (Eds.), Proc. IMA Conf. on Mathematical Modelling for Materials Processing, Bristol, Clarendon Press, Oxford, 1991.

2.25 W. F. Zoetelief, G. W. M. Peters and H. E. H. Meijer, "*Numerical Simulation of the Multi-component Injection Molding Process*," Int. Polym. Process, 12, 1997, 216-277.

2.26 F. P. Folgar and C. L. Tucker, "*Orientation Behaviour of Fibers in Concentrated Suspensions,*" J. Reinforced Plastics and Compos., 3, 1984, 98-119.

2.27 X. J. Fan, N. Phan-Thien and R. Zheng, "*A Direct Simulation of Fiber Suspensions,*" J. Non-Newtonian Fluid Mech., 74, 1998, 113-136.

2.28 N. Phan-Thien and R. Zheng, *Macroscopic Modelling of the Evolution of Fibers orientation During Flow,* in: T.D. Papathanasiou, D.C. Guell (Eds.), *Flow-Induced Alignment in Composite Materials,* Woodhead, Cambridge UK, 1997, Ch. 3.

2.29 G. B. Jeffery, "*The Motion of Ellipsoidal Particles Immersed in Viscous Fluid,*" Proc. Roy. Soc. Lond. A., 102, 1922, 161-179.

2.30 Y. Yamane, Y. Kaneda and M. Doi, "*Numerical Simulation of Semi-dilute Suspensions of Rodlike Particles in Shear Flow,*" J. Non-Newtonian Fluid Mech., 54, 1994, 405-421.

2.31 S.G. Advani and C.L. Tucker III, "*The Use of Tensors to Describe and Predict Fibers orientation in Short Fiber Composites,*" J. Rheol., 31, 1987, 751-784.

2.32 M. Doi, "*Molecular Dynamics and Rheological Properties of Concentrated Solutions of Rodlike Polymers in Isotropic and Liquid Crystalline Phases*," J. Polym. Sci. Polym. Phys. Ed., 19, 1981, 229-243.

2.33 E. J. Hinch and L. G. Leal, "*Constitutive Equations in Suspension Mechanics. Part 1. Approximate Forms for a Suspension of Rigid Particles Affected by Brownian Rotations*," J. Fluid Mech., 76, 1976, 187-208.

2.34 V. Verleye and F. Dupret, "*Prediction of Fibers orientation in Complex Injection Molded Parts*," Proc. ASME Winter Annual Meeting, 28 November-3 December 1993, New Orleans, LA.

2.35 J. S. Cintra and Jr. C. L. Tucker III, "*Orthotropic Closure Approximations for Flow-induced Fibers orientation*," J. Rheol., 39, 1995, 1095-1122.

2.36 F. P. T. Baaijens, "*Calculation of Residual Stress in Injection Molded Products,*" Rheol. Acta, 30, 1991, 284-299.

2.37 K. M. B. Jansen, "*Residual Stresses in Quenched and Injection Molded Products,*" Int. Polym. Proces., 9, 1994, 82-89.

2.38 F. Boitout, J. F. Agassant and M. Vincent, "*Elastic Calculation of Residual Stresses in Injection Molding: Influence of Mold Deformation and Pressure in the Liquid,*" Int. Polym. Proces., 10, 1995, 237-242.

2.39 G. Titomanlio and K. M. B. Jansen, "*In-mold Shrinkage and Stress Prediction in Injection Molding,*" Polym. Eng. Sci., 36, 1996, 2041-2049.

2.40 W. F. Zoetelief, L. F. A. Douven and A. J. Ingen-Housz, "*Residual Thermal Stresses in Injection Molded Products,*" Polym. Eng. Sci., 36, 1996, 1886-1896.

2.41 L. Caspers, VIp, *An Integral Approach to the Simulation of Injection Molding,* Ph.D. Thesis, Eindhoven University of Technology, 1996.

2.42 W. C. Bushko and V. K. Stokes, "*Solidification of Thermoviscoelastic Melts Part 1. Formulation of Model Problem,*" Polym. Eng. Sci., 35, 1995, 351-364.

2.43 W. C. Bushko and V. K. Stokes, "*Solidification of Thermoviscoelastic Melts Part 2. Effects of Processing Conditions on Shrinkage and Residual Stresses,*" Polym. Eng. Sci., 35, 1996, 365-383.

2.44 W. C. Bushko and V. K. Stokes, "*Solidification of Thermoviscoelastic Melts. Part 3. Effects of Mold Surface Temperature Differences on Warping and Residual Stresses,*" Polym. Eng. Sci., 36, 1996, 322-335.

2.45 W. C. Bushko and V. K. Stokes, "*Solidification of Thermoviscoelastic Melts. Part 4. Effects of Boundary Conditions on Shrinkage and Residual Stresses,*" Polym. Eng. Sci., 36, 1996, 658-675.

2.46 R. B. Bird, R. C. Armstrong and O. Hassager, "*Dynamics of Polymeric Liquids: Fluid Mechanics*," 2nd ed., 1, Wiley, New York, 1987.

2.47 R. I. Tanner, *Engineering Rheology*, 2nd ed., Oxford Press, London, 1988.

2.48 J. D. Ferry, *Viscoelastic Properties of Polymers*, 3rd ed., Wiley, New York, 1980.

2.49 T. D. Papathanasiou and D. C. Guell (Eds.), *Flow-induced Alignment in Composite Materials*, Woodhead, Cambridge, UK, 1997.

2.50 R. A. Schapery, "*Thermal Expansion Coefficients of Composite Materials Based on Energy Principles*," J. Compos. Mater., 2, 1968, 380-404.

2.51 J. C. Halpin and J. L. Kardos, "*The Halpin-Tsai Equations: A Review*," Polym. Eng. Sci., 16, 1976, 344-352.

2.52 C. W. Camacho, C. L. Tucker III, S. Yalvac and R. L. McGee, "*Stiffness and Thermal Expansion Predictions for Hybrid Short Fiber Composites*," Polym. Compos., 11, 1990, 229-239.

2.53 R. F. Eduljee, R. L. McCullough and J. W. Gillespie, Jr, "*The Influence of Aggregated and Dispersed Textures on the Elastic Properties of Discontinuous-fiber Composites*," Comp. Sci. Tech., 50, 1994, 381-391.

2.54 W. J. Liou and C. I. Tseng, "*Creep Behavior of Nylon-6 Thermoplastic Composites*," Polymer Composites, 8, 1997, 492-499.

2.55 R. Zheng, P. Kennedy, N. Phan-Thien, and X. J. Fan, "*Thermoviscoelastic simulation of Thermally and Pressure-induced Stresses in Injection Molding for the Prediction of Shrinkage and Warpage for Fiber-reinforced Thermoplastics,*" Journal of Non-Newtonian Fluid Mechanics, 84, 1999, 159-190.

2.56 K. Ramani and B. Moriarty, "*Thermoplastic Bonding to Metals Via Injection Molding for Macro-Composite Manufacture*," Polymer Engineering and Science, 38, 5, 1998, 870-877.

CHAPTER 3

AN OVERVIEW OF THE POLYMER-TO-METAL DIRECT-ADHESION HYBRID TECHNOLOGIES FOR LOAD-BEARING AUTOMOTIVE COMPONENTS

3.1. Abstract

The work published in the open literature dealing with various polymer metal hybrid (PMH) approaches used to promote direct (adhesive-free) adhesion between metal and injection-molded thermoplastics is reviewed and critiqued. Different approaches are categorized as: (a) micro-scale polymer-to-metal mechanical interlocking; (b) in-coil or stamped-part pre-coating for enhanced adhesion; and (c) chemical modifications of the injection-molded thermoplastics for enhanced polymer-to-metal adhesion. For each of these approaches their suitability for use in load-bearing body-in-white (BIW) components is discussed. In particular, the compatibility of these approaches with the BIW manufacturing process chain (i.e. (pre-coated) metal component stamping, BIW construction via different joining technologies, BIW pre-treated and painting operations) is presented. It has been found that while considerable amount of research has been done in the PMH direct-adhesion area, many aspects of these technologies which are critical from the standpoint of their use in the BIW structural applications have not been addressed (or addressed properly). Among the PMH technologies identified, the one based on micro-scale mechanical interlocking between the injection-molded thermoplastic polymer and stamped-metal structural component appears to be most promising.

3.2. Introduction

Traditionally, metals and plastics have been fierce competitors in automotive manufacturing practice. In sharp contrast, the two classes of materials are integrated within the polymer metal hybrid (PMH) technologies in a singular component/sub-assembly. The driving

philosophy behind the PMH technologies has been to (utilizing the systems approach) combine the structural and non-structural needs of many components into a singular, fully-optimized sub-assembly, in order to deliver a customer specific solution. An underlying integrated construction enables greater system benefit than the typical merging of two proximal parts.

The first example of a successful implementation of this technological innovation in practice was reported at the end of 1996, when the front end of the Audi A6 (made by Ecia, Audincourt/France) was produced as a hybrid structure, combining sheet steel with elastomer-modified polyamide PA6 - GF30 (type: Durethan BKV 130 from Bayer). A key feature of hybrid structures is that the materials employed complement each other so that the resulting hybrid material can offer structural performance which is not present in either of the two constituent materials independently.

Currently, polymer metal hybrids (PMHs) are replacing all-steel structures in automotive front-end modules at an accelerated rate. Moreover, new PMH technologies are being introduced as alternatives to the over-molding method first established by Bayer. In addition to their aforementioned use in the front-end modules, PMHs are currently being used in instrument-panel and bumper cross-beams, door modules, and tailgates applications as well as in non-automotive applications, ranging from appliance housings to bicycle frames.

The main PMH technologies currently being employed in the automotive industry can be grouped into three major categories: (a) Injection over-molding technologies; (b) Metal over-molding technologies combined with secondary joining operations; and (c) Adhesively-bonded PMHs. In the following, a brief description is provided for each of these groups of PMH manufacturing technologies.

In the injection over-molding process (originally developed and patented by Bayer [3.1]), metal inserts with flared through-holes are stamped, put in an injection mold and over-molded

with 30% short glass-fiber reinforced nylon 6 to create a cross-ribbed supporting structure. The metal and nylon are joined by nylon melt penetrating through-holes to form rivets that provide mechanical interlocks. Because an injection molding press opens in one direction, cross-rib geometry was initially limited to just two dimensions. Recently, multi-directional ribbing was produced using this process by adding side motion to the tooling. Significant boosts in the load-bearing capability of U-shaped steel stampings were observed. A simplified solid model of the PMH component produced by injection over-molding is displayed in Figure 3-1.

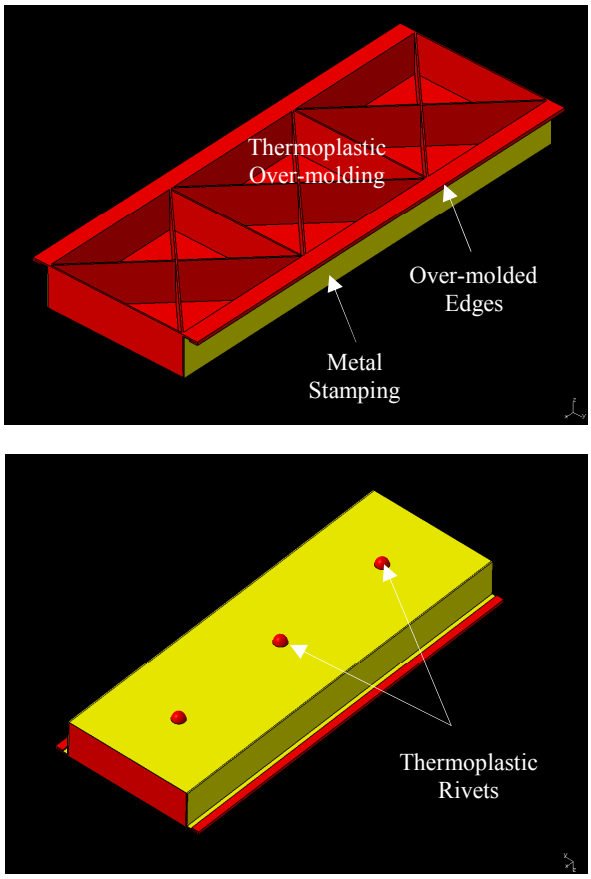

Figure 3-1: Two Views of a Simplified Prototypical Injection Over-molding PMH BIW Load-bearing Component

In the metal over-molding PMH technology, which was developed and patented by Rhodia [3.2] and adopted for the front-end module used on a 2004 light truck in South America, a steel stamping is placed in an injection mold, where its underside is coated with a thin layer of reinforced nylon. In a secondary operation, the plastics-coated surface of the metal insert is ultrasonically welded to an injection molded nylon sub-component. In this process, a closed-section structure with continuous bond lines is produced which offers a high load-bearing capability. The hollow core of the part permits functional integration like cable housings and air or water channels. Additionally, gas or water injection-molding can be employed to produce a stiffer, thinner coating for enhanced load-bearing capabilities and increased functional integration. A lower-cost variation of the metal over-molding PMH technology is Rhodia's so called Plastic-Metal Assembling process. A U-shaped steel stamping with punched holes and a nylon injection molded component, which contains columns or heat stakes that can lock into the stamping holes, are produced separately. The two sub-components are subsequently joined by riveting the ends of the plastic columns using ultrasonic welding or heat staking. A simplified (exploded) solid model of the PMH component produced by metal over-molding is displayed in Figure 3-2.

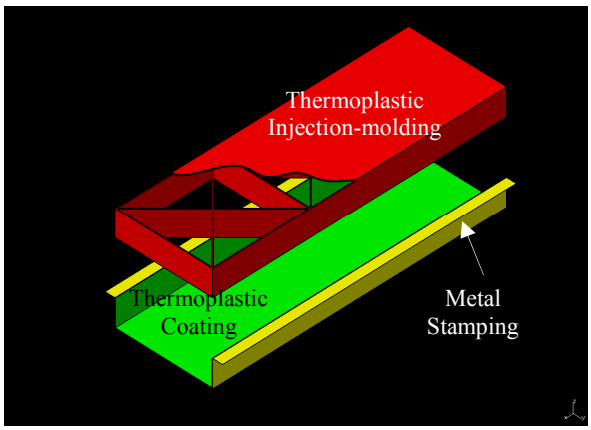

Figure 3-2: A Simplified Prototypical BIW Load-bearing Components Manufactured Using the Metal Over-molding PMH Technology

Adhesively-bonded PMHs were developed and patented by Dow Automotive [3.3] and were introduced in 2003 in prototype form for a Volkswagen front-end module. In this PMH technology, glass-fiber reinforced poly-propylene is joined to a metal stamping using Dow's proprietary low-energy surface adhesive (LESA). The acrylic-epoxy adhesive does not require pre-treating of the low surface-energy poly-propylene and is applied by high-speed robots. Adhesive bonding creates continuous bond lines, minimizes stress concentrations and acts as a buffer which absorbs contact stresses between the metal and polymer sub-components. The latest LESA grade, Grade 74030, provides a good compromise between stiffness and toughness as well as improved adhesion and faster cure. To help maintain alignment of the sub-components during curing of the adhesive, snap features are designed into the sub-components. Adhesively-bonded PMHs enable the creation of closed-section structures which offer high load-bearing capabilities and the possibility for enhanced functionality of hybrid parts (e.g. direct mounting of air bags in instrument-panel beams or incorporation of air or water circulation inside door modules). A simplified (exploded) solid model of the PMH component produced by adhesion bonding is displayed in Figure 3-3.

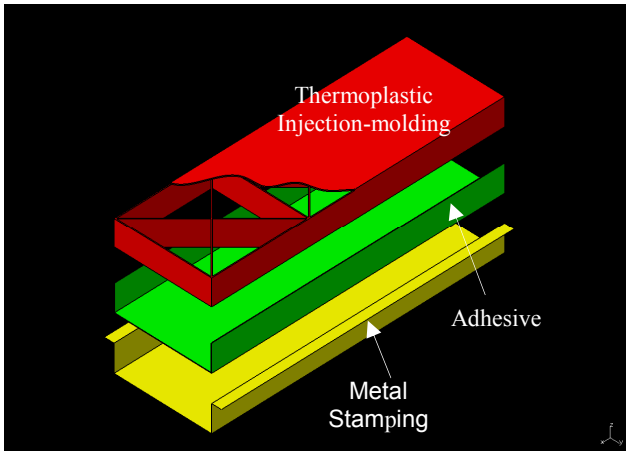

Figure 3-3: A Simplified Prototypical BIW Load-bearing Component Manufactured Using the Adhesive-bonding Technology

While the aforementioned PMH technologies have demonstrated their potential and are being widely used in various non-structural and load-bearing automotive components, they nevertheless display some significant shortcomings. For example, in many applications, to maintain the structural integrity of the part, hole punching needed for polymer-to-metal interlocking in the injection over-molding process may not be allowed. Similarly, stamped-edges over-molding may be restricted. In the case of adhesively-bonded PMHs, the adhesive cost, long curing time and the ability of the adhesive to withstand aggressive chemical and thermal environments encountered in the paint-shop during BIW pre-treatment and E-coat curing may be an issue. Consequently, alternative lower-cost PMH technologies for structural load-bearing BIW component which are compatible with the BIW manufacturing process chain are being sought. One of such technologies, which is the subject of the present work, is the so called direct-adhesion PMH technology in which the joining between the metal and thermo-plastic sub-components is attained through direct-adhesion of injection-molded thermo-plastics to the metal without the use of interlocking rivets/over-molded edges or structural adhesives [3.4]. There are several potential advantages offered by this technology over the ones discussed above: (a) Polymer-to-metal adhesion strengths (ca. 35MPa [3.4]) comparable with those obtained in the case of thermo-setting adhesives are feasible but only at a small fraction of the manufacturing cycle time; (b) The shorter cycle time and the lack of use of an adhesive allow for more economical PMH-component production; (c) Unlike the adhesive-bonding technology, joining is not limited to simple and non-interfering contact surfaces; (d) Reduced possibility for entrapping air in undercuts of a complex surface; (e) No holes for the formation of interlocking rivets are required and, hence, structural integrity of the part is not compromised; and (f) Overall reduction in the constraints placed upon the design complexity of the PMH component. A simplified solid

model of the PMH component produced by polymer-to-metal direct-adhesion is displayed in Figure 3-4.

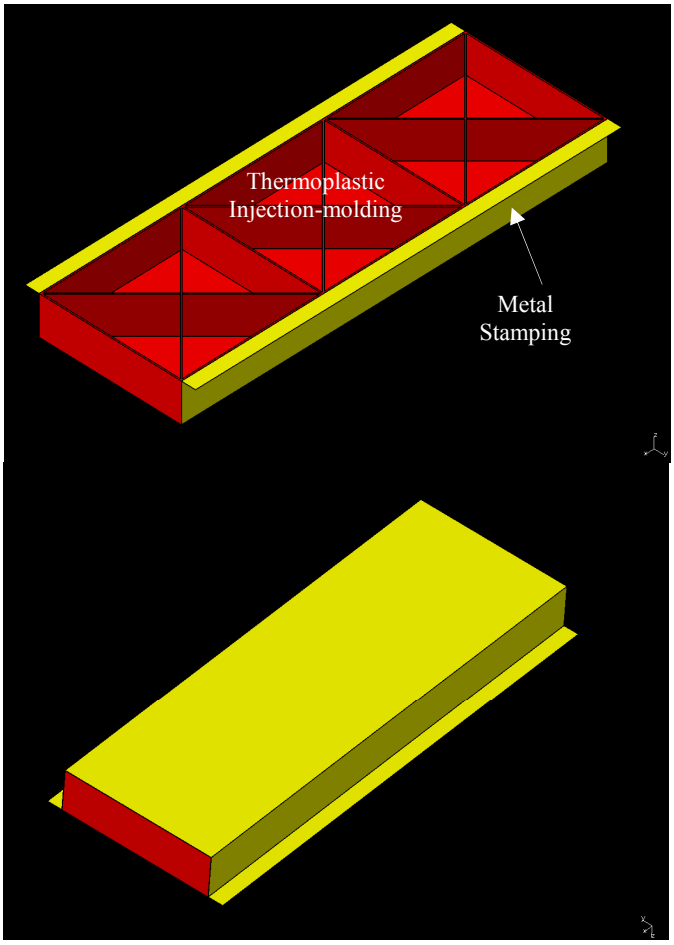

Figure 3-4: Two Views of a Simplified Prototypical Direct-adhesion PMH BIW Load-bearing Component

In the present chapter, an overview of the state-of-the-art polymer-to-metal direct-adhesion approaches is provided. Since no well accepted classification of these approaches can be found in the open literature, an attempt is made here to classify different efforts. In addition, a critical assessment for each of these approaches is provided with respect to their suitability for use in BIW load-bearing automotive applications and with respect to their compatibility with the BIW manufacturing process chain.

Based on the work published in the open literature, all polymer-to-metal direct-adhesion efforts can be classified as: (a) micro-scale mechanical interlocking approaches [e.g. 3.5-3.7]; (b) in-coil or stamped-part metal priming with silane or other adhesion promoters [e.g. 3.8,3.9]; (c) chemical modifications of the injection-molding thermo-plastic material for enhanced adhesion to metal [e.g. 3.10,3.11]; and (d) other approaches aimed at enhancing polymer-to-metal direct-adhesion [e.g. 3.12-3.15]. In the following four sections a detailed overview of each of the approaches is provided. It should be noted that the key objective of the present work is to critically assess the potential of direct-adhesion PMH technologies in BIW load-bearing applications. Hence, significant body of work dealing with polymer-to-metal adhesion developed within the electronic packaging field is not presented, since the approaches used employed very thin (10-100μm) metal and/or polymeric structures and were not compatible with the BIW manufacturing process chain.

As stated earlier, the objective of the present work is to assess the potential of different polymer-to-metal direct-adhesion approaches for BIW load-bearing components both from the component function standpoint and the stand point of compatibility with the BIW manufacturing process chain. In traditional all-metal BIW manufacturing practice, components are stamped in the press shop, joined (typically by welding) in body shop and the constructed BIW pre-treated and painted in paint shop. In the case of injection over-molding BIW PMH components, stamped metal subcomponents are "*hybridized*" with thermoplastic ribbing structure in injection molding shop. Hence to assess the suitability of various direct-adhesion PMH technologies for BIW load-bearing applications, their compatibility with various processes taking place in press shop, injection molding shop, body shop and paint shop will be considered. Specific aspects of the BIW manufacturing process chain capability are discussed in the following three sections.

It should be noted that the present chapter is part of the ongoing research which deals with a total life-cycle approach to the selection of materials, and manufacturing/processing technologies in the light-weight engineering of the automotive BIW structural applications.

Within such an approach, all the key BIW manufacturing process steps are considered. These steps include, metal-subcomponent manufacturing by stamping in the process shop, PMH component or thermo plastic subcomponent manufacturing in the injection-molding shop, BIW construction by various joining processes in the body shop, BIW pre-treatment and painting in the paint shop, component performance and durability in service, and end-of-life considerations including disassembly, shredding, materials segregation, separation and recycling.

3.3. Micro-scale Polymer-to-metal Mechanical Interlocking

3.3.1. Technology Overview

Within the micro-scale polymer-to-metal mechanical-interlocking approach, the required level of adhesion strength is attained via the infiltration of (and, upon cooling, the interlocking with) the micron-size roughness features of the metal substrate with thermoplastic melt. The mechanism of plastic-to-metal adhesion should be distinguished from the standard *insert over-molding* process which relies on the shrink-fit phenomenon and special under-cut geometrical features for good polymer-to-metal adherence.

The most comprehensive investigation of the micro-scale polymer-to-metal mechanical interlocking available in the open literature was conducted by Ramani and co-workers [3.5-3.7]. In the work of Ramani and co-workers [3.5-3.7], adhesion between low-carbon-steel or 6061 aluminum metal substrates and injection-molded poly-carbonate was investigated. Metal surfaces were prepared using the following sequence of steps: grit blasting with ca. 0.5μm average-size Al_2O_3 particles, scrubbing with a nylon brush and ultra-sonic cleaning in isopropyl alcohol. Metal substrates were then oven heated (in some cases), placed in the mold and over-molded with poly-

carbonate. A full factorial study was carried out to determine the effect of the following four parameters:

(a) metal-substrate temperature; (b) injection-machine screw linear velocity; (c) thickness of the injection over-molded poly-carbonate; and (d) injection-molding packing/holding pressure on the polymer-to-metal adhesion strength. A comprehensive set of mechanical tests and Scanning Electron Microscopy (SEM) studies were conducted in order to reveal details of the adhesive mechanism and correlate the mechanical testing results with the morphology of the polymer/metal interface. The results obtained in the work of Ramani and co-workers [3.5-3.7] can be summarized as follows: (a) between the four process parameters investigated, the metal-substrate temperature has, by far, the largest effect on to the polymer-to-metal adhesion strength; (b) No adhesion between polymer and metal is obtained in the cases in which the metal substrates were not heated. In these cases, it was found that polymeric melt freezes upon its contact with the metal-substrate during injection molding. In other words, polymeric melt does not manage to infiltrate the micron-size roughness features of the metal substrate and fails to mechanically interlock to it; (c) Under the optimal process conditions (metal substrate pre-heating temperature ~210ºC, screw linear velocity ~11cm/s and the over-molding thickness ~0.5mm), an adhesion strength as high as 40 MPa is obtained; and (d) A standard deviation of ±10MPa for the adhesion strength is typically found for a given set of process parameters. This finding suggests that a tight control of the manufacturing process is needed to ensure a high-level of product consistency.

Ramani and co-workers [3.5-3.7] also address the issue of residual-stress development during injection over-molding. Their studies clearly revealed that the fast cooling (which is preferred from the stand point of the reduction of the cycle time) leads to the development of higher residual stresses compromising the integrity and durability of the polymer/metal adhesion bonding. This observation was made both in the case of amorphous (e.g. poly-ether-imide, PEI)

and semi-crystalline (e.g. poly-ether-ether-ketone, PEEK) polymers. While the residual stresses are the result of differential properties between polymers and metal and, hence, cannot be avoided, the work of Ramani and co-workers [3.5-3.7] clearly showed that the extent of residual stresses can be greatly reduced by proper design of the injection over-molding process.

3.3.2. Potential Application in BIW Structure

As discussed earlier, each of the polymer-to-metal direct-adhesion approaches has to meet a number of process/product related requirements before it can be considered as a potentially viable technology for use in BIW load-bearing PMH applications. Among such specific requirements, the most important ones appear to be: (a) metal-stamping surface preparation needed to ensure the necessary level of polymer-to-metal adhesion strength. A comprehensive finite-element analysis of the structural response of the direct-adhesion PMH test structures [3.4] revealed that a minimum adhesion strength of ca. 10MPa is needed in order to achieve a sufficient level of load transfer between the metal stamping and the injection-molded plastic insert; (b) compatibility with the standard injection over-molding PMH manufacturing process; (c) ability of the PMH component to withstand the BIW pre-treatment and painting processes; and (d) durability of the polymer-to-metal adhesion bond, particularly under fatigue and high-humidity conditions. In the remainder of this section, the ability of the micro-scale polymer-to-metal mechanical interlocking approach to meet these requirements is presented. Similar format will be used in the subsequent sections.

Metal-surface Preparation Requirements

Efficient micro-scale mechanical interlocking entails the presence of micron-size rough (preferably oil-free and clean) metal surfaces with a sufficiently high (minimum ca. 200^{o}C) temperature. The achievement of the needed level of surface roughness does not appear to be a major challenge and can be ensured through proper surface texturing of the stamping dies. The

constraint that the metal-stamping surface is oil-free and clean is somewhat negotiable, since the adhesion mechanism is mechanical and not chemical, in character. Heating of the metal stamping prior to their placement into the injection-molding mold appears to be a serious shortcoming for the micro-scale mechanical interlocking process. Among the potential undesirable consequences of metal-stamping pre-heating are: (a) metal-stamping warping/distortions; (b) metallurgical changes leading to a loss of strength; (c) a higher injection-tooling material cost; (d) additional step(metal-stamping pre-heating) has to be introduced prior to the injection-molding step, etc. Most of these problems appear to be surmountable through the integration of an induction-heating coil in the injection-molding mold. Induction heating is non-contact heating (relies on the induction of Eddie currents, which are resistively dissipated within the metal substrate in the form of joule heating) and fast (seconds to minutes, thus more compatible with the injection-molding process time).

Compatibility with the Injection-molding Process

If induction heating can be integrated in the injection-molding process, micro-scale mechanical interlocking could become a viable polymer-to-metal direct-adhesion PMH-technology alternative.

Compatibility with Paint-shop Treatment

While the work of Ramani and co-workers [3.5-3.7] focused on poly-carbonate, (maximum service temperature ~120-150^{o}C), other thermoplastic (e.g. nylon) with a higher maximum service temperature (needed to ensure survivability of the PMH component during BIW pre-treatment and painting operations, in particular during the ca. 190^{o}C/30minute E-coat baking treatment) should be amendable to the mechanical-interlocking mechanism. Some problems regarding complete infiltration of micron-size roughness features may arise when

thermo-plastics with glass-fiber reinforcements are used. The extent of these problems can not be assessed, at the present time, due to absence of the relevant experimental data.

Durability of Polymer-to-metal Bond

Since the polymer-to-metal adhesion, in the present case, relies on purely mechanical (interlocking) phenomena, the adhesion bonding is not expected to be severely compromised by prolonged exposure to humidity or elevated temperatures. As far as the fatigue resistance of the polymer/metal hybrid interface is concerned, the situation is less clear. On a more macroscopic scale level, polymer-to-metal mechanical interlocking appears to yield a continuous (stress-concentration free) bonding which is not typically very prone to fatigue failure. Conversely, on a finer length-scale, major stress concentration effects are expected giving rise to a type of bonding which is normally quite sensitive to cyclic loading. It appears, hence, that there is perhaps an ideal surface/roughness topology which would maximize durability of the plastic-to-metal mechanical-interlocking bonding with respect to mechanical and thermal fatigue conditions. This is similar to the use of particular optimal roughness to promote retention of oil during stamping and different optimal roughness to promote paint adhesion.

Summary Remarks

Based on the simple engineering analysis presented above, it appears that with the proposed integration of induction heating into the injection-molding mold, the micro-scale polymer-to-metal mechanical interlocking approach can become a viable PMH direct-adhesion polymer BIW load-bearing components manufacturing technology.

3.4. Primed-Metal Surfaces for Enhanced Polymer Adhesion

3.4.1. Technology Overview

Within this approach, an enhanced adhesion between metal-stamping and injection-over molded thermo-plastics is attained by priming the metal surface prior to the injection-molding process. The most frequently used primer is silane which owing its amino and vinyl functional groups acts as a "*coupling agents*" which promotes adhesion between inorganic and organic materials. For silane to act as an adhesion promoter, its organo-reactive moieties should be in contact with polymer and metal which can be achieved by coating the metal substrate with silane just prior to injection molding of the polymer [20]. It is generally believed that the silane coupling reactions take place in the following sequence: (a) hydrolysis of the alkoxy group which results in the production of hydrogen; (b) formation of the hydrogen bonds at the polymer/metal interface; (c) interfacial condensation of the functional groups; and lastly (e) interfacial chemical reactions with the polymer and metal resulting in the formation of interfacial bonds [3.21].

One of the most comprehensive studies of primed-metal/injection over-molded thermoplastic adhesion was carried out by Shah [3.8]. In the work of Shah [3.8], bonding occurring at the interface between injection molded poly-(vinyl chloride), PVC, and cold-rolled mild steel substrates (pre-coated with thin coatings of amino-silane) were investigated using a variety of analytical and spectroscopic analysis (e.g. X-ray photoelectron spectroscopy, XPS, and Fourier transform infrared spectroscopy, FTIR). The silane coating was formed by adsorption of γ-amino-propyl-triethoxy-silane, γ-APS, or N-(2-amino-ethyl-3-amino-propyl) trimethoxy-silane, γ-AEAPS, from 2% aqueous solutions onto polished steel substrates. PVC was injection molded onto the silane pre-coated steel substrates and annealed at temperatures up to 170^{o}C for times as long as 30 minutes. After extensive experimental investigation of the steel/silane/PVC interfaces, the bonding mechanism was rationalized as follows: Amine hydrochloride complexes appear to

form by protonation of amino groups of the silanes with HCl that was liberated from PVC during the onset of thermal dehydro-chlorination. Furthermore, quaternization or nucleophilic substitution of labile pendent allylic chloride groups by amino groups on the silanes takes place, thus grafting PVC onto the aminosilanes. It was determined that PVC having β-chloroallyl groupings along its chains showed better adhesion with steel pre-coated with amino-silanes and that generation of allylic chloride groups in PVC chains was the rate limiting step in the reaction between PVC and aminosilane. Interdiffusion of the polymer phase and the silane phase was found to be also critical in obtaining good adhesion.

Additionally, a fairly comprehensive investigation of the effect of metal-stamping surface priming on the polymer-to-metal direct-adhesion has been carried out by Sasaki et al. [3.9]. In the work of Sasaki et al. [3.9], adhesion of injection over-molded poly-amide 6 (PA6) thermoplastic polymer and stainless steel plates pre-coated with triazine trithiol polymer (TTP) was investigated. Adhesion strength between PA6 and the pre-coated stainless steel plates was found to be relatively large (~6 MPa). To rationalize the nature of the adhesion mechanisms, X-ray photoelectron spectroscopy (XPS) and nuclear magnetic resonance (NMR) were used. In addition, simplified (model) systems consisting of stainless steel plates, TTP coating (chemically oxidized with amines and nylon oligomer) were investigated. The XPS results revealed the formation of iron and/or chromium mercaptide at the stainless steel/TTP interfaces. Furthermore, formation of chemical bonds via nucleophilic substitution of terminal amino groups in PA6 was observed at the PA6/TTP interfaces.

3.4.2. Potential Application in BIW Structure

In assessing suitability of the primed-metal enhanced polymer-to-metal adhesion approaches for BIW load-bearing components, the same four suitability aspects as the one discussed in Section 3.3.2 will be considered.

Metal-surface Preparation Requirements

The experimental work presented in Refs. [3.8,3.9] clearly revealed that pre-treatment of the metal-stamping surfaces (e.g. SiC-grit grinding followed by water based 1μm-Al2O3 slurry polishing and thorough rinsing) is imperative to attaining good polymer-to-metal adhesion. This is a major disadvantage for this direct-adhesion PMH approach, since it is generally desirable to postpone any metal-stamping pre-treatment until paint shop. Leaving the drawing compound/oil on metal stampings until paint shop does not only simplify the manufacturing process (i.e. reduces the number of processes) but also prevents in-shipping damage of the metal-stampings.

Compatibility with the Injection-molding Process

Primed-metal surfaces enhanced polymer-to-metal adhesion approach appears not to be fully compatible with the standard injection over-molding process. The concern is that the in-mold primer (even just partial) curing requires several minutes while a typical injection-molding cycle lasts only few seconds. This shortcoming can be somewhat overcome by heating the mold and/or increasing the injection-molding temperature and using the heat carried by the mold and the polymer to attain (at least partial) curing of the primer. The final stage of primer curing can then be achieved during the E-coat curing treatment in paint shop.

Compatibility with Paint-shop Treatment

Since the maximum service temperature for PVC (by Shah [3.8]) is typically below 100ºC, this material is not compatible with the paint-shop component-survivability requirements and, thus, is not suitable for the BIW structural PMH components. On the contrary, the PA6 used by Sasaki et al [3.9] can withstand temperature way in excess of 200ºC (particularly if reinforced with glass fibers). While the ability of the polymer-to-metal bonding to withstand high temperature was not directly investigated by either Shah [3.8] or Sasaki et al. [3.9], the covalent nature of the chemical bonding observed suggests that the bonding strength should not be

seriously compromised by the BIW chemical (e.g. degreasing) pre-treatment or the thermal (e.g. the E-coat curing) treatment. Mechanical loading subjected to the BIW structure during pre-treatment (power-spray washing) and/or painting (polymer/metal thermal-expansion mismatch stresses), on the other hand, can compromise the integrity of the PMH components if the primer has not cured sufficiently.

Durability of Polymer-to-metal Bond

In the work of Shah [3.8] and Sasaki et al [3.9], the durability of PMH components based on direct-adhesion between polymers and metal in the presence of a primer was not directly investigated. Hence, no definite statements can be made here regarding the suitability of this approach to the BIW load-bearing components with respect to long-term reliability of such components and their exposure to prolonged high-humidity high-temperature environment and in severe cyclic loading. Nevertheless, since interfacial bonding is primarily covalent in nature, one can speculate that the PMH components processed in this way would not seriously suffer from low durability.

Summary Remarks

In summary, the primed-metal surface enhanced polymer-to-metal adhesion approach entails a new process step (a metal-stamping surface cleaning and pre-treatment step) in press shop or in injection-molding shop, which are not very economically attractive options in the overall BIW manufacturing production scheme. Once such additional process step is introduced, the remaining requirements associated with the primed-metal surface options are not significant and can be readily met with the current BIW manufacturing practice. It should be noted, however, that the last conclusion was based more on a sound engineering judgment than on the basis of experimental data which could fully support such contention.

3.5. Chemical Modifications of Polymer for Enhanced Adhesion

Within this approach, various chemical modifications are made either with the polymerized thermoplastics or within its monomeric resin in order to enhance polymer-to-metal direct-adhesion. While this approach is frequently used by the major automotive OEMs and their first and second-tier suppliers, very little information is available in the open literature.

3.5.1. Technology Overview

Among the studies pertaining to chemical modifications of thermoplastic materials, the work shared by Salladay and Stevens [3.10] with the present authors is perhaps most comprehensive. The work of Salladay and Stevens [3.10] involves chemical modification of poly-amide with self-ordering poly-(ester-amide) block co-polymer (a hot-melt adhesive-like material). The material displays an exceptionally high adhesion strength (>20MPa) even in the cases in which metal surfaces were covered with drawing compound/oil prior to injection over-molding.

An additional approach which falls into the categories of chemical-modification based polymer-to-metal adhesion-enhancement involves chemical modification of the thermoplastic resin, rather than chemical modification of the polymerized thermoplastic material. This approach is most comprehensively applied in the work of Berry and Namkanisorn [3.11], who examined the effect of various concentrations of styrl silane added directly into styrene (monomers) resin onto the ability of the resin to directly bond to aluminum upon polymerization. Experimental investigations of the aluminum/poly-styrene interfaces included interfacial fracture toughness and adhesion strength measurement and X-ray photo-electron spectroscopy (XPS) characterizations of the fracture surfaces, in test coupons processed under different metal substrate pre-treatment conditions, silane concentrations and polymerization process conditions. The results obtained clearly revealed that metal-surface preparation via either chromic-sulfuric acid etching or phosphoric acid anodization is highly critical for attaining good polymer-to-metal adhesion. The

concentration of styrl silane in styrene resin was found to affect the thickness of the polymer-to-metal bonding interface and, in turn, the bond strength. Surface treatment of metal substrate ensures that a sufficient density of binding sites is available to provide a grafted or tethered polymer interfacial layer. When the thickness of such layer (controlled by the concentration of silane in the styrene monomers) becomes comparable with the average distance between the polymer-chain entanglement points, the polymer-to-metal adhesion strength reaches its maximum value. The concentration of silane in the resin is also found to affect the bond-strength sensitivity to the presence of moisture. On the anodized aluminum surface, a significant contribution to polymer-to-metal adhesion is found to be associated with micro-scale mechanical interlocking.

3.5.2. Potential Application in BIW Structure

Metal-surface Preparation Requirements

The two investigations reviewed in this section revealed that in the case of chemically-modified polymeric materials, no significant metal-surface pre-treatments are needed to obtain the desired level of polymer-to-metal adhesion strength. This is highly encouraging, since no introduction of additional process steps in press/injection-molding shop appears necessary. In sharp contrast, in the case of chemically modified resin, the experimental results clearly revealed that metal-surface preparation via either chromic-sulfuric acid etching or phosphoric acid anodization is highly critical for attaining good polymer-to-metal adhesion. These types of surface pre-treatments, due to their chemical nature, are highly undesirable.

Compatibility with the Injection-molding Process

Both of the investigations reviewed, show significant incompatibility with the standard injection over-molding practice. In the work of Salladay and Stevens [3.10], pronounced adhesion of the thermoplastic melt to the mold is generally observed, hampering the part ejection process.

While this problem can be generally rectified through the use of mold-release agents and relatively large draft angles, neither of these approaches is very attractive. Since the thermoplastic melt is generally reinforced with glass fibers, mold-release agent is typically removed from the mold surfaces by the injected polymeric melt after only few cycles and would have to be re-applied. As far as an increased draft angle is concerned, this condition coupled with a relatively-large minimum injection-moldable wall thickness of the fiber-reinforced thermo-plastics, typically leads to injection moldings with an excessive weight.

As far as the chemical modification of the monomer resin approach is concerned, this approach entails minutes-long in-mold curing times to ensure at least partial curing of the resin. Such times are not compatible with the seconds-long injection-molding cycle times

Compatibility with Paint-shop Treatment

To obtain the needed level of polymer-to-metal adhesion, Salladay and Stevens [3.10] modified PA6 (a thermoplastic material with relatively high maximum service temperature) with a low temperature hot melt thermoplastic adhesive material. This seriously compromised the thermal stability of the resulting material, questioning if the associated PMH components could survive the E-coat curing treatment. Based on the unpublished work of Salladay and Stevens [3.10], the PMH components based on chemically modeled PA6 could withstand chemical and mechanical loadings encountered during BIW pre-treatment and painting.

As far as the PMH approach based on chemical modifications of the resin is concerned serious incompatibility with the pre-treatment/paint-shop processes can be observed. Insufficiently cured resin could not generally withstand neither a chemical attack from BIW degreases nor mechanical loads (during spray washing). In other words, serious compromise in the structural integrity of the PMH component can occur prior to painting. As far as the E-coat

curing treatment is concerned, it is likely that this treatment would help further cure the resin that endanger structural integrity of the PMH component.

Durability of Polymer-to-metal Bond

Neither of the two studies reviewed above examined long-term durability of the associated PMH components. What is clear, nevertheless, is that the nature of the polymer-to-metal bonding is non-covalent and to some extent non-chemical. Such bonding is typically sensitive to a prolonged exposure to moisture/high-temperature and fatigue.

Summary Remarks

Based on the analysis presented above, neither chemically modified polymeric material nor chemically-modified resin based PMH approaches appear to be viable technologies for the BIW load-bearing automotive components.

3.6. Other Polymer-to-metal Direct-adhesion Approaches

3.6.1. Technology Overview

The polymer-to-metal direct-adhesion approaches reviewed in Sections 3.3-3.5 were primarily concerned with the potential use of these approaches in PMH (non-necessarily BIW load-bearing) components. The review of the literature revealed other efforts which were not focused on the PMH technology but address the issue of adhesion enhancement and, hence, can have some bearings onto the identification of the optimal direct-adhesion PMH technology for the BIW structural components. Among such approaches is commercial pre-coating of in-coil sheet metal with organic coatings with proven high adhesion to specific injection-molding thermoplastics. For example, reactive poly-vinylidene-fluoride (PVDF) is known to display good adhesion to both (surface pre-treated) metals and commodity thermoplastics (poly-amide, poly-propylene, etc.) [3.14]. These materials are currently being used as substitution for the stainless

steel and exotic alloys commonly specified for fluid contact components such as piping, process vessels, pumps, valves, etc. The present authors were not able to locate any public-domain reports dealing with the use of sheet-metal pre-coated with high-adhesion organic coatings in automotive BIW applications. On the other hand, there are numerous examples of the use of polymer pre-laminated sheet-metal [e.g. 3.15]. The can-making research revealed that polymer-coating survivability during the manufacturing operations involved in can making may become a serious issue. The most demanding operation in can making is ironing because of the high pressures involved as well as the necessary generation of new surfaces. While ironing is not generally involved in the production of BIW components, the problem of coating survivability during stamping operations has to be resolved before the organically pre-coated sheet-metal approach can be considered as a viable BIW load-bearing PMH component manufacturing technology.

Another potential approach to direct-adhesion PMH technologies is the use of (color) base-coats which are known to adhere well to metal substrates and which were chemically-modified to enhance their adhesion to the injection molded thermo-plastics. Reports of the investigation of such coats are typically found in studies dealing with painting of the injection molded parts [e.g. 3.12,3.13]. Consequently, adhesion to metal parts is not typically considered. Nevertheless, if generally good adhesion of such base coats to metals is not compromised by their chemical modification, the approach could be of interest to the direct-adhesion PMH technology. In Refs. [3.12,3.13], the development of a new base coat with improved adhesion to the thermo-plastic olefin (TPO) part is presented. The new coat was obtained by chemically modifying the standard base-coat formulations with olefinic diol. Using various tests (e.g. a cross-hatch tape adhesion-strength test, a test to determine adhesion-strength sensitivity to prolonged humidity/temperature exposure, a fuel-exposure resistance test, a thermal shock test, etc.), good adhesion was found to exist between the modified base-coat and the TPO part without the use of

adhesion promoter (e.g. chlorinated poly-olefins) or surface treatments (e.g. flame, plasma, etc.). It was also stated that improved transfer efficiency of the applied base-coat with the TPO part can be obtained via making the TPO part electrically conductive and using electrostatics. TPO usually consists of poly-propylene, poly-ethylene, block copolymer poly-propylene, ethylene propylene diol monomer (EPDM) rubber and talc. In automotive engineering, TPO is typically used for bumper fascia and body side moldings. TPO is not normally used in the BIW structural components since its melting temperature is too low, i.e. in a 160-180^{o}C range. The modified base coat was sprayed on the TPO surface and the coated TPO part baked at a temperature of 130^{o}C for 30 minutes to ensure full curing of the base coat. The results obtained show that the base coat modified with olefinic diol can adhere well to an injection-molded TPO part without the use of an adhesion promoter and/or surface treatment. However, the coat curing time (30 minutes) is way too long in comparison to the time taken for a typical injection molding cycle (several seconds). In addition, the melting temperature for standard TPO grades is unacceptably low for a BIW frame component. Fortunately, some TPO grades (e.g. Thermorun TT-811, Un-filled, Mitsubishi Chemical) have the melting temperature as high as 260^{o}C and may be expected to survive the E-coat baking treatment in paint shop. The outstanding problem associated with prolonged in-mold curing of the base coat can perhaps be overcome via the integration of induction heating in the mold, as discussed earlier. If this is the case, PMH components can be produced by spraying the base coat (just prior to injection molding) over the interior surface of a U-shape BIW metal stamping and injection over-molding in-mold induction-heated stamping to ensure sufficient in-mold curing of the coat.

3.6.2. Potential Application in BIW Structure

In general, the public-domain information for the PMH technologies listed under "*Other polymer-to-metal direct-adhesion approaches*" is incomplete and no definite judgment (beyond

the statements made in Section 3.6.1) can be made regarding their potential application in BIW structural components.

3.7. The Effect of Water/Moisture on the Polymer-to-Metal Adhesion

In the previous sections, the effect of water (either absorbed by the polymer, or attracted to the polymer/metal interface) on the durability of BIW load-bearing direct-adhesion PMH components was mentioned very briefly. The reason for this was that the relevant research published in the open literature did not address, in sufficient detail, this otherwise very important problem. Nevertheless, because of the great importance of this problem in properly assessing the suitability of different direct-adhesion PMH technologies in BIW load-bearing automotive components, a brief discussion pertaining to the effect of water/moisture is presented in this section. When assessing durability of the BIW load-bearing PMH components, the effect of moisture on both the polymer and metal has to be considered. Moisture absorbed in polymeric materials can lead to a wide range of effects, some of which are reversible (i.e. can be erased on removal of water) while the others are irreversible (i.e. result in permanent changes in the performance of polymers). Plasticization (i.e. loss in stiffness and strength associated with a depression in the glass transition temperature) and swelling are examples of the reversible processes. Among the irreversible changes in polymeric materials are: (a) hydrolysis effects which are enhanced under tensile stress in alkaline water; (b) polymer oxidation; (c) microstructural damage induced by the formation of micro-cavities; etc. It is generally believed that absorbed water cannot be totally removed from polar polymers by thermal annealing since the residual water is strongly bonded to polar sites.

Water can also lower the polymer-to-metal adhesion strength. It is generally observed that there is a critical water concentration/humidity level below which environmental attack on the polymer/metal interface does not occur. It is also generally believed that water-induced loss of

adhesion is a result of chemical reactions between adsorbed water molecules and the OH groups of the polymer, which cause the breaking of inter-chain hydrogen bonds and displacing adsorbed OH groups from the surface of the substrate. Other mechanisms have also been proposed. For example, Gledhill and Kinloch [3.16] suggested that for adhesion joints, where only secondary forces are the mechanism of adhesion, the intrinsic stability of the polymer/metal-substrate interface in the presence of an absorbed liquid may be evaluated from a consideration of the thermodynamic work of adhesion. Typically, the work of adhesion for a dry adhesive/substrate has a positive value, indicating thermodynamic stability of the interface. However, the introduction of water may induce a negative value of the work of adhesion, which indicates that the interface is unstable and the polymer may be easily displaced from the substrate by water. It has been observed by many researchers [3.17-3.19] that the presence of water/moisture can hydrolyze interfacial metal oxide and result in the formation of a hydrated oxide layer between the underlying metal substrate and the polymer, which is mechanically weak and is the likely interfacial failure location. To summarize, the aforementioned findings suggest that a loss of adhesion strength can result from either the effect of water on the interfacial layer of polymer and/or interfacial layer of metal.

In general, one can expect that the non-mechanical bonding between metal and thermoplastic polymer is affected by the polar character of the polymer. In polar plastics, bonding is not fully covalent and the time-averaged electron charge density is somewhat unbalanced leading to the formation of electrical dipoles. These dipoles, when present at the polymer/metal interface, affect the electron distribution at the metal side, producing London dispersion bonding. Such bonding is generally absent in non-polar polymers. Polymethyl-methacrylate (PMMA), poly-amide (PA), poly-vinyl-chloride (PVC) and poly-carbonate (PC) are examples of polar polymers, while poly-tetrafluoroethylene (PTFE), poly-ethylene (PE), poly-propylene (PP) and

poly-styrene (PS) are examples of non-polar polymers. The discussion presented above suggests that, from the standpoint of maximum chemical polymer-to-metal adhesion, polar polymers are preferred. Unfortunately, polar polymers tend to absorb excessive amount of water which, as discussed earlier, can cause undesirable micro-structural changes in the polymers, introduce internal stresses by swelling and weaken the polymer/metal interface. This makes the identification of the optimal thermoplastic polymer for the polymer-to-metal direct-adhesion PMH applications quite difficult. What is clear; however, is that micro-scale mechanical interlocking approach to the BIW load-bearing PMH technology will be least affected by the presence of water.

Since poly-amide (nylon) possesses a relatively high maximum service temperature (required for the PMH technology compatibility with the E-coat curing treatment), it is important to address the problem of water adsorption (surface phenomenon) and water absorption (bulk phenomenon) on the nylon/metal adhesion and nylon properties. The family of nylons consists of several different types, e.g. nylon 6, nylon 6/6, nylon 6/12, etc. The numbers refer to the number of methyl units (-CH2-) residing on each side of the nitrogen atoms (amide groups) which influences the property profiles of the material. Polarity (and, hence, moisture absorbance) decreases with an increase in the separation and with a decrease in location regularity of the very polar amide groups. At the same time, thermal stability is lowered due to higher flexibility and mobility in these methyl unit sections of the main chain. As these units increase in length making the molecules appear more like polyethylene, as is the case of nylon 6/12, the properties of the nylon shift slightly toward those of polyethylene. Consequently, nylon 6/12 possesses lower modulus, higher elongation, lower strength, lower thermal distortion temperature, lower hardness and lower melting point than nylon 6/6. At the same time, moisture absorption in nylon 6/12 (more expensive than nylon 6/6) is approximately half of that of nylon 6/6 ensuring that the

properties of the former are much more consistent and experience less humidity-induced fluctuations. Based on these findings, one can anticipate that a moderately polar nylon would be optimal, among the nylon family, for the direct-adhesion PMH applications.

3.8. Summary and Conclusions

Based on the results obtained in the present work, the following main summary remarks and conclusions can be drawn:

1. A comprehensive review is provided of the public-domain literature dealing with various polymer-to-metal direct-adhesion efforts.

2. The efforts and their results were critically assessed with respect to their potential use in the BIW load-bearing applications. The analysis included both the consideration of the functionality and durability of the BIW load-bearing components and the compatibility of various PMH technologies within the BIW manufacturing process chain.

3. The overview of the literature revealed that while considerable amount of research has been done in the PMH direct-adhesion area, many aspects of these technologies which are critical from the standpoint of their use in the BIW structural applications have not been addressed (or addressed properly).

4. Among the PMH technologies identified, the one based on micro-scale mechanical interlocking between the injection-molded thermoplastic polymer and stamped-metal structural component appears to be most promising. It should be noted that this conclusion was influenced by the number and completeness of the investigations and their results for different direct-adhesion PMH technologies.

3.9. References

3.1 O. J. Zoellner and J. A. Evans, "*Plastic-Metal Hybrid. A New Development in the Injection Molding Technology,*" ANTEC 2002 Annual Technical Conference, Sanfrancisco, CA, 2002, 1-4.

3.2 *Plastic-Metal Hybrid Material*, http://www.hbmedia.net/polymotive/polymotive/2003/01/articles/frontend1.shtml

3.3 D. Recktenwald, "*Advanced Adhesives Foster Hybrid Structures*," Machine Design, 77, 21, November 2005, 124-126.

3.4 M. Grujicic, V. Sellappan, G. Arakere, N. Seyr and M. Erdmann, "*Computational Feasibility Analysis of Direct-Adhesion Polymer-To-Metal Hybrid Technology for Load-Bearing Body-In-White Structural Components*," Journal of Materials Processing Technology, 195, 2008, 282-298.

3.5 K. Ramani and B. Moriarty, "*Thermoplastic Bonding to Metals via Injection Molding for Macro-Composite Manufacture*," Polym. Eng. Sci., 38, 5, 1998, 870-877.

3.6 K. Ramani and W. Zhao, "*The Evolution of Residual Stresses in Thermoplastic Bonding to Metals*," Int. J. Adhesion and Adhesives, 17, 4, 1997, 353-357.

3.7 K. Ramani and J. Tagle, "*Process-Induced Effects in Thin-Film Bonding of PEKEKK in Metal-Polymer Joints*," Polymer composites, 17, 6, 1996, 879-886.

3.8 P. Shah, *Adhesion of Injection Molded PVC to Silane Primed Steel,* M.S. Thesis, University of Cincinnati, 2005.

3.9 H. Sasaki, I. Kobayashi, S. Sai, T. Omoto and K. Mori, "*Direct Adhesion of Nylon Resin to Stainless Steel Plates Coated with Triazine Thiol Polymer by Electropolymerization During Injection-Molding*," Japanese Journal of Polymer Science and Technology, 55, 8, 1998, 470-476.

3.10 J. Salladay and J. Stevens, *New Business Identification and Development*, Private Communication, October 2006.

3.11 D. H. Berry and A. Namkanisorn, "*Fracture Toughness of a Silane Coupled Polymer-Metal Interface: Silane Concentration Effects*," The Journal of Adhesion, 81, 2005, 347-370.

3.12 M. Mikulec, "*Feasibility of Automotive Coatings Designed for Direct Adhesion to TPO Materials*," ANTEC 1997 Conference: Plastics-Saving the Planet, 3, 1997, 2775-2779.

3.13 C. A. Kondos and C. F. Kahle, II, "*Basecoats with Direct Adhesion to TPO Materials*," SAE Technical Papers on CD-ROM, 1998.

3.14 A. Bonnet and R. Perrinaud, *Many benefits can be gained by substituting fluoropolymer resins for the stainless steel and exotic alloys commonly specified for fluid contact components,* http://www.chem.info.

3.15 S. A. Marcus, United States Patent No: 4,452,375, *Manufacture of Draw-Redraw Cans Using Steel Sheet Material Film Laminated or Extrusion Coated with a High Density Polyethylene Graft Co-polymer*, June 5, 1984, Michigan.

3.16 R. A. Gledhill and A. J. Kinloch, "*Environmental Failure of Structural Adhesive Joints*", Journal of Adhesion, 6, 1974, 315-330.

3.17 J. D. Venables, "*Adhesion and Durability of Metal-Polymer Bonds*", Journal of Materials Science, 19, 1984, 2431-2453.

3.18 G. D. Davis, P. L. Whisnant and J. D. Venables, "*Subadhesive Hydration of Aluminum Adherends and Its Detection by Electrochemical Impedance Spectroscopy*", J. Adhesion Sci. Technol., 9, 1995, 433-442.

3.19 A. J. Kinloch, M. S. G. Little and J. F. Watts, "*The Role of the Interphase in the Environmental Failure of Adhesive Joints*", Acta Mater., 48, 2000, 4543-4553.

3.20 P. W. Erickson, E. P. Pleuddemann, *Composite Materials 6*, New York, Academic Press, 1974.

3.21 E. P. Pleuddemann, *Silane Coupling Agents*, New York, Plenum-Press, 1991.

CHAPTER 4

SELECTION OF THE SPRAYING TECHNOLGIES FOR OVER-COATING OF METAL-STAMPINGS WITH THERMOPLASTICS FOR USE IN DIRECT-ADHESION POLYMER METAL HYBRID LOAD-BEARING COMPONENT

4.1. Abstract

The suitability of various polymer-powder spraying technologies for coating of metal stampings used in polymer metal hybrid (PMH) load-bearing automotive-component applications is considered. The suitability of the spraying technologies is assessed with respect to a need for metal-stamping surface preparation/treatment, their ability to deposit the polymeric material without significant material degradation, the ability to selectively overcoat the metal-stamping, the resulting magnitude of the polymer-to-metal adhesion strength, durability of the polymer/metal bond with respect to prolonged exposure to high-temperature/high-humidity and mechanical/thermal fatigue service conditions, and compatibility with the automotive body-in-white (BIW) manufacturing process chain. The analysis revealed that while each of the spraying technologies has some limitations, the cold-gas dynamic-spray process appears to be the leading candidate technology for the indicated applications.

4.2. Introduction

Over the last decade, polymer metal hybrid (PMH) structures have been used in variety of automotive applications ranging from the instrument-panel cross-beams via the roof-panel-cross-support to the entire front-end vehicle modules. The main idea behind the PMH technology is to use a system level approach in order to combine the structural and non-structural functions of a number of components, into a singular fully-optimized sub-assembly (typically consisting of a metal-stamping core and plastic injection-molded overcoat containing multiple ribs). This

approach generally yields, due to its underlying material/structure system-integration approach, greater system-level benefits relative to those obtained by simple merging/joining of the proximate parts/components.

The subject of the present work is the use of the PMH technology in load-bearing BIW automotive components. An example of such a component is depicted in Figures 4-1(a)-(b). The component in question is generally referred to as the "*rear longitudinal beam*" which connects, on the front end, to the rocker panel, on the middle to the shock tower, while at the rear end it connects to the rear cross beam. The traditional all-metal design of this component is displayed in Figure 4-1(a) and includes three components: (a) main U-shape channel beam; (b) a reinforcement plate and (c) a cover plate. The latter two components are spot welded to the first one. It should be noted that the cover plate is slightly translated in Figure 4-1(a) in order to reveal the location of the reinforcing plate. The PMH rendition of the same component is depicted in Figure 4-1(b). The reinforcement plate has been replaced with an injection-molded thermoplastic rib-like sub-structure, while the thickness of the cover-plate (not shown in Figure 4-1(b) for clarity) is reduced.

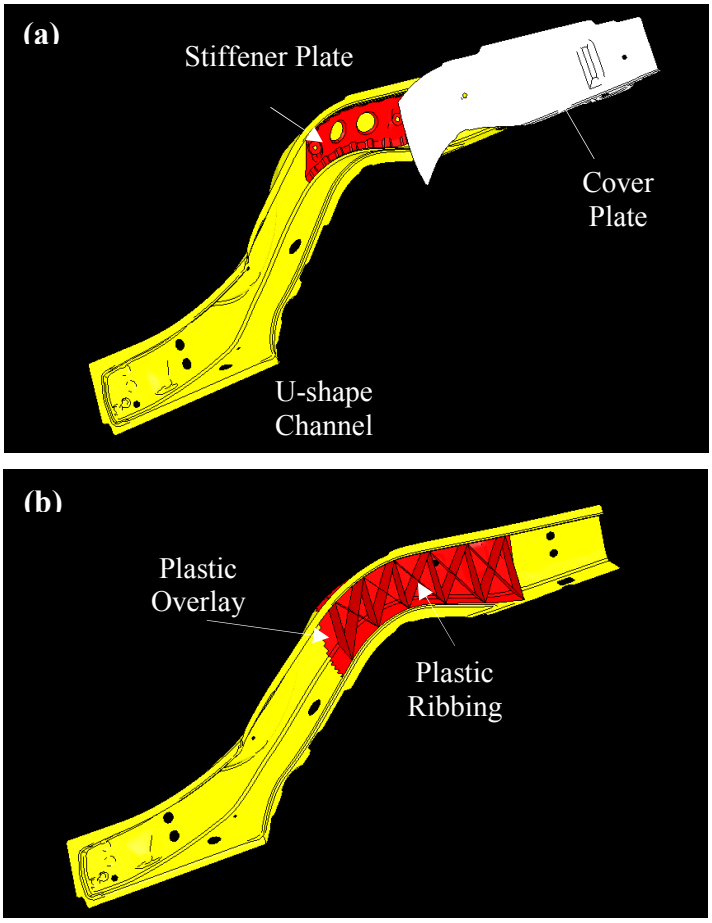

Figure 4-1: An Example of the: (a) All-metal and (b) PMH Load-bearing Automotive Component

The main PMH technologies currently being employed in the automotive industry can be grouped into three major categories: (a) Injection over-molding technologies [4.1]; (b) Metal-over-molding technologies combined with secondary joining operations [4.2]; and (c) Adhesively-bonded PMHs [4.3]. A detailed description for each of these groups of PMH manufacturing technologies can be found in our recent work [4.4]. Hence, only a brief overview of each is given below.

In the injection over-molding process, metal inserts with matching flared through-holes are stamped, placed in an injection mold and over-molded with short glass fiber-reinforced

thermoplastics to create a cross-ribbed supporting structure. The metal and plastics are joined by the rivets which are formed by the polymer melt penetrating through-holes in the metal stamping(s). Such rivets then provide mechanical interlocks between the plastics and the metal. In the metal over-molding PMH technology, a steel stamping is placed in an injection mold, where its underside is coated with a thin layer of reinforced thermoplastics. In a secondary operation, the plastics-coated surface of the metal insert is ultrasonically welded to an injection molded glass-reinforced thermoplastic sub-component. In this process, a closed-section structure with continuous bond lines is produced which offers a high load-bearing capability. In the adhesively-bonded PMH technology, glass fiber-reinforced poly-propylene is joined to a metal stamping using Dow's proprietary low-energy surface adhesive (LESA) [4.4]. The acrylic-epoxy adhesive does not require pre-treating of the low surface-energy poly-propylene and is applied by high-speed robots. Adhesive bonding creates continuous bond lines, minimizes stress concentrations and acts as a buffer which absorbs contact stresses between the metal and polymer sub-components. Adhesively-bonded PMHs enable the creation of closed-section structures which offer high load-bearing capabilities and the possibility for enhanced functionality of hybrid parts (e.g. direct mounting of air bags in instrument-panel beams or incorporation of air or water circulation inside door modules).

While the aforementioned PMH technologies have demonstrated their potential and are being widely used in various non-structural and load-bearing automotive components, they nevertheless display some significant shortcomings. For example, in many applications, to maintain the structural integrity of the part, hole punching needed for polymer-to-metal interlocking in the injection over-molding process may not be allowed. Similarly, stamped-edges over-molding may be restricted. In the case of adhesively-bonded PMHs, the adhesive cost, long curing time and the ability of the adhesive to withstand aggressive chemical and thermal

environments encountered in the paint-shop during BIW pre-treatment and E-coat curing may be an issue. Consequently, alternative lower-cost PMH technologies for structural load-bearing BIW component which are compatible with the BIW manufacturing process chain are being sought. One of such technologies, which is the subject of the present work, is the so called direct-adhesion PMH technology in which the joining between the metal and thermo-plastic sub-components is attained through direct-adhesion of injection-molded thermo-plastics to the metal without the use of interlocking rivets/over-molded edges or structural adhesives [4.4]. There are several potential advantages offered by this technology over the ones discussed above: (a) Polymer-to-metal adhesion strengths (ca. 35MPa [4.4]) comparable with those obtained in the case of thermo-setting adhesives are feasible but only at a small fraction of the manufacturing cycle time; (b) The shorter cycle time and the lack of use of an adhesive allow for more economical PMH-component production; (c) Unlike the adhesive-bonding technology, joining is not limited to simple and non-interfering contact surfaces; (d) Reduced possibility for entrapping air in undercuts of a complex surface; (e) No holes for the formation of interlocking rivets are required and, hence, structural integrity of the part is not compromised; and (f) Overall reduction in the constraints placed upon the design complexity of the PMH component.

In our previous work [4.4], it was shown that, in order to ensure a good load transfer between the polymer and the metal sub-components in the direct-adhesion PMH structures, a plastic overlay (with a large contact surface area with the metal stamping) is needed in addition to the plastic rib-like structure. An example of such an overlay is depicted in Figure 4-1(b). Furthermore, our previous work [4.4] has demonstrated that if the overlay is produced simultaneously as the ribbing structure using conventional injection molding, the weight of the resulting PMH component would be excessively high. The primary reason for this was the existence of a minimal injection-moldable part wall thickness, which in the case of short glass

fiber-reinforced nylon 6 (the material most commonly used in the injection over-molding PMH technology) amounts to ~2mm (and becomes even larger as the need for drafting is accommodated). To overcome this limitation, it is suggested [4.4] that the overlay should be fabricated using one of the polymer-powder spraying technologies. Such technologies enable fabrication of coating layer with ca. 0.5mm thickness and, hence, could substantially reduce the PMH-component weight. Once the overlay has been spray formed, the plastic ribbing structure can be injection molded against it.

In the present work, a brief overview of the main polymer-powder spraying technologies and an analysis of their suitability for use in the direct-adhesion PMH technologies aimed at load-bearing BIW components are presented. In order to carry out such suitability assessment a number of suitability criteria have been developed. Some of these criteria are related to the PMH-component manufacturability, others with respect to the long-term durability of the PMH-component while the remaining ones with respect to the compatibility of the PMH-component/process with the BIW manufacturing process chain. It should be noted that the far-reaching objective of the present work is to critically assess the potential of direct-adhesion PMH technology in BIW load-bearing applications. Hence, significant body of work dealing with polymer-to-metal adhesion developed within the electronic packaging field is not presented, since the approaches used employed very thin (10-100μm) metal and/or polymeric structures and were not compatible with the BIW manufacturing process chain.

As stated earlier, the objective of the present work is to assess the potential of different polymer-powder spraying technologies for use in direct-adhesion PMH load-bearing BIW components both from the component function standpoint and the stand point of compatibility with the BIW manufacturing process chain. In traditional all-metal BIW manufacturing practice, components are stamped in the press shop, joined (typically by welding) in body shop and the

constructed BIW pre-treated and painted in paint shop. In the case of injection over-molding BIW PMH components, stamped metal subcomponents are "*hybridized*" with thermoplastic ribbing structure in injection molding shop. Hence to assess the suitability of various polymer-powder spraying technologies for BIW load-bearing applications, their compatibility with various processes taking place in press shop, injection molding shop, body shop and paint shop will be considered. Specific aspects of the BIW manufacturing process chain capability are discussed in the following sections.

It should be also noted that the present chapter is part of the ongoing research which deals with a total life-cycle approach to the selection of materials, and manufacturing/processing technologies in the light-weight engineering of the automotive BIW structural applications. Within such an approach, all the key BIW manufacturing process steps are considered. These steps include, metal-subcomponent manufacturing by stamping in the process shop, PMH component or thermoplastic sub-component manufacturing in the injection-molding shop, BIW construction by various joining processes in the body shop, BIW pre-treatment and painting in the paint shop, component performance and durability in service, and end-of-life considerations including disassembly, shredding, materials segregation, separation and recycling.

4.3. Overview of Polymer-powder Spray Processes

In this section a brief overview is given of the major polymer-powder spraying technologies. Since the final goal of the present work is to assess the suitability of these technologies for plastic-overlay deposition needed in the direct-adhesion PMH technology, the spraying processing are presented using a common platform. Such platform includes the consideration of the following aspects of each process: (a) problem description; (b) variation of the process; (c) depositing materials (d) substrate materials; (e) depositing/substrate materials pre-treatment; (f) part post-treatment; (g) major advantages and (h) main limitations.

4.3.1. Cold-gas Dynamic Spray

Process Description

The cold-gas dynamic spray process, often referred to as "*cold spray*", is a high-rate coating and free-form fabrication process in which fine, solid powder particles (generally 1 to 50 μm in diameter) are accelerated to high velocities (ca.100m/s for polymeric materials) by entrainment in a (often supersonic) jet of compressed (propellant) gas. The solid particles are directed toward a substrate, where during impact, they undergo plastic deformation and bond to the surface, rapidly building up a layer of the depositing material. Cold spray as a coating technology was initially developed in the mid-1980s at the Institute for Theoretical and Applied Mechanics of the Siberian Division of the Russian Academy of Science in Novosibirsk [4.5,4.6]. The Russian scientists successfully deposited a wide range of pure metals, metallic alloys, polymers and composites onto a variety of substrate materials. In addition, the Russian scientists demonstrated that very high surface deposition rates on the order of 5 m^2/min (~ 300 ft^2/min) are attainable using the cold-spray process.

In a typical cold-spray process, a compressed propellant gas of an inlet pressure on the order of 30 bar (500 psi) enters the device and flows through a converging/diverging DeLaval-type nozzle to attain a high velocity. The solid powder particles are metered into the gas flow upstream of the converging section of the nozzle and are accelerated by the rapidly expanding gas. To achieve higher gas flow velocities in the nozzle, the compressed gas is often preheated. However, while preheat temperatures as high as 900^o K are sometimes used, due to the fact that the contact time of spray particles with the hot gas is quite short and that the gas rapidly cools as it expands in the diverging section of the nozzle, the temperature of the particles remains substantially below the initial gas preheat temperature and, hence, below the melting temperature

of the powder material. A simple schematic of the cold-gas dynamic spray process is shown in Figure 4-2.

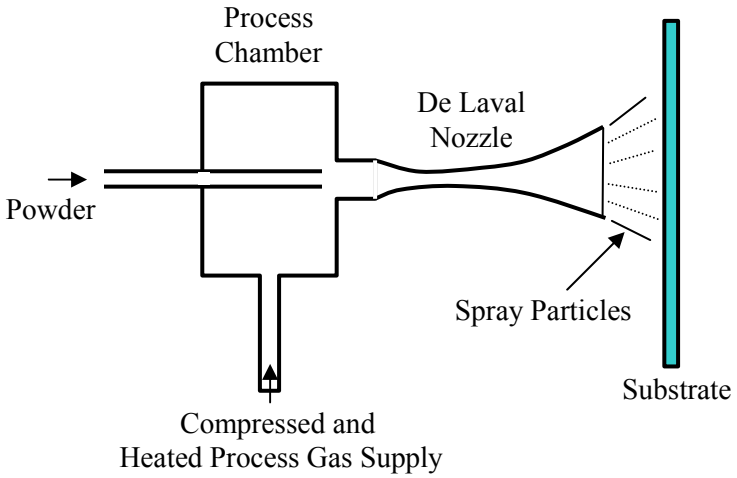

Figure 4-2: A Schematic of the Cold-gas Dynamic-spray Process

The actual mechanism by which the solid particles deform and bond during cold spray is still not well understood. It is well-established; however, that in the case of metallic feed particles and the metallic substrates extensive localized plastic deformation takes place during the impact. This causes disruption of the thin surface (oxide) films and enables an intimate conformal contact between the particles and the substrate/deposited material. The intimate conformal contact of clean surfaces combined with high contact pressures are believed to be necessary conditions for particles/substrate and particles/deposited material bonding. As far as the bonding mechanism between the sprayed polymer and metallic substrates is concerned, the picture is much less clear. It is generally believed, however, that micron-scale mechanical interlocking between the two materials at the polymer/metal interfaces plays an important role.

Variations of the Process

With the exception of some differences in the carrier-gas and powder delivery systems and nozzle designs, no distinct variations of the cold-gas dynamic-spray process could be identified.

Depositing Materials

A wide range of ductile (metallic and polymeric) materials can be successfully deposited by the cold spray while non-ductile materials such as ceramics can be deposited only if they are co-cold-sprayed with a ductile (matrix) material.

Substrate materials

Since a good combination of strength and ductility of the substrate is a critical component of the process, metallic materials are typically used as substrates.

Pre-treatment

To obtain higher jet speeds, the carrier gas is typically pre-heated to a couple of hundreds of degrees of Celsius. In the case of plastic powder materials, cleaning/degreasing and pre-heating of the substrate appear to have a positive effect in attaining larger deposition yields and higher polymer-to-metal adhesion strengths [4.7].

Post-treatment

Typically no post-treatment is needed for cold-sprayed parts.

Advantages

Because of its low-temperature operation, the cold-spray process generally offers a number of advantages over the thermal-spray processes when used for deposition of the polymeric materials. Among these advantages, the most important appear to be [4.8,4.9]: (a) The amount of heat delivered to the coated part is relatively small so that microstructural changes in

the substrate material are minimal or nonexistent; (b) Due to the absence of in-flight oxidation and other chemical reactions, thermally- and oxygen-sensitive depositing materials can be cold sprayed without significant material degradation; (c) "*Peening*" effects caused by the impinging powder particles can give rise to potentially beneficial compressive residual stresses in cold-spray deposited materials [4.8] in contrast to the highly detrimental tensile residual stresses induced by solidification shrinkage accompanying the conventional thermal-spray processes; and (d) Cold spray of the polymeric materials offers exciting new possibilities for cost-effective and environmentally-friendly alternatives to the conventional solvent-based painting technologies.

Disadvantages

Due to visco-elastic (i.e. strain-rate dependent) nature of the thermoplastic materials and the mechanical-interlocking character of the polymer-to-metal bonding, a relatively narrow, material and particle-size dependent processing window is typically available for successful cold-spray deposition of thermoplastic coatings.

4.3.2. Electrostatic Powder Coating Spray Process

Process Description

Electrostatic-spray powder-coating process utilizes a powder-air mixture delivered to the spray gun from a fluidized-bed feed system. Within the gun, the powder is electro-statically charged and directed toward a grounded metal substrate being coated. A simple schematic of the electrostatic-spray powder-coating process is shown in Figure 4-3.

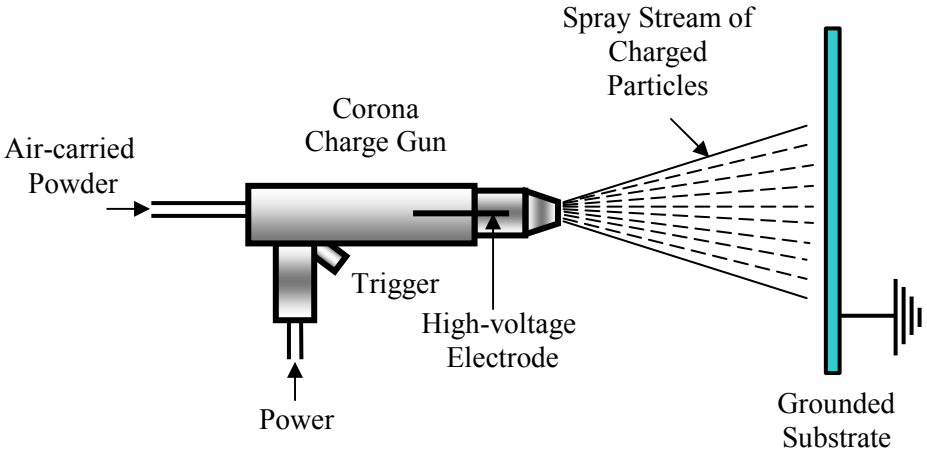

Figure 4-3: A Schematic of the Corona Spray Process

Variations of the Process

There are two basic variations of this process which mutually differ with respect to the way the electrostatic charge is applied to the powder: (a) within the "*corona*" electrostatic spray process, the powder is charged via an electrode subjected to a high negative DC voltage; and (b) in the "*tribo-charge*" electrostatic spray process, the powder is charged by friction accompanying the contact between the powder particles and the spray-gun inner lining.

Depositing Material

Currently, in excess of 90% of thermosetting coatings are deposited using the electrostatic spray process, while the process is also widely used for the deposition of variety of thermoplastic coatings (e.g. nylon, vinyl, poly-olefins)

Substrate material

Since electrical grounding of the substrate is a critical component of the process, metallic materials are typically used as substrates.

Pre-treatment

To remove the moisture, air is typically passed through a drying bed. Powder must be electro-statically charged. Standard cleaning/degreasing of the metal substrate is required. For thicker coatings (0.1-0.5mm), substrate preheating is necessary.

Post-treatment

Curing/fusion of the deposited powder is required and can be carried out at different temperatures (curing/fusing cycles as short as 20-60 seconds at temperatures around 200^{o}C are typically needed)

Advantages

High deposition efficiency since the over-sprayed powder is reclaimed, short cycle time, high adaptability to automation, suitable for a large variety of depositing and substrate materials.

Disadvantages

Difficulties in attaining uniform coating thickness in parts with complex geometries.

4.3.3. Fluidized-bed Powder Coating Process

Process Description

In the fluidized-bed powder coating process, the coating powder is held in a container which is at its bottom separated from an air chamber (commonly referred to as "*plenum*") by a perforated plate. Compressed air is introduced into the plenum and through the perforated plate, into the coating-particle bed. As the compressed air passes through the bed it lifts the particles causing them to get suspended and to form a "*fluidized bed*" of the particle/air mixture. When the substrate is brought into a contact with the fluidized bed, coating takes place.

Variations of the Process

There are two basic variations of the fluidized-bed powder coating process: (a) a conventional process and (b) an electrostatic process. Schematics of these processes are given in Figures 4-4(a)-(b). Within the conventional fluidized-bed powder coating process, the part to be coated is preheated and lowered into the fluidized-particle bed. In the electrostatic fluidized-bed powder coating process, particles in the fluidized bed are charged using a high-voltage DC electrode. While the metallic part is electrically grounded and suspended above the fluidized bed, electrostatic interactions between fluidized-bed charged particles and the grounded substrate then causes particle acceleration toward the substrate and, in turn, to the formation of the coating on the part.

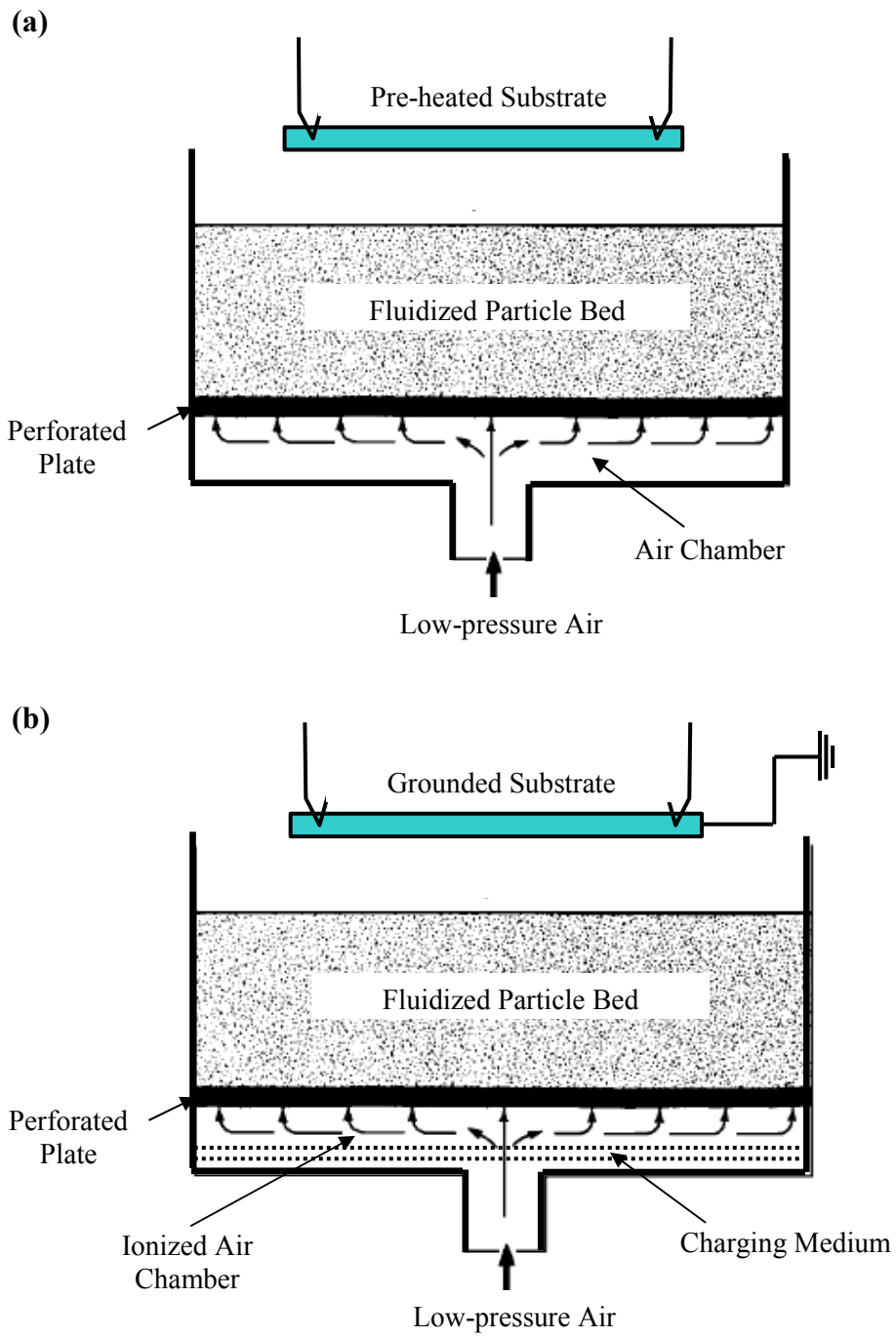

Figure 4-4: A Schematic of the: (a) Conventional and (b) Electrostatic Fluidized-bed Process

Depositing Material

Both versions of the fluidized-bed powder-coating process are widely used for the deposition of common thermoplastics (e.g. nylon, vinyl, poly-olefins, etc.) and common thermosets (e.g. epoxy, acrylics, etc.)

Substrate material

Typically metallic materials are used as substrates and in the case of the electrostatic fluidized-bed powder coating process, electrical grounding of the part entail a high-level of electrical conductivity of the part material.

Pre-treatment

With the exception of drying and electrostatic charging of the powder (in the case of electrostatic fluidized-bed process) no special powder pretreatment is required. Standard cleaning/degreasing of the substrate is required. In the case of the conventional process, the part is pre-heated and, often, pre-primed for improved coating adhesion.

Post-treatment

Relatively short (3-5 min) post-coating heat treatment (at ca. 200^{o}C) is typically required to ensure smooth and less porous coating (in the case of thermoplastic) and complete curing (in the case of thermosets).

Advantages

One of the main advantages of the fluidized-bed powder coating process is uniformity in the coating thickness and the microstructure. Essentially perfect material-transfer efficiency is typically attained. Also, in the case of the electrostatic fluidized-bed process, no preheating of the substrate is required.

Disadvantages

Main limitations of the fluidized-bed powder coating process are: (a) suitable for relatively small to middle-size parts; (b) generally not suitable for coating of selected portions of the part; (d) in the case of the electrostatic process, the inside corners of the part are typically less coated due to the interplay of the so-called "*Faraday cage effect*".

4.3.4. Thermal Spray Powder Coating Process

Process Description

Within the thermal spray powder coating process, powder particles in a 1-50μm size range are (at least partially melted) inside a spray gun and accelerated to high-velocities (ca. 40-100 m/s for flame, 400-800 m/s for HVOF, 80-300 m/s for plasma coating process) toward the substrate. Upon impact, the particles splatter onto the surface building a coating layer.

Variations of the Process

All the thermal spray processes are generally classified as combustion and electric processes. Among the combustion type thermal spray processes the ones most frequently used for the deposition of plastic are flame and high-velocity oxygen fuel (HVOF) spraying processes. Schematics of these two thermal spray processes are given in Figures 4-5(a)-(b). The fundamental difference between these two processes is that in the case of flame spraying the powder material is fed continuously to the tip of the spraying gun where it is melted in a fuel/gas flame and propelled to the substrate in a stream of carrier gas (typically air). Usually, acetylene, propane and methyl acetylene-propadiene are used as fuel. Within the HVOF process fuel and oxygen are pre-mixed, combusted in a confined space and accelerated to supersonic speeds in an extended nozzle. While the powder particles are injected into the flame. Consequently, the resulting coating is characterized by a high-density, low-porosity and a high bond-strength.

Among the electrical thermal spray coating processes, the one most frequently used for the deposition of plastic coatings is plasma-arc spray process. Within this process, powder particles are melted within the spray gun by an electric arc created between an internal central-line electrode and the gun nozzle (which acts as a second electrode). A pressurized inert gas is passed between the electrodes where it is heated to very high temperatures to form a plasma gas. As the powder particles are introduced into the plasma gas, they are melted and propelled toward the substrate. A schematic of the plasma-arc spray process is given in Figure 4-5(c).

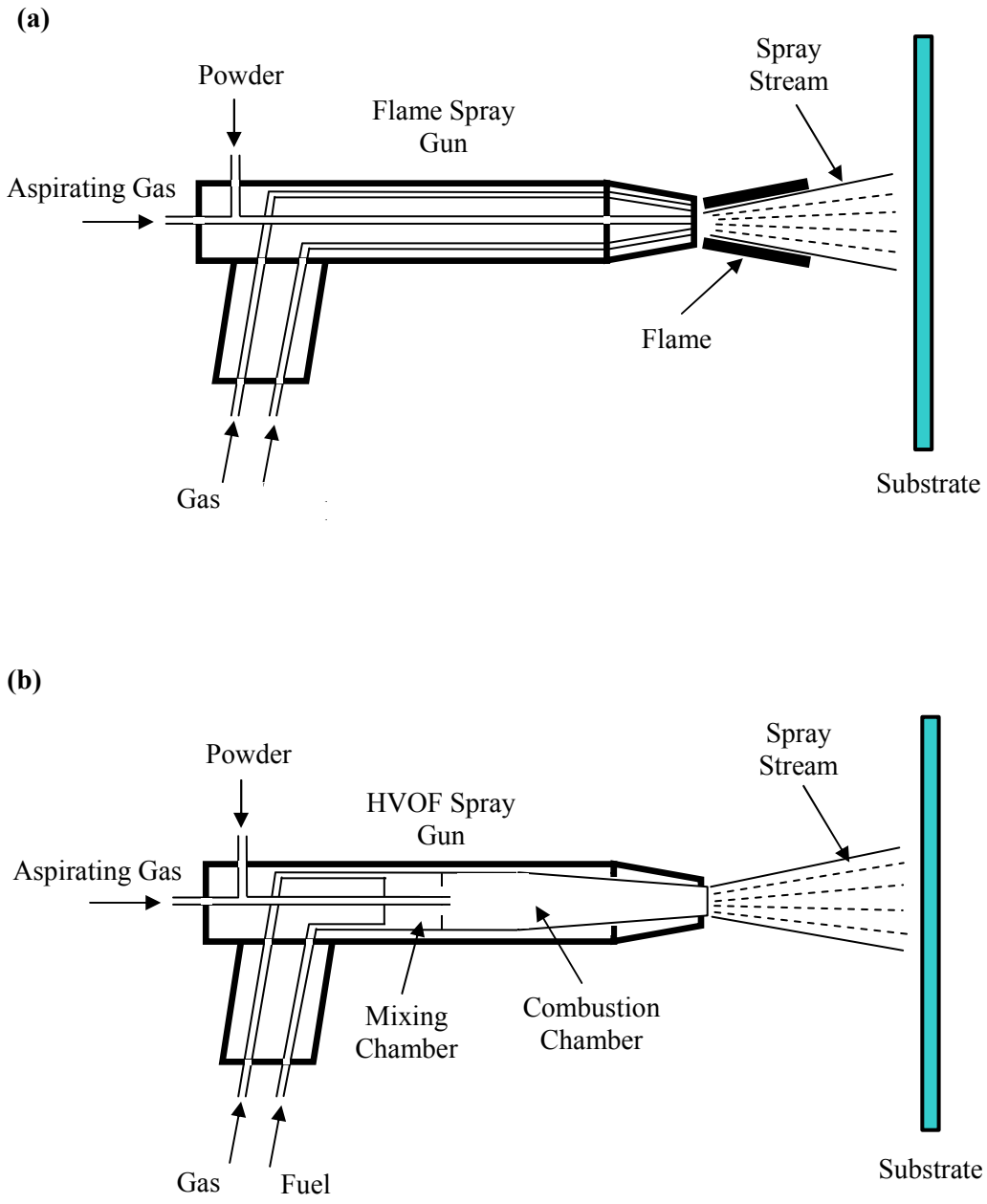

Figure 4-5: A Schematic of the: (a) Flame; (b) High-velocity Oxygen Fuel (HVOF) and (c) Plasma-arc Thermal Spray Process

(c)

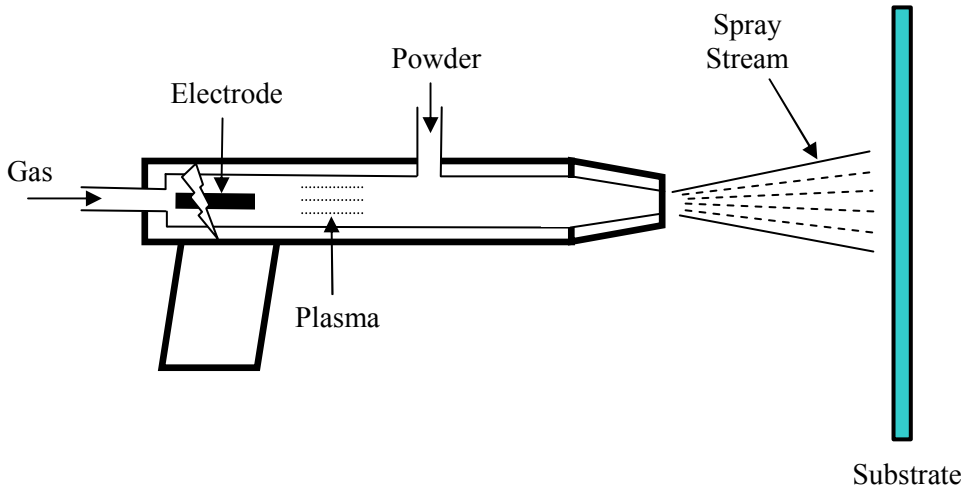

Figure 4-5: Continued…

Depositing Material

A wide variety of metallic, ceramic and polymeric coating materials can be used.

Substrate material

Likewise, a variety of metallic, ceramic and polymeric materials can be used as substrate materials.

Pre-treatment

No particular pre-treatment of the polymeric powder is required while standard grit blasting, cleaning/degreasing of the substrate is normally required. Pre-heating of the substrate is generally not a pre-requisite for good adhesion bonding.

Post-treatment

Typically no post-treatment of the thermal spray coated parts is required.

Advantages

Among the main advantages of the thermal spray processes are: (a) no requirements exist with respect to substrate pre-heating; (b) a large variety of depositing and substrate materials can be utilized; and (c) low-porosity, high-density coating can be readily produced (particularly in the HVOF process).

Disadvantages

Potential for thermal degradation and oxidation of the coating material and the substrate appear to be the main concerns accompanying thermal spray deposition processes.

4.4. Selection of the Powder Coating Process

To select the most suitable powder coating process (among the ones discussed in the previous section), the standard decision matrix approach was used [4.10]. The decision matrix approach entails the definitions of constraints (i.e. the conditions which must be satisfied) and criteria (i.e. the conditions which are used to judge the suitability of a given solution alternative). To define the constraints and the criteria for selection of the powder coating process for the BIW load-bearing application at hand, the Quality Functional Deployment (QFD) approach was utilized [4.11]. The QFD approach provides guidance for converting the customer needs (i.e. quality) into the technical/engineering specifications (i.e. functions) of the product /process to be designed (selected, in the present case) or service to be offered. The needs of the customer (an injection-molding shop, in the present case) are simply defined as: "*A polymer powder coating process is needed which will require little pre-treatment of metal stampings and polymer powder, be easily integrated into the existing process chain within the shop, be readily automated and safe, have cycle time comparable with that for plastic-rib structure injection process, can be used to deposit relatively-high melting-point polymers, produce strong and durable polymer-to-metal bond, require little post-coat treating, and, above all be inexpensive.*" These needs are then

converted into a list of specific engineering requirements, i.e. constraints and criteria, given below.

For the case at hand which involves thermoplastic-overlay fabrication at selected locations within the interior of a U-shape load-bearing BIW structural component, the following four constraints were identified:

1. The process must be able to coat only pre-selected portions of the metal-stamping substrate without a requirement for extensive masking;

2. The process must be able to deposit relatively-high melting-point thermoplastics (e.g. nylon) which can withstand a typical 190^{o}C/30min E-coat curing treatment in the paint shop;

3. The process must ensure a minimal polymer-to-metal adhesion strength of ca. 5MPa; and

4. The total coating cycle time must be comparable with the injection molding cycle time (when coating is carried out just prior to injection molding) and thus have duration of several seconds, not minutes.

Fulfillment of these constraints by the powder-coating process alternatives is presented in Table 4-1. It is seen that with the exception of the electrostatic spraying process and the electrostatic fluidized bed process which require post-coat heat treatment and with the exception of the conventional fluidized-bed process which entails extensive masking of the metal stamping, all the constraints are met by the remaining powder-coating spray technologies. While, in general, short cycle-time infra-red radiation-based post-coat heat-treating processing is available to remedy the aforementioned deficiencies of the electrostatic spraying and the electrostatic fluidized bed processes, high geometrical complexity of the BIW components and the need for a line-of-sight renders the infra-red radiation treatment not very effective. It should also be noted that, in the case of the cold-gas dynamic spray process no public-domain data could be located

pertaining to the ability of this process to deposit nylon. To overcome this deficiency, a simple computational analysis of the cold-gas dynamic-spray process involving formation of a nylon coat on top of a metallic substrate is presented in Section 4.6. This analysis suggested that nylon can be cold-sprayed, provided the particles velocity and temperature are kept within well defined ranges. Based on all these considerations, it was concluded that all the powder-coating spray processes considered in the previous section except for the electrostatic spray process are viable candidates for the overlay fabrication. The next question to be answered is "*Which of the processes is the most attractive alternative?*" This question will be answered by constructing the appropriate decision matrix.

The decision matrix approach enables evaluation and ranking of competing alternative solutions to a problem using a list of weighted (ranking) criteria. The method is commonly used in situations involving the selection of a simple alternative solution and the decision involves consideration of a number of criteria. To construct the appropriate decision matrix the following steps are generally followed:

(a) An extensive list of criteria which are used to judge the suitability of an alternative solution is created via project-team brainstorming, input from the customer(s) and through the use of the QFD method;

(b) The list from (a) is critically evaluated and one or more list reduction tools (e.g. multi-voting) are used to obtain the final list of criteria;

(c) Next, relative importance of each criterion is assessed by assigning a relative weighting factor to each. Table 4-2 contains a list of the final criteria, their weighting factors and a brief justification for the assigned importance (i.e. the weighting factor) to each criterion. The results listed in Table 4-2 were obtained using pair-wise comparison between different criteria in order to assess their relative importance. As a result of each two-criteria comparison, score 0 is

assigned to both criteria if they are judged equally important, score 1 is assigned to the more important criterion and score -1 to the less important criterion. The pair-wise comparison approach used in the present work is summarized in Table 4-3. The results appearing in the last column of Table 4-3 and the justification presented in the last column of Table 4-2 were used to assign the weighting factor for each of the criteria, Column 2, Table 4-2;

(d) Next, a two-dimensional matrix (the decision matrix) is constructed by listing the criteria with their weights along one (horizontal or vertical) direction and the alternative solutions along the other;

(e) Each alternative is then evaluated with respect to its ability to accommodate each of the criteria and the corresponding score is assigned. Most frequently, one of the following two ways for score assigning are used: (i) a fixed scale (e.g. 1-5. with a higher score denoting a superior solution) is used for each criterion and a score (e.g. 3) is assigned to given alternative. (e.g. cold-gas dynamic spray) for the given criterion (e.g. minimal need for metal-substrate pre-heating); or (ii) within each criterion, the alternative solutions are ranked and given a score based on their ranking (with score 1 being the least favorable alternative with respect to the criterion in question, score 2 being the second least favorable alternative, etc.). The first method of score assigning is used in the present work; and

(f) Lastly, scores for each alternative are multiplied with the corresponding criterion weighting factor and summed to get a total score for each alternative, last row, Table 4-4. The alternatives with the highest overall score are then closely examined to obtain the final single choice.

The decision matrix pertaining to the selection of the optimal powder spray coating technology for the fabrication of thermoplastic overlay at selected (interior) locations of a typical U-shape BIW load-bearing direct-adhesion PMH component considered in the present work is

given in Table 4-4. The results displayed in Table 4-4 suggest that the cold-gas dynamic-spray process is the most suitable alternative for the fabrication of a nylon overlay in the interior of a U-shape BIW load-bearing direct-adhesion PMH component. A careful examination of the results displayed in Table 4-4 indicates that the main reasons for the cold-gas dynamic-spray process being identified as the best alternative are a relatively low cost and the ability of the process to deposit the thermoplastic material without causing any thermal degradation to it.

Table 4-1: Fulfillment of the Requirements Imposed by the PMH Direct-adhesion BIW Load-bearing Components onto the Candidate Powder Coating Technologies

Process	Variations of Process	Constraints			
		1	2	3	4
		Selective Coating without masking	Nylon Compatible	Minimum Adhesion Strength 5 MPa	Cycle Time in Seconds
Cold-gas Dynamic Spray	N/A	Yes	Yes (Section V)	Yes	Yes
Electrostatic Spray	Corona-Charge	Yes	Yes	Yes	No (due to post-coat treatment)
	Tribo-Charge	Yes	Yes	Yes	No (due to post-coat treatment)
Fluidized Bed	Conventional	No (due to need for extensive masking)	Yes	Yes	Yes
	Electrostatic	No (due to need for extensive masking)	Yes	Yes	No (due to post-coat treatment)
Thermal Spray	Flame	Yes	Yes	Yes	Yes
	HVOF	Yes	Yes	Yes	Yes
	Plasma-arc	Yes	Yes	Yes	Yes

Table 4-2: Final List of Ranking Criterion, Weighting Factors and Justification of Importance of the Criteria Used in the Decision Matrix Approach

Ranking Criterion	Weighting Factor	Justification of Importance
1. Minimal need for metal-substrate pre-treatment (e.g. sanding, grit blasting, cleaning/degreasing, etc.)	2	It is desirable, but not absolutely critical, to be able to leave drawing compound on the stamping to minimize the possibility for surface damage and not to have to introduce additional cleaning process step in the injection-molding shop.
2. Minimal need for metal-substrate pre-heating	3	Metal-substrate pre-heating is an additional process step in the injection molding shop and can degrade metallic-material properties.
3. Minimal additional requirements for powder pre-treatment (e.g. screening, drying, etc.)	2	Any additional powder pre-treatment would introduce a new process step in the injection molding shop and unnecessarily increase the overlay fabrication cost.
4. Ability to coat uniformly intrinsic geometrical features of the metal substrate	5	Uniform coating thickness is critical for ensuring a proper transfer of load between polymer and metal and for controlling the overall weight of the overlay.
5. Minimal thermal/chemical degradation of the depositing and substrate materials	5	Thermal/chemical degradation of the depositing and substrate materials can seriously jeopardize materials properties and, hence, functionality of the PMH component.
6. Minimal need for post coating treatment	3	If the post coating treatment does not seriously compromise the overall overlay-fabrication cycle time, it is a less critical requirement.
7. Minimal overlay manufacturing cost	5	In addition to reducing the component weight, the PMH approach should not compromise (if not reduce) the overall manufacturing cost.
8. Maximal ease of automation	5	Automation is a critical element of the effort to reduce the overall manufacturing cost.

Table 4-3: A Pair-wise Comparison Matrix Used to Assign a Relative Weighting Factors to the Powder-coating Process-selection Criteria

Criteria	Substrate Pre-treat	Substrate Pre-heat	Powder Pre-treat	Uniform Coating	Material Degradation	Post-coat Treatment	Cost	Automation	TOTAL
Substrate Pre-treat	0	-1	0	-1	-1	0	-1	-1	-5
Substrate Pre-heat	1	0	1	-1	-1	-1	-1	-1	-3
Powder Pre-treat	0	-1	0	-1	-1	-1	-1	-1	-6
Uniform Coating	1	1	1	0	0	1	0	0	4
Material Degradation	1	1	1	0	0	1	0	0	4
Post-coat Treatment	0	1	1	-1	-1	0	-1	-1	-2
Cost	1	1	1	0	0	1	0	0	4
Automation	1	1	1	0	0	1	0	0	4

Table 4-4: Decision Matrix for Powder Coating Deposition Process for PMH Overlay Fabrication. Weighting Factors are Given Within Parenthesis in the First Column. Scoring is Done on a 1-5 Scale

Criterion and Weight	Alternative Solutions			
	1	2	3	4
	Cold-gas Spray	Flame Spray	HVOF Spray	Plasma-arc Spray
1. Substrate Pre-treatment (2)	5x2=10	3x2=6	3x2=6	3x2=6
2. Substrate Pre-heating (3)	4x3=12	5x3=15	5x3=15	5x3=15
3. Powder Pre-treatment (2)	5x2=10	5x2=10	5x2=10	5x2=10
4. Uniform Coating (5)	3x5=15	3x5=15	3x5=15	3x5=15
5. Material Degradation (5)	5x5=25	3x5=15	2x5=10	1x5=5
6. Post-coat Treatment (3)	5x3=15	4x3=12	5x3=15	5x3=15
7. Cost (5)	4x5=20	4x5=20	3x5=15	3x5=15
8. Automation (5)	4x5=20	4x5=20	3x5=15	3x5=15
TOTAL	127	113	101	96

4.5. Cost Analysis for the Overlay Fabrication

As discussed in the previous section, the cost is an important criterion in choosing the most suitable powder coating process for the direct adhesion PMH load-bearing BIW applications at hand. In the decision matrix, Table 4-4, each of the alternative solutions was assigned a score in the criterion 7 using an estimated cost associated with the use of the coating process in question. While a detailed discussion of the procedure used in assessing the total manufacturing cost associated with the overlay fabrication process is beyond the scope of the present chapter, a brief account of this procedure is presented in the remainder of this section.

In general, the total manufacturing cost, C_m, is segregated into contributing components as follows:

$$C_m = C_{mat} + C_{cap} + C_{tool} + C_{cons} + C_{power} + C_{op} + C_{maint} \quad (4.1)$$

where C_{mat}, C_{cap}, C_{tool}, C_{cons}, C_{power}, C_{op} and C_{maint} are respectively the material, capital equipment, tooling, consumables, power, operating and maintenance costs (for the coating deposition process in the present case).

The coating material cost, C_{mat}, is obtained by multiplying the weight of the coating with the unit-weight cost of the coating material and dividing the result by the powder-coating process deposition efficiency. The unit-weight material cost is determined using the so-called *"tiered-volume pricing model"*, i.e. it is based on total planned production volume for the PMH component.

The capital cost, C_{cap}, is assessed using the so-called *"straight-line depreciation"* method. Within this method, the value of the capital equipment is assumed to depreciate linearly with time between its initial-purchase price and the *"salvage"* value. The C_{cap} is then computed by dividing the difference between the capital equipment initial-purchase price and its salvage

value by the expected life time of the equipment (in years) and by the number of parts coated per year.

Tooling manufacturing cost, C_{tool}, includes the cost of fixtures used to hold the part during pretreatment and coating. Since tooling is not perceived as a major cost component, is reusable and is not expected to be significantly different for the powder-coating alternative processes analyzed, C_{tool} was not assessed.

The cost of consumables, C_{cons}, includes the cost of material such as grinding/polishing medium, detergents, degreasers, fuel, oxidizing and carrier gases, etc., simple procedures were used to assess C_{cons}. For example, in the case of consumed gases, the C_{cons}, is obtained by multiplying the gas mass-flow rate with a typical cycle time and the gas cost per unit mass.

The (electric) power cost, C_{power}, is taken to include five main components (where applicable): (a) spray-gun power consumption cost; (b) gas-compressor power cost; (c) part pre-treatment and/or post-treatment heating cost; (d) gas heater power cost; and (e) powder-delivery system energy cost.

The operating cost, $C_{op,}$ is assessed by multiplying a fixed labor rate with the total coating-deposition cycle time and an (indirect/overhead-cost) burden factor.

The maintenance cost, C_{main}, was decomposed into the following two components: (a) the cost of labor and parts to service the equipment and (b) cost of downtime associated with lost production, idle employees, etc.

The results of the powder-coating cost analysis (per part coated) are presented in Table 4-5. The data used during the calculation of the results presented in Table 4-5 were obtained by consulting at least three equipment manufactures and/or service providers per each powder-coating process considered. The input received was averaged and the average values were used in the cost analysis. Some of the key input data used are listed in Table 4-6. It should be also noted

that a number of assumptions/simplifications were used in the cost analysis and the most important ones among these can be summarized as:

1. The part displayed in Figure 4-1(b) was used as a prototypical BIW load-bearing component, so the area (ca. 1370 cm^2) to be coated was assessed for this part;

2. An average coating thickness of 0.5 mm was assumed and the volume of coating material used was assessed as the product of the coating area and coating thickness divided by the coating-efficiency factor;

3. 400,000 parts are assumed to be coated per year over a period of eight years (typical production-life of a vehicle model);

4. The capital equipment needed is dedicated for coating the part at hand;

5. Comparable worker skills (and thus comparable labor cost) are required for each of the coating-process alternatives; and

6. Comparable metal-stamping surface pre-treatment requirements are entailed by each of the powder spraying process.

To assess the robustness of the overall cost-analysis results (last row, Table 4-5), the input data were perturbed within reasonable limits and the cost analysis repeated. This procedure changed the numbers in the last row of Table 4-5, but not the ranking of the competing powder coating processes.

Table 4-5: Cost Analysis for the Alternative Powder Coating Processes

Cost Component ($)	Powder Coating Process			
	1	2	3	4
	Cold-gas Spray	Flame Spray	HVOF Spray	Plasma-arc Spray
C_{mat} Material Cost	0.3365	0.3883	0.3365	0.3883
C_{cap} Capital Cost	0.0356	0.0148	0.0238	0.0445
C_{con} Consumable Cost	0.2138	0.1438	1.027	0.0476
C_{power} Power Cost	0.0107	0.0296	0.0170	0.0391
C_{op} Operational Cost	0.2524	1.1649	0.5048	0.7766
TOTAL COST	0.8490±0.1274	1.7415±0.2612	1.9068±0.2860	1.2961±0.1944

Table 4-6: Parameters Used in the Construction of Table 5.

Parameter (Units)	Powder Coating Process			
	1	2	3	4
	Cold-gas Spray	Flame Spray	HVOF Spray	Plasma-arc Spray
1. Coating Efficiency (N/A)	0.6-0.9	0.6-0.7	0.7-0.8	0.6-0.7
2. Deposition Rate (kg/h)	20	5	10	7.5
3. Capital Cost ($)	1,20,000	50,000	80,000	1,50,000
4. Salvage Value ($)	6,000	2,500	4,000	7,500
5. Carrier-gas Pressure (MPa)	3	0.5	1	0.5-2
6. Gun Wattage (kW)	-	20-40	20-40	40-80
7. Powder-feeder Wattage (kW)	0.6-0.7	0.2	0.5	0.2
8. Carrier-gas, Oxygen, Fuel Flow Rates (cm^3/s)	Carrier-gas (Nitrogen) 10,000-15,000	Oxygen 700-800 Fuel (Acetylene) 210-220	Oxygen 10,000-20,000 Fuel (Acetylene) 2,000-4,000	Carrier-gas (Argon) 300-400

4.6. Computational Analysis of the Cold-gas Dynamic-spray Process

As discussed previously, no public-domain data can be found for the cold-spray fabrication of nylon coatings. Nylon is of interest in the case of the overlay fabrication since: (a) it can withstand a typical 190°C/30min E-coat curing heat-treatment applied to the BIW in the paint shop and (b) since the injection-molded rib-like structure is likely to be made of the glass fiber-reinforced nylon, nylon overlay will guarantee good overlay/rib-structure adhesion strength.

To overcome the lack of data pertaining to cold-gas dynamic-spraying of nylon, a computational analysis of this process carried out in a companion work [4.12]. A brief overview of the procedure and the results is given in the remainder of this section.

The (transient non-linear dynamics) computational analysis of the nylon-particles/metal-substrate interactions involves the solution of mass, momentum and energy conservation equations. The solution is obtained using a second-order accurate explicit control-volume computational analysis and the commercial code AUTODYN [4.13].

Due to the presence of large elastic strains accompanying thermoplastic coating formation during particle/substrate interactions, a multi-material Eulerian formulation of the transient non-linear dynamics problem is selected. Within the Eulerian formulation, a fixed computational grid is selected to discretize the computational space and the particles and the substrate materials are allowed to move through the grid and mutually interact. Materials models available in the AUTODYN material database were used to represent the constituent behavior of nylon and steel. The material models include three basic components; (a) an equation of state (defines the density and temperature dependencies of the pressure); (b) a strength model (defines the deviatoric stress during elastic and elastic/plastic deformation steps); and (c) a failure model (defines the evolution of stress within material elements undergoing micro-structural damage/failure). Nylon is represented using a polynomial equation of state, a three-parameter visco-elastic strength model and a minimum (negative) hydrostatic pressure failure model. The material model for steel includes a linear equation of state, a Johnson-Cook strength model and a Johnson-Cook failure model.

The steel substrate is initially assigned roughness characteristics consistent with those observed in zinc-galvanized mild formable steel. The diameter of spherical nylon particles was selected from a narrow normal distribution with mean value of 10μm. All the particles were

assigned the same initial velocities and their altitude with respect to the substrate top surface was assigned using a stochastic procedure.

An example of the initial configuration of the computational domain is displayed in Figure 4-6(a). The evolution of the materials in the particles and the substrate with time is displayed in Figures 4-6(b)-(d). The formation of the nylon coating is evident. Close examination of the particles/substrate interfaces reveal that the deposited thermoplastics forms a full conformal coating with the substrate. This finding suggests that nylon can be cold-gas dynamic-sprayed in such a way that good mechanical interlocking between the depositing material and the substrate may be achieved to ensure the necessary level of polymers-to-metal adhesion strength. The surface roughness evident in Figure 4-6(d) typically becomes quite small at longer simulation times.

It should be noted that the results of the computational analysis (like the ones displayed in Figures 4-6(a)-(d)) are greatly affected by the particle velocity, temperature and average size. If these are not properly selected, the depositing particles, following an impact with the substrate, either bounce back, incompletely coat the substrate, or break-up into several fragments and get scattered around. Neither of these scenarios is desirable from the standpoint of attaining a good polymer-to-metal adhesion resistance [4.12].

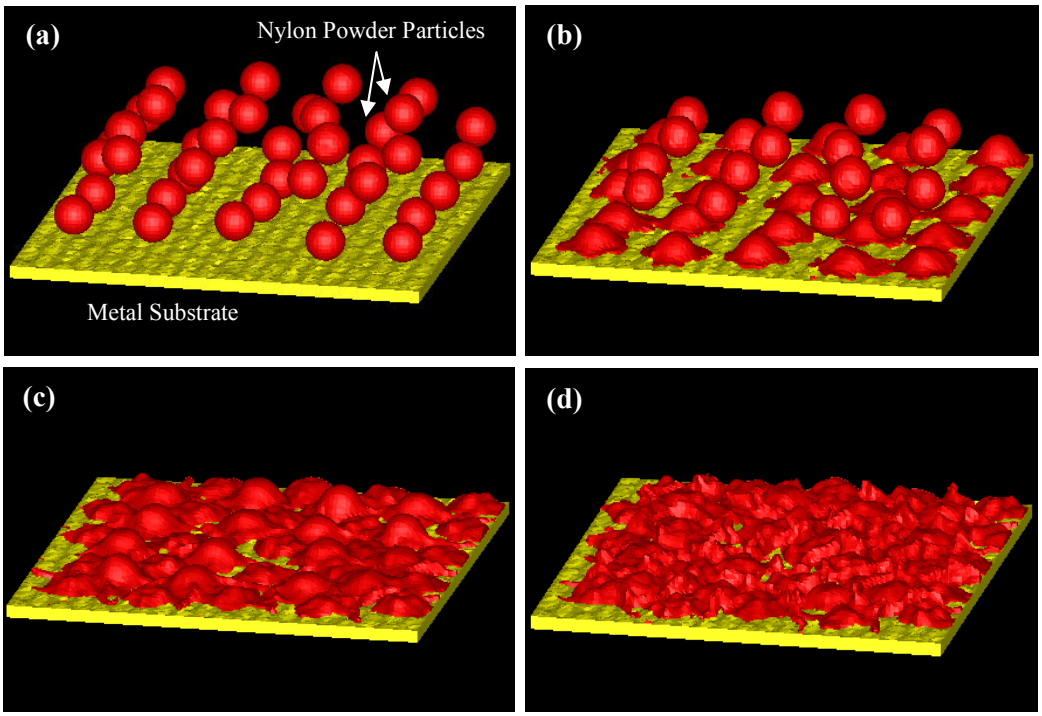

Figure 4-6: Temporal Evolution of the Coating and Substrate Materials During Cold-gas Dynamic-spray: (a) 0ms; (b) 0.1ms; (c) 0.2ms; and (d) 0.3ms

4.7. Summary and Conclusions

Based on the results obtained in the present work, the following main summary remarks and conclusions can be drawn:

1. A comprehensive review is provided of the public-domain literature dealing with various powder-coating processes suitable for the fabrication of an overlay within a U-shape BIW metal-stamping structural component which will be subsequently hybridized using the polymer-to-metal direct-adhesion injection-molding process.

2. After the product (overlay coating) requirements and the capabilities/attributes of the various processes were identified, a set of engineering-design tools (e.g. the quality functional deployment, decision matrix, etc.) were used to identify the screen-out non-suitable processes and to rank the remaining ones;

3. A detailed cost analysis is carried out while assessing the criteria used for ranking the candidate powder-coating processes.

4. Cold-gas dynamic-spray process was identified as a prime candidate for the BIW structural-component hybridization application at hand.

5. While no public domain data exist regarding the ability of the cold-gas dynamic-spray process to deposit nylon a transient non-linear computational analysis carried out in a companion work suggested that such a process is feasible.

4.8. References

4.1 O. J. Zoellner and J. A. Evans, *"Plastic-Metal Hybrid. A New Development in the Injection Molding Technology,"* ANTEC 2002 Annual Technical Conference, Sanfrancisco, CA, 2002, 1-4.

4.2 *Plastic-Metal Hybrid Material,* http://www.hbmedia.net/polymotive/polymotive/2003/01/articles/frontend1.shtml

4.3 D. Recktenwald, *"Advanced Adhesives Foster Hybrid Structures,"* Machine Design, 77, 21, November 2005, 124-126.

4.4 M. Grujicic, V. Sellappan, G. Arakere, N. Seyr and M. Erdmann, *" Computational Feasibility Analysis of Direct-Adhesion Polymer-To-Metal Hybrid Technology for Load-Bearing Body-In-White Structural Components,"* Journal of Materials Processing Technology, 195, 2008, 282-298.

4.5 A. P. Alkhimov, A. N. Papyrin, V. F. Dosarev, N. I. Nestorovich, and M. M. Shuspanov, *"Gas dynamic spraying method for applying a coating,"* US Patent 5,302,414, April 12, 1994.

4.6 A. O. Tokarev, Met. Sci. Heat. Treat., 35, 1996, 136.

4.7 Y. Xu and I. M. Hutchings, *"Cold Spray Deposition of Thermoplastic Powder,"* Surface and coating technologies, 201, 6, 2006, 3044-3050.

4.8 R. C. McCune, A. N. Papyrin, J. N. Hall, W. L. Riggs, P. H. Zajchowski, *"An exploration of the cold gas-dynamic spray method for several material systems,"* Thermal Spray Science and Technology, ASM International, 1995, 1–5.

4.9 J. Vlcek, *"A systematic approach to material eligibility for the cold spray process,"* International Thermal Spray Conference and Exhibition, May 5–8, Orlando, Florida, 2003.

4.10 D. G. Ullman, *"The Mechanical Design Process,"* McGraw-Hill Professional, 2002.

4.11 A. Olewnik and K. Lewis, *"Can a House Without a Foundation Support Design?,"* Proceeding IDETC/CIE, Long Beach, CA, 2005, 1-11.

4.12 M. Grujicic, B. Pandurangan, W. C. Bell, M. Daqaq, L. Ma, N. Seyr, M. Erdmann and J. Holzleitner, " *A Computational Analysis and Suitability Assessment of Cold-Gas Spraying of Glass-Fiber Reinforced Poly-Amide 6 for Use in Direct-Adhesion Polymer Metal Hybrid Automotive Components,"* Applied Surface Science, 254, 2008, 2136-2145.

4.13 AUTODYN-2D and 3D, Version 6.1, User Documentation, Century Dynamics Inc., 2006.

CHAPTER 5

SUITABILITY ANALYSIS OF A POLYMER METAL HYBRID TECHNOLOGY BASED ON HIGH-STRENGTH STEELS AND DIRECT POLYMER-TO-METAL ADHESION FOR USE IN LOAD-BEARING AUTOMOTIVE BODY-IN-WHITE APPLICATIONS

5.1. Abstract

A comprehensive set of computational engineering analyses is carried out in order to assess the suitability of a "*direct adhesion*" polymer metal hybrid (PMH) technology for use in load-bearing automotive body-in-white (BIW) components. Within the direct adhesion PMH technology, load transfer between stamped sheet-metal and injection-molded rib-like plastic subcomponents is accomplished through a variety of nanometer-to-micron scale chemical and mechanical phenomena which enable direct adhesion between the two materials. The resultant adhesion strength in a 5-10MPa range has been assessed. In the present work it has been investigated if such level of adhesion strength is sufficient to restore the component's stiffness in the cases when stiffness has been compromised by substituting a twin-shell large-thickness drawing-quality-steel design of a prototypical BIW component with a single-shell lower-thickness high-strength-steel and polymer-hybridized design of the same component. The results obtained suggest that meeting the bending stiffness requirements is the most challenging task and if such requirements do not control the overall component design, weight savings in a 4.5-7.0% range can be obtained.

5.2. Introduction

Traditionally, metals and plastics are fierce competitors in many automotive engineering applications. This paradigm is gradually being abolished as the polymer-metal-hybrid (PMH) technologies, developed over the last decade, are finding ways to take full advantage of the two

classes of materials by combining them into a singular component/sub-assembly. By employing one of the several patented PMH technologies, the automotive original equipment manufacturers (OEMs) have succeeded in engaging flexible assembly strategies, decreasing capital expenditures and reducing labor required for vehicle manufacture.

The basic concept utilized in all PMH technologies is illustrated in Figures 5-1(a)-(b). An open-channel thin-wall sheet-metal component can readily buckle under compressive load, Figure 5-1(a). With very little lateral support, provided by a thin-wall rib-like injection-molded plastic subcomponent, the buckling resistance (and the stiffness) of the component can be greatly increased (while the accompanied weight increase is relatively small).

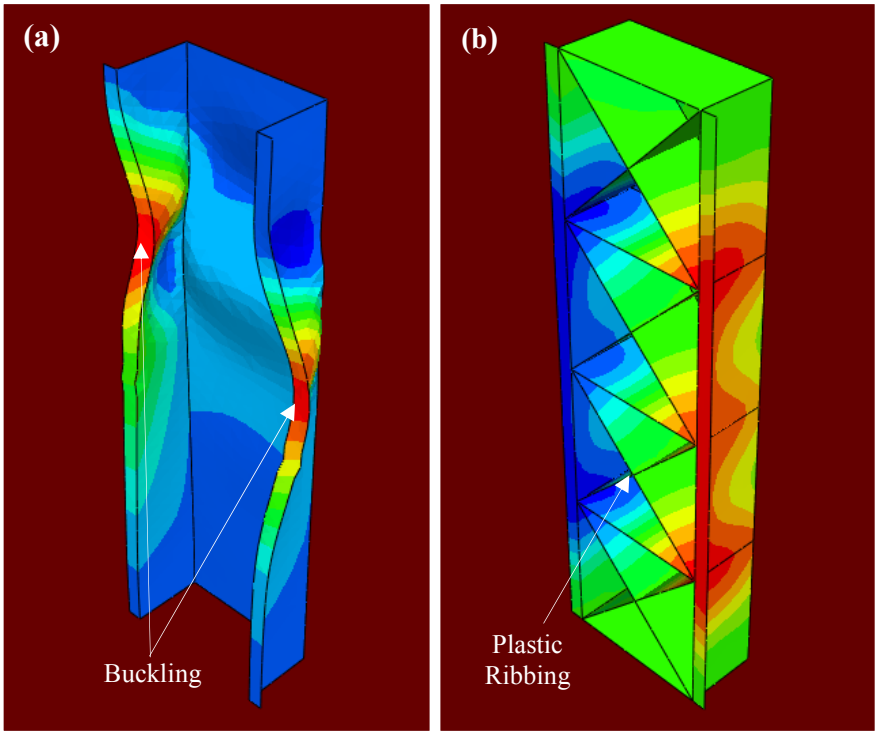

Figure 5-1: The Basic Concept Utilized in the Polymer Metal Hybrid (PMH) Technologies. Buckling in an Open-channel All-metal Component in (a) Has Been Prevented by a Rib-like Plastic Substructure in (b) Which Provides the Needed Lateral Support

Three main PMH technologies are currently being used by the automotive OEMs and their tier 1 and tier 2 suppliers: (a) Injection over-molding technologies; (b) Metal over-molding technologies combined with secondary joining operations; and (c) Adhesively-bonded PMH technologies. Only a brief description of these technologies will be given in the present chapter since they were reviewed in great details in our recent work [5.1].

Within the injection over-molding technologies [5.2], a metal-stamping profile is placed in an injection mold and polymer (typically glass fiber reinforced nylon) is injected around the profile. The plastic wraps around the edges of the sheet metal and/or through carefully designed flared holes or buttons. There are no secondary operations required and the drawing oils/greases do not need to be removed from the metal stamping.

Within the metal over-molding technologies [5.3], a steel stamping is placed in an injection mold in order to coat its underside with a thin layer of reinforced nylon. In a secondary operation, the polymer-coated surface of the metal insert is ultrasonically welded to an injection molded nylon subcomponent. In this process, a closed-section structure with continuous bond lines is produced which offers a high load-bearing capability. The hollow core of the part permits functional integration like cable housings and air or water channels.

Within the adhesively-bonded technologies [5.4]., glass-fiber reinforced poly-propylene is typically joined to a metal stamping using an adhesive which does not require pre-treating of the low surface-energy poly-propylene and can be applied by high-speed robots. Adhesive bonding creates continuous bond lines, minimizes stress concentrations and acts as a buffer which absorbs contact stresses between the metal and polymer subcomponents. Adhesively-bonded PMHs also enable the creation of closed-section structures which offer high load-bearing capabilities and the possibility for enhanced functionality of hybrid parts (e.g. direct mounting of

air bags in instrument-panel beams or incorporation of air or water circulation inside door modules)

Among the many technical and economic benefits offered by the PMH technologies, the following appear to be the most important:

(a) Reduction of the number of components;

(b) Production of the integrated components ready to assemble;

(c) Weight reduction compared to the traditional all-metal solutions;

(d) Additional design and styling freedom;

(e) Production of in-mold features like brackets, bosses and attachment points;

(f) Safety improvement due to lowered center of gravity of the vehicle;

(g) Often a several-fold increase in the bending strength of stamped metal sections which is attributed to the ability of plastics-subcomponent to assist the metal stamping to maintain its cross-section properties throughout the loading cycle and to delay the onset of failure due to localized buckling; and

(h) Improved damping in the acoustic range (relative to their all-steel counterparts, often as high as four times lower initial decibel reading measured in a simple hammer-strike test)

A comprehensive review of the PMH-technologies used in the automotive applications, carried out as part of the present work, revealed that these technologies were mainly used in non-structural (bolt-on) BIW components. In the cases of structural (load-bearing) automotive BIW applications, the PMH components in question (e.g. rear cross-roof beam, instrument-panel support beam, etc.) were not the main load-bearing components but rather the ones providing lateral support for the main load-bearing components. Weight reductions in these PMH components were attained by removing one of the sheet-metal stamped shells from the original all-metal twin-shell design of the component. Subsequently, the remaining sheet-metal stamped

shell was hybridized with a plastic ribbing substructure to recover component's stiffness and the buckling resistance lost during the removal of the other sheet-metal shell. In these PMH technologies, the sheet-steel grades used were not changed, i.e. formable steel grades with at least 15-20% ductility were used. Consequently, hybridization of the (originally all-metal) components did not entail consideration of manufacturability of the (remaining single-shell) metal subcomponent.

In more recent efforts, the automotive PMH technologies have begun to rely more on the use of high-strength and, thus, low-ductility steels for metal subcomponents. The essential philosophy behind this approach is displayed schematically in Figures 5-2(a)-(c). Figure 5-2(a) shows that, as steel grades with higher strengths are introduced, the sheet-metal thickness (and thus the subcomponent weight) can be reduced. Meanwhile subcomponent-strength requirements continue to be met, Figure 5-2(b). However, since the Young's and shear moduli of various steel grades differ by no more than a percent (material stiffness is a micro-structure insensitive property), the stiffness of the component, as well as its buckling resistances, continue to decrease as the sheet-steel thickness is reduced, Figure 5-2(c).

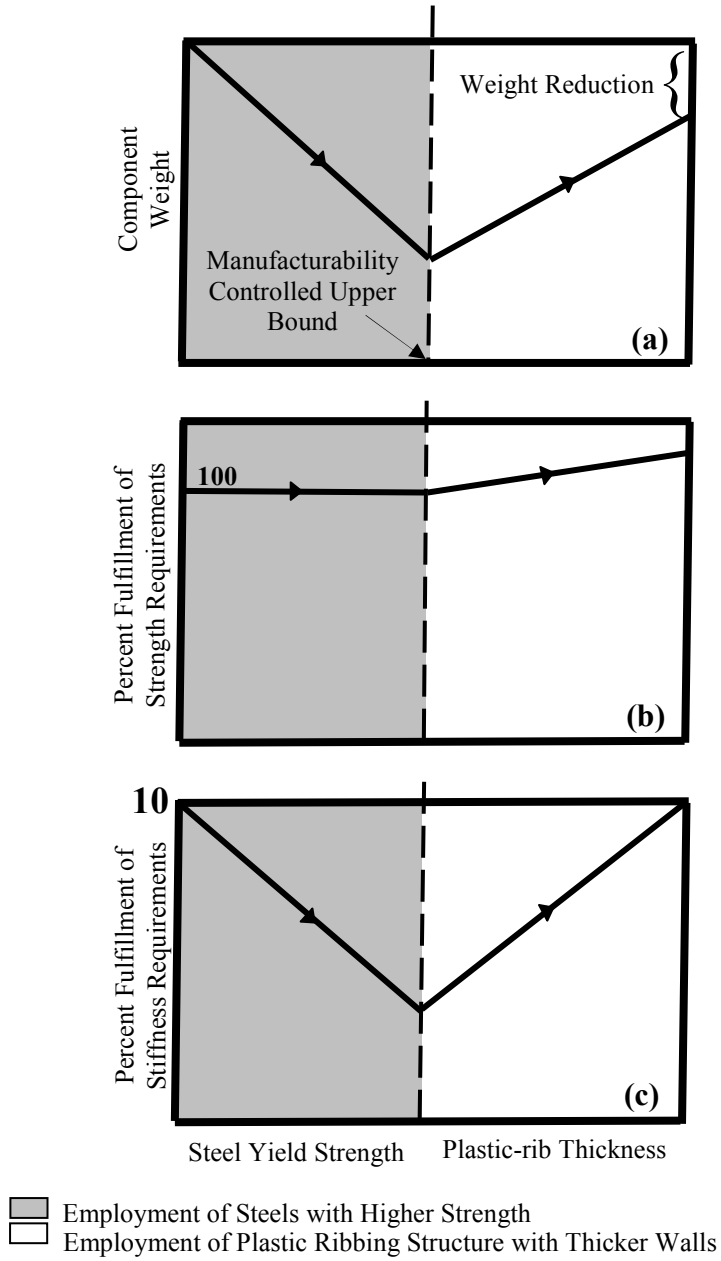

Figure 5-2: Concept Analysis for the Direct-adhesion PMH Technology Based on the Use of High-strength Steels. Please See Text for Details

In addition, as higher-strength steel grades are introduced, the metal subcomponent manufacturability by stamping becomes questionable. A maximum steel strength is ultimately reached past which the subcomponent can not be stamped out without intervening measures (e.g. the introduction of additional stages in the component's stamping process chain, the use of heated blanks, etc.) which are generally quite costly. If steel grades with yield strengths lower than the aforementioned upper bound are used, then a sheet-metal subcomponent can be produced using the standard stamping process and the subcomponent will be lighter and will meet the strength requirements. To attain the fulfillment of stiffness and buckling-resistance requirements, the metal subcomponent should be subsequently hybridized using an injection-molded plastic rib-like substructure. As discussed earlier some of the PMH technologies (e.g. injection overmolding and metal-overmolding based on the use of heat-staking) require fabrication of a number of holes (few millimeter in diameter) in the metal subcomponent to enable polymer-to-metal mechanical interlocking. In the case of high-formability steels, this normally does not present any serious challenges and holes can be punched in the stamped-out metal subcomponent. The situation is drastically different in the case of high-strength steel stampings. These steels possess relatively low ductility even in their as-received conditions and, after the component is stamped out, one can not expect that a significant ductility level remains in the metal subcomponent. Hole punching may present a problem and be accompanied by cracking of the stamped part and/or punch deformation/cracking. It is hence, unrealistic, under normal circumstances, to contemplate the use of the PMH technologies which entail holes in the metal-stamping for polymer-to-metal mechanical interlocking. Clearly, the adhesively-bonded PMH technology can be used in these applications. However, the low surface energy adhesives which must be used to adhesively bond thermoplastic and metal are quite expensive and their ability to withstand a typical (30min/190^{o}C)

E-coat curing treatment in the paint-shop is not yet well established. Likewise, long-term durability of the adhesively-bonded joints has not been fully established.

Among the newest efforts aimed at overcoming the aforementioned limitations of the standard PMH technologies is the so-called "*direct-adhesion*" PMH technology [5.1,5.5-5.9] in which various nanometer- and micron-scale chemical and mechanical phenomena are utilized to obtain direct bonding between the injection-molded plastics and the stamped metal subcomponents. The following potential main advantages offered by this technology have been identified in our prior work [5.1]:

(a) Polymer-to-metal adhesion strengths (20-30MPa) comparable with those obtained in the case of thermo-setting adhesives are feasible but only at a small fraction of the manufacturing cycle time;

(b) The shorter cycle time and the lack of use of an adhesive allow for more economical PMH-component production;

(c) Unlike the adhesive-bonding technology, joining is not limited to simple and non-interfering contact surfaces;

(d) Reduced possibility for entrapping air in undercuts of a complex surface;

(e) No holes for the formation of interlocking rivets are required and, hence, structural integrity of the part is not compromised; and

(f) Overall reduction in the constraints placed upon the design complexity of the PMH component

As implied by its name, the direct-adhesion PMH technology relies (at least partly) on polymer-to-metal adhesion to attain the required level of mechanical connectivity between the two materials. In our previous work [5.5] various possible polymer-to-metal adhesion mechanisms (such as micro-scale mechanical interlocking, metal-substrate priming, chemical

modifications of the plastics, etc.) were reviewed with respect to suitability and potential for use in the direct-adhesion PMH technology. In the present chapter, a comprehensive set of the computational analyses is carried out in order to assess feasibility of the direct-adhesion PMH technology with respect to meeting the strength, stiffness, durability and manufacturability requirements for a typical load-bearing BIW component as well as the requirements concerning compatibility with the BIW manufacturing process chain.

The organization of the chapter is as follows: The selection of a prototypical PMH component to be analyzed and its geometrical model are presented in Section 5.3.1. Determination of the functional requirements for the selected PMH component is carried out in Section 5.3.2. Details concerning the replacement of the all-metal design of the component in question and its PMH rendition are discussed in Section 5.3.3. Manufacturability of the high-strength steel sheet-metal subcomponent is investigated in Section 5.3.4. Hybridization of the component using a rib-like plastic substructure and manufacturability of the component in its PMH rendition by injection molding are discussed in Section 5.3.5. The results obtained in the present work are presented and discussed in Section 5.4. The key conclusions resulted from the present work are summarized in Section 5.5.

5.3. Computational Procedures

5.3.1. Geometrical Model for a Prototypical PMH Load-bearing BIW Component

Suitability of the direct-adhesion PMH technology for use in load-bearing automotive BIW components is investigated in the present work by carrying out a set of computational analyses. A prototypical load-bearing BIW component, the rear cross-roof beam, Figures 5-3(a)-(b), is used in all the analyses. In its original all-metal rendition, Figure 5-3(a), the rear cross-roof beam consists of two metal stampings spot welded to each other along the flanges to form a close-box beam-like component. The ends of the rear cross-roof beam are spot welded to a pair of

brackets and attached to the C-pillars. In addition to providing a load-path between and a lateral support for the C-pillars, the rear cross-roof beam provides support for the roof panel and the rear window. In its PMH rendition, the rear cross-roof beam contains only the lower steel stamping and its interior is hybridized with injection-molded plastic ribbing substructure, Figure 5-3(b).

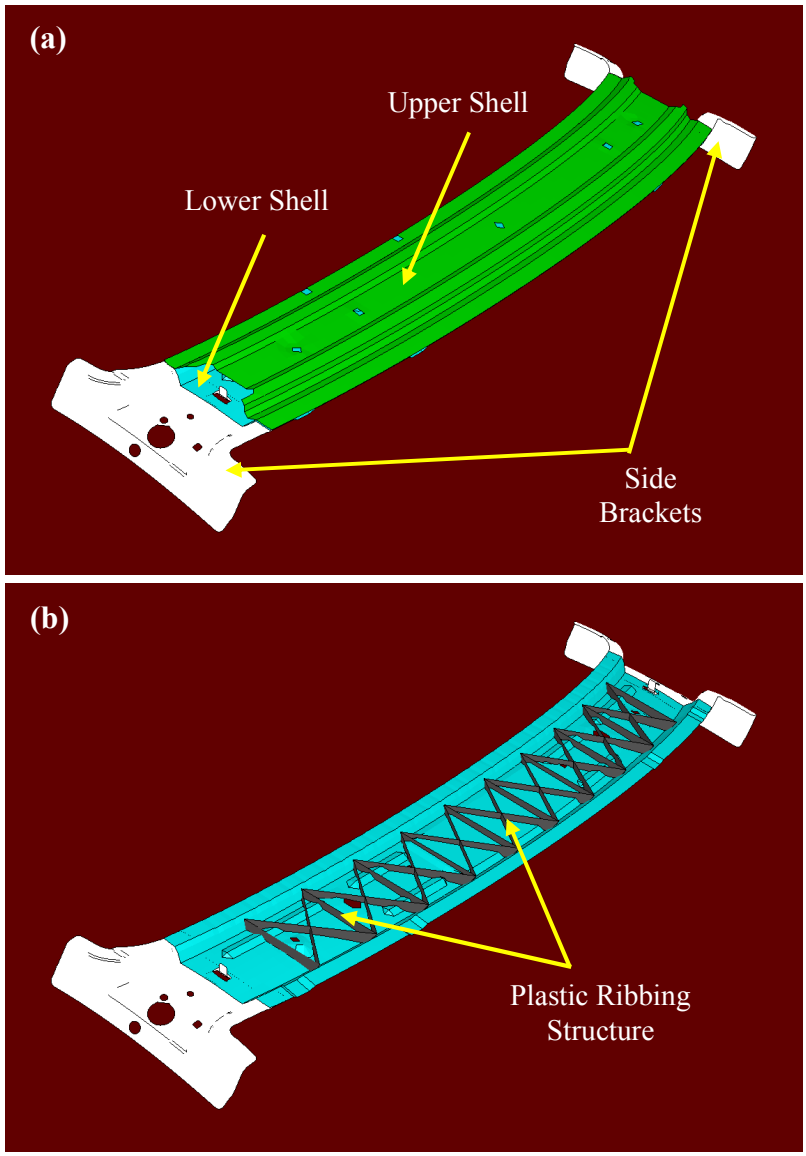

Figure 5-3: A Rear Cross-roof Beam with the Adjoining Side Brackets Analyzed in the Present Work: (a) the All-metal Design; and (b) the PMH Rendition

5.3.2. Determination of the Functional Requirements

The starting assumption in the present work is that the rear cross-roof beam in its original all-metal design is made of 0.6mm thick Cold Rolled Drawing Quality (CRDQ) formable steel with a nominal yield-strength of ca. 186MPa and that it satisfies all the strength, stiffness, durability and manufacturability requirements. Since the quantitative measures of these requirements were not available at the beginning of the present work, they were determined computationally. A set of structural-mechanics finite-element analyses is carried out and the results used to define the functional requirements for the direct-adhesion PMH-rendition of the rear cross-roof beam component. Specific computational analyses carried out in the present work included:

(a) Quasi-static bending, torsion and compression analyses to assess the component's stiffness and, possibly, its buckling resistance;

(b) Dynamic impact analyses to assess the components ability to absorb energy (referred as the component's dynamic strength); and

(c) Single-step stamping manufacturing process analyses to confirm manufacturability of the original formable-steel metal subcomponent and examine manufacturability of its high-strength steel rendition.

In all the finite element analyses carried out in the present work, the following coordinate system was used: (a) the positive x-direction goes from the rear to the front of the vehicle, (b) the positive y-direction goes from the passenger (right-hand) side to the driver (left-hand) side, and (c) the positive z-direction is oriented upward.

5.3.3. Twin-shell to Single-shell Transition

As a first step toward the hybridization of the rear cross-roof beam, the upper shell is removed and the sheet-metal thickness is increased until the original dynamic strength (i.e. the energy absorption capability) of the component is restored. Since the steel grade used at this point

is identical to the one used in the original twin-shell design and since the close-box shell is, in general, structurally more efficient than an open-box shell, the twin-shell to single-shell redesign of the rear cross-roof beam, with the attainment of the component strength, is typically accompanied by a weight increase. Furthermore, due to the larger sheet-metal thickness in the case of single-shell design, the component manufacturability by stamping needs also to be reconfirmed. Details pertaining to the stamping-process manufacturability analyses carried out in the present work can be found in Section 5.3.4. As far as the restoration of the dynamic strength in the single-shell all-metal rendition of the rear cross-roof beam is concerned, it was found to take place when the sheet-metal thickness was increased to at least 1.5mm (the initial sheet metal thickness in twin-metal shells was 0.6mm).

Next, a set of dynamic impact analyses is carried out using the single-shell design but with steel grades with progressively higher yield-strength levels. For each steel grade, this sheet-metal thickness is lowered until the component strength requirements are exactly met. At this point, manufacturability of the component by stamping is examined. If the component is found to be manufacturable, the procedure is repeated until a further increase in the steel-grade strength would result in a component which can not be made by a single-stage stamping process without possibility for blank wrinkling and/or cracking/splitting. At this point, the last steel grade used is accepted as the final material choice and the steel strength (as well as the other mechanical properties) not varied in the remainder of the work.

5.3.4. Stamping-process Manufacturability Analysis

Suitability Manufacturability of the lower shell by a single-step stamping process has been investigated using Altair Engineering's HyperForm software, 1 Step module [5.13], a finite-element based sheet-metal forming simulation program. For the given shape of the metal stamping and its thickness and for the given set of mechanical properties of the steel used,

HyperForm provides several forming-feasibility criteria to assess critical areas with potentials for formation of wrinkles and splits, or localized thinning. In addition, HyperForm enables an accurate prediction of the original blank shape (important for improved material utilization) and provides fast assessment of various forming scenarios.

Within the 1Step HyperForm program used in the present work, one of the so-called "*Inverse One-Step*" methods is implemented. In an inverse one-step method, the finished part shape is the only geometry input. Further inputs pertain to the specification of material properties, friction coefficient, and external boundary conditions. Inverse one-step methods are therefore very useful for use in the early (product design and design for manufacturability) feasibility analyses. In these types of analyses, very little may be known about the intended tooling process or tooling information may not even be available. Thus, the inverse one-step geometry-only analyses render predictions regarding potential blank thinning, wrinkling and/or splitting based solely on the final shape of the stamped component. In other words, the effect of tool timing during the stamping process is not taken into consideration.

The basic procedure carried out in an inverse one-step analysis is as follows: (a) The final shape of the stamped part is input into the program along with material properties, friction coefficient, binder surfaces and the binder pressure; (b) That finished shape is then flattened to obtain the original blank shape. As the final part is being flattened, its mesh will be stretched and/or compressed; and (c) The computed mesh distortions are then inverted (i.e. it is assumed that as the initial blank is being stamped into the final part, it will undergo the strains which are inverses of the strains calculated during the final-part flattening process. Clearly, the procedure described is overly simplified and does not fully account for the role of tooling. Nevertheless, the inverse one-step method was used in the present work since the tooling information was not available.

Within the HyperForm, the average flow strength of steel, (defined as a true-stress rather than an engineering-stress quantity) is defined by the following power-law relation:

$$\bar{\sigma} = K\left(\varepsilon_0 + \bar{\varepsilon}\right)^n \tag{5.1}$$

where K is a strength coefficient, ε_0 a pre-strain coefficient defined as: $\varepsilon_0 = \left(\sigma_y / K\right)^{\frac{1}{n}}$, σ_y the initial yield strength, $\bar{\varepsilon}$ an equivalent plastic strain (defined as a true-strain not as an engineering-strain quantity) and n strain hardening exponent. The strength coefficient is normally defined as: $K = \sigma_{UTS}\left(e^n / n^n\right)$ where, σ_{UTS} is the ultimate tensile strength (defined as an engineering-stress quantity) and $e = 2.718$

Another important property of sheet-steel is the thinning resistance, typically referred to as the *R* value. The *R* value is a simple measure of the deep-drawability of a given sheet metal and typically has different values in in-plane directions with an angle of 0^o, $\pm 45^o$, and 90^o with respect to the rolling direction. The *R* value is defined as a ratio of the true lateral strain and the true through-the-thickness strain obtained in a sheet-metal tensile test. Based on the average *R* value one can construct a Formability limit diagram (*FLD*) which graphically identifies the major strain (the maximum tensile strain)/ the minor strain (the other in-plane strain) deformation states, which can potentially lead to the formation of wrinkles and splits. A schematic of the FLD diagram is depicted in Figure 5-4.

The right-hand side of the FLD in which both the major and minor strains are positive (tension) corresponds to the deformation states found in bi-axially stretched areas of a blank. Conversely, the left-hand side of the plot where the minor strain is negative (compression) corresponds to the deformation states typically found in deep-drawn sections of a blank. Several curves are identified in Figure 5-4. The top-most curve labeled "*FLC*" (stands for the Formability

Limit Curve) separates a *"safe"* region (below the curve) from a *"non-safe"* region (the region above the curve in which splits in sheet-metal blanks are likely to occur). On the right-hand side of the FLD diagram, a *"+45^o Stretch"* line is also drawn and correspond to the balanced biaxial stretching condition under which the major and the minor strain are numerically equal. Clearly, no deformation states below this line are allowed since such deformation states will make the minor strain larger than the major strain. On the left hand side of the FLD plot, there is a *"Tension"* line which defines the major vs. minor strain relation obtained in a simple tensile test. The *"-45^o Draw"* line corresponds to the case when the major strain and the minor strain are of equal magnitude (i.e. when the through-the-thickness strain is zero). Lastly there is a *"Compression"* line which defines the major-strain vs. minor-strain relation under an in-plane compression test. The critical areas on the deep-drawing side of the FLD are above the FLC line (implies splitting) and below the -45^0–Draw line (implies potential wrinkling). The areas just below the -45^0–Draw line have lower tendency for wrinkling formation than the areas under the Compression line. Operationally, to minimize the tendency for splits formation, the FLC line is lowered by several percents along the major-strain axis and the resulting line referred to as the *"Marginal FLC"* line.

For different steel grades considered in the present work, the FLD has been constructed using the following procedure. The +45^o-Stretch,-45^o-Draw, Tension and Compression lines are readily determined from the knowledge of the average *R* value, To construct the FLC (and, thus, the marginal FLC) lines additional information is required before they can be constructed. In the present work, the Keeler model [5.10] was used to assess the *"plane-strain"* FLC point (i.e. the major-strain value corresponding to the zero minor-strain value at the FLC curve). The Keeler model defines this level of the major strain in percents as:

$$FLD_O = \frac{n}{0.21}\left[23.3 + 14.1t\right] \tag{5.2}$$

where t is the steel-sheet thickness in mm. The remainder of the FLD is obtained by employing the computational procedure proposed by Pepelnjak and Kuzman [5.11] which relies on numerical simulations of the Marciniak testing procedure using ABAQUS/Standard finite element program. A detailed account of this procedure will be presented in a future communication. Curve fitting of the computational results revealed that they can be represented quite well using the following functions for the left-hand and the right-hand sides of the FLD diagrams, respectively:

$$e_{major}^{left} = \ln(1 + FLD_0) - e_{\min or} \tag{5.3}$$

and

$$e_{major}^{right} = \ln(1 + FLD_0) + 0.18(1 - e^{-5.838(e^{e\min or} - 1)}) \tag{5.4}$$

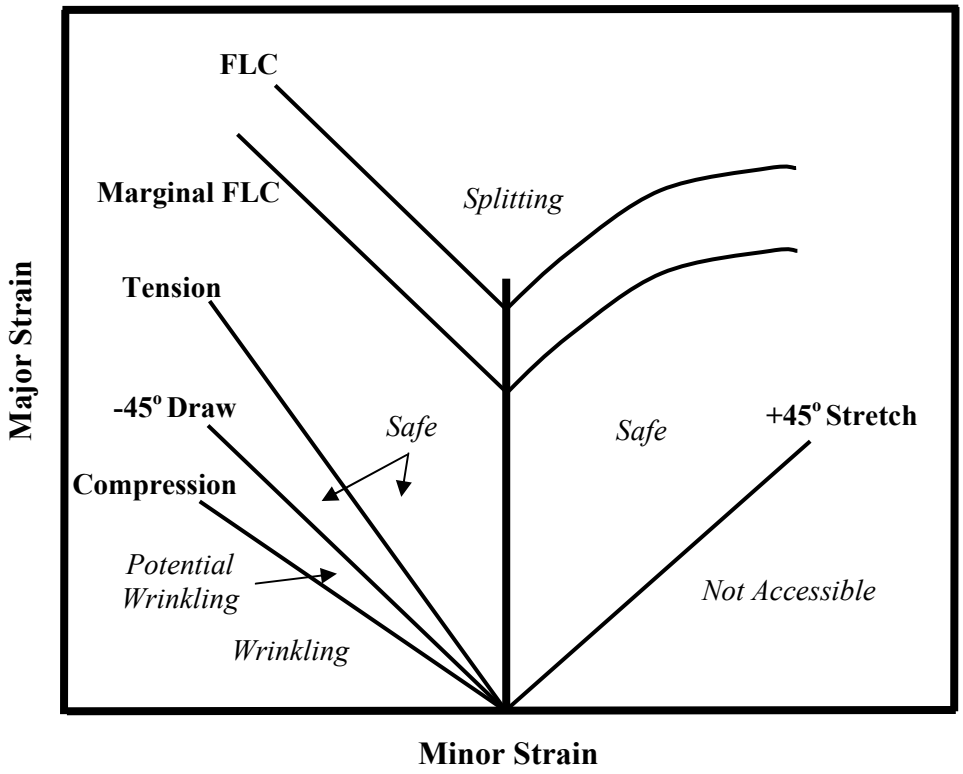

Figure 5-4: A Schematic of the Formability Limit Diagram (FLD)

5.3.5. Hybridization of Single-shell Component

The next step in a series of computational analyses is to introduce an injection-molded ribbing substructure into the single-shell component interior and to increase the rib-wall thickness until stiffness requirements for the component are met. In our previous work [5.6], a comprehensive design concept-level (topology) and detailed-level (size and shape) optimization analyses were used to identify the optimal design for the injection-molded plastic substructure. Consequently, the optimal design of this substructure obtained in Ref. [5.6] is adopted in the present work and, in order to attain the needed level of stiffness and buckling resistance, only the thickness of each rib is increased using a constant scaling factor.

It should be also noted that, as discussed in our previous work [5.7], to attain the required level of polymer-to-metal adhesion strength, the interior of the single-shell component should be

cold-gas sprayed (prior to injection molding) with 0.2-0.3mm-thick layer of the same material as the one used for the injection molded substructure. This approach ensures: (a) that drawing compound/oil residues are removed from the metal surface: (b) that the sprayed material forms an overcoat which is fully conformed with the substrate (critical for the attainment of good mechanical interlocking between the sprayed plastic and the metal); and (c) provides an ideal substrate for adhesion of the injection-molded rib-like substructure.

In all quasi-static calculations of the bending, torsion and compression response of the rear cross-roof beam in its PMH rendition, a constant (conservative) value of the polymer-to-metal adhesion strength between the sprayed overcoat and the metal substrate (σ_{adh}=5MPa) is used since such level of adhesion is attainable through direct-adhesion effects [1]. Furthermore, perfect bonding is assumed between the overcoat and the injection-molded plastic substructure.

As it was done in our previous work [5.1,5.5-5.9], the plastic substructure is assumed to be made of Durethan BKV 130 H2.0 (a 30wt.% glass-fiber filled Nylon 6, elastomer modified with enhanced heat-age resistance). The following rheological and thermal properties of Durethan BKV 130 H2.0 were used in the injection molding mold-filling, material-packing and part cooling analysis (discussed in next section): the viscosity is shear-rate and temperature dependent and was defined using the cross-WLF model as presented in our previous work [5.1], specific heat, C_p= 1909J/kg·K, thermal conductivity, k=0.14W/m·K, glass transition temperature, $T_{trans=}$479.0K. In addition, the following thermo-mechanical properties were used for the in-mold stress-development, post-ejection shrinkage/warping and quasi-static and dynamic structural analyses of the PMH rendition of the rear cross-roof beam: Young's modulus, E=7GPa, Poisson's ratio, ν=0.4, yield strength, σ_y=150MPa, linear strain-hardening tangent modulus, h=100MPa, linear thermal expansion coefficient, α=4·10^{-5}.

It should be noted, however, that the thermo-mechanical properties for Durethan BKV 130 H2.0 given above pertain to the properties of this material in its *as-received* (isotropic) condition. The actual properties used in the in-mold stress-development, post-ejection shrinkage/warping and quasi-static and dynamic structural analyses were both anisotropic and non-uniform throughout the part and were obtained by combining the mold-filling results pertaining to the local orientation of the glass-fibers with a rule-of-mixture computational scheme for determination of the effective (two-phase) material properties [5.1]. That is, interactions between the melt flow and the glass-fiber reinforcements generally lead to the alignment of the fibers with the local flow direction, and, in turn, cause the fiber-reinforced injection-molded plastic material to become anisotropic. The information regarding the spatial distribution of the (anisotropic) material properties resulting from the Moldflow mold-filling /packing calculations (stored in a *.xml* type file) is converted using a general mathematical package Matlab [5.15] into a material-data file. The syntax of the material file was made consistent with the requirements of ABAQUS/Standard and ABAQUS/Explicit [5.14].

The overcoat-plastics/substrate-metal interfaces have been modeled in the present work using the *"cohesive zone framework"* originally proposed by Needleman [5.16]. The cohesive zone is assumed to have a negligible thickness when compared with other characteristic lengths of the problem, such as the plastics-wall thickness, the width of metal-stamping grooves, or the characteristic lengths associated with the stress/strain gradients. The mechanical behavior of the cohesive zone is characterized by a traction–displacement relation, which is introduced through the definition of an "*interfacial potential"*. The perfectly bonded plastic/metal interface is assumed to be in a stable equilibrium, in which case the potential ψ has a minimum and all tractions vanish. For any other configuration, the value of the potential is taken to depend only on the displacements discontinuities (jumps) across the interface. A comprehensive account of the

constitutive law used to model the overcoat-plastics/substrate-metal adhesion can be found in our recent work [5.9] and hence will not be considered here any further.

All the quasi-static bending, torsion and compression analysis of the single-shell rear cross-roof beam in the PMH rendition were carried out using the same procedure as the one presented in Section 5.3.2 for the twin-shell all metal design of this component.

5.3.6. Manufacturability of the PMH Component by Injection Molding

Finally, manufacturability of the PMH component by a standard insert injection molding process is investigated. The objective is to ensure that the component is free of flaws (e.g. weld lines, entrapped air, incompletely-filled sections, excessive in-mold residual stresses which can cause distortions/warping of the PMH component after ejection from the mold, etc. Such manufacturability analysis is carried out in the present work using Moldflow Plastic Insight computer program [5.12]. Since a detailed discussion pertaining to the use of this program was presented in our recent work [5.1], only a brief overview is given here.

Within Moldflow, mass, momentum and energy conservation equations are solved numerically to model the processes associated with polymeric-melt mold filling, mold packing, melt solidification, polymer reinforcing-fiber orientation distribution, in-mold residual stress development, etc. To carry out the manufacturability analysis, the final design of the PMH component is directly imported in Moldflow, runner system and gates constructed, a cooling system provided (if required) and a mold filling/packing analysis carried out. The analysis carried out in the present work was particularly useful for identification of the minimal manufacturable rib-wall thickness, the optimal locations of injection points (gates) with respect to minimization of the effects of unbalanced flow, failure-conducive weld-lines, air traps, etc.

Since perfect adhesion is considered at the plastic-overcoat/injection-molded plastic interfaces, the in-mold stresses could be calculated using the *"Stress*" module of Moldflow

Plastics Insight. While the injection-molded PMH component resides in the mold, it is constrained and can not distort. However, after ejection, the component can undergo shrinkage and warping. Due to the presence of adhesion at the overcoat-plastics/substrate-metal interfaces, shrinkage and warping analyses were carried out using ABAQUS/Standard. In these analyses, the same finite element mesh is utilized as that used in the filling and packing analyses, except that a set of interfacial cohesion elements is added to model explicitly the effect of adhesion at the plastics/metal interfaces. Furthermore, the computed in-mold stresses, as well as temperatures and element-based through-the-thickness variations in thermo-mechanical properties of the injected thermoplastic material are exported from Moldflow Plastics Insight to ABAQUS/Standard. The exported in-mold stresses and temperatures are then used to define the initial conditions in the PMH component right after its ejection and, in turn, to construct the loading term in the coupled thermo-mechanical finite element equations. Next, a boundary condition is applied by constraining all six degrees of freedom for a single node of the metal stamping in order to prevent the PMH component from undergoing a rigid body motion. Also, free convection boundary conditions are prescribed on all free surfaces. Furthermore, since the ejected PMH component spends some amount of time at the temperature at which thermoplastics exhibit viscous behavior, a linear visco-elastic residual-stress and warping finite element analysis is performed in the present work.

5.4. Presentation of the Results and Discussion

5.4.1. Geometrical Model for a Prototypical PMH Load-bearing Component

All sheet-metal and injection-molded plastic components analyzed in the present work are modeled as shell parts with a constant thickness. A typical mesh used in the present work is displayed in Figure 5-5. Typically, an average element edge-length of ca. 10mm was used. The upper and the lower metal shells are joined along their flanges using 5-mm diameter spot welds at

a center to center distance of ~10mm. In the same way, the side brackets are joined to the lower shell. During the dynamic impact analysis, the roof panel was utilized, Figure 5-5, (in addition to the components mentioned earlier) and it was also spot welded to both the upper/lower shell and the side brackets. The spot welds are modeled as Cartesian and Cardan connectors whose mechanical properties were given in our prior work [5.1].

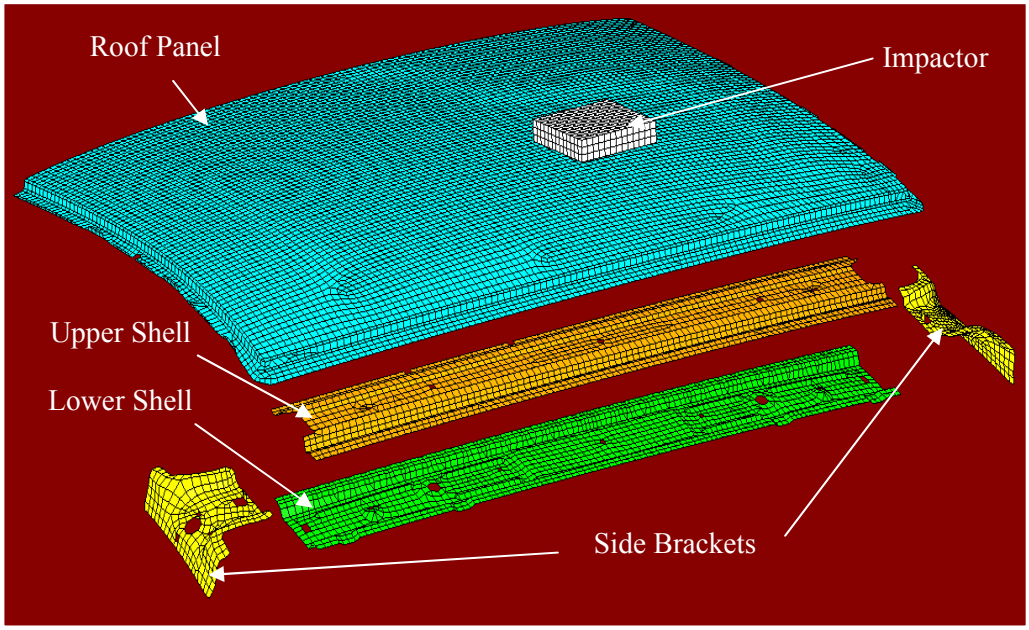

Figure 5-5: Typical Finite Element Meshes Used in the Quasi-static and Dynamic-impact Analyses of the Rear Cross-roof Beam Assembly

Quasi-static (bending, torsion and compression) tests were conducted by first defining two coupling surfaces (one at each end bracket). Loading is then applied by defining the displacement-based boundary conditions to the reference nodes of these coupling surfaces. Contact interactions between the adjacent components are modeled using a *hard-contac*t algorithm (i.e. direct contact of the surfaces is required for the contact pressure to develop) with a friction coefficient of 0.15. The stiffness and the corresponding buckling resistance of the rear cross-roof beam with respect to a given mode (bending, torsion, compression) of loading is obtained by monitoring the relations between the reaction force/reaction-moment and the corresponding displacement/ rotation at one of the coupling-surface reference nodes. All quasi-static calculations were carried out using ABAQUS/Standard; a finite-element general purpose computer program [5.14]

Dynamic impact analyses were carried out using ABAQUS/Explicit finite-element computer program [5.14]. In a typical dynamic impact analysis, a 500kg square-shaped plate is propelled at a 40 km/h initial speed in the negative vertical direction towards the roof-panel covered rear cross-roof beam. The edges of the side brackets, and the outer edges of the roof panel (other than the one which were spot welded to the upper/lower metal shell) are kept fixed. The dynamic strength of the rear cross-roof beam is quantified by the maximum downward intrusion of the plate. Contact interactions between the plate and roof panel as well as between the other components are modeled using the same hard-contact algorithm described above. To prevent hour-glassing of the reduced-integration shell elements, a default value of the hourglass stiffness was used.

5.4.2. Determination of the Functional Requirements

Typical quasi-static computational results pertaining to the functional-requirements determination for the original twin-shell all-metal rear cross-roof beam are displayed in Figures 5-6-5-8 for the bending, torsion and compression load cases, respectively. In Figures 5-6-5-8, part (a) shows the deformed configuration while part (b) displays the corresponding mechanical-response curve. In Figures 5-6(b), 5-7(b) and 5-8(b), the initial slope of the mechanical-response curves is used to quantify the component's stiffness, while the maximum value of the reaction-force/reaction-moment is used as a measure of the component's buckling resistance (both with respect to the given mode of loading).

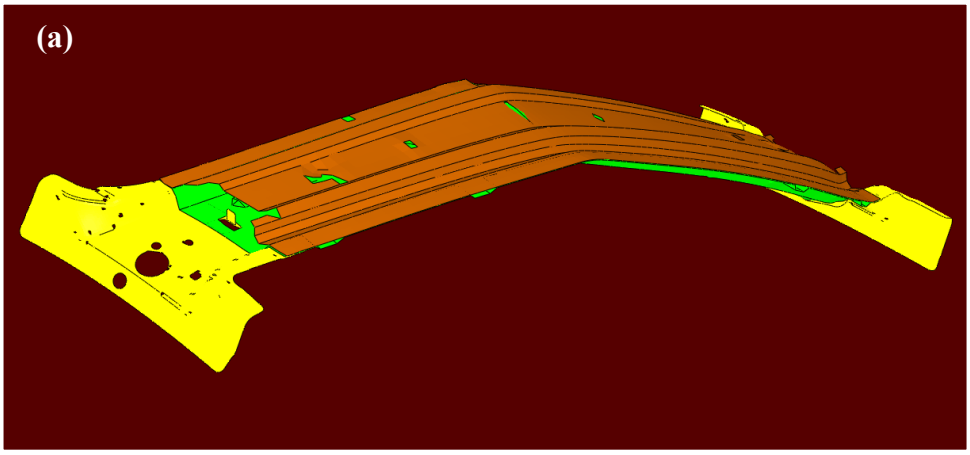

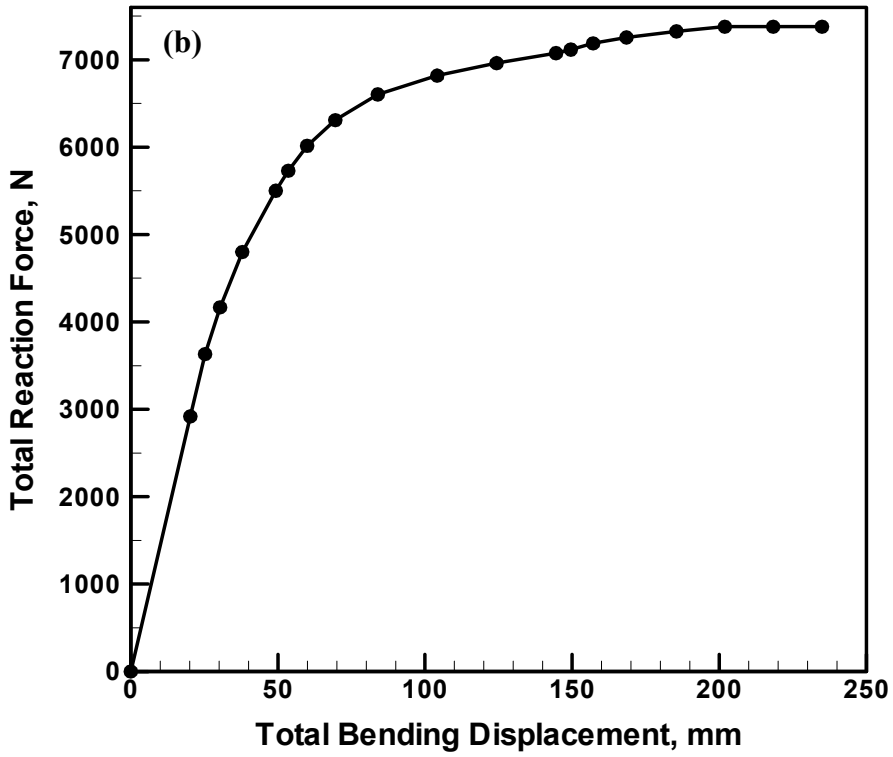

Figure 5-6: Typical Deformed Configuration Obtained in the Quasi-static Bending Analysis; and (b) the Corresponding Mechanical Response Curve

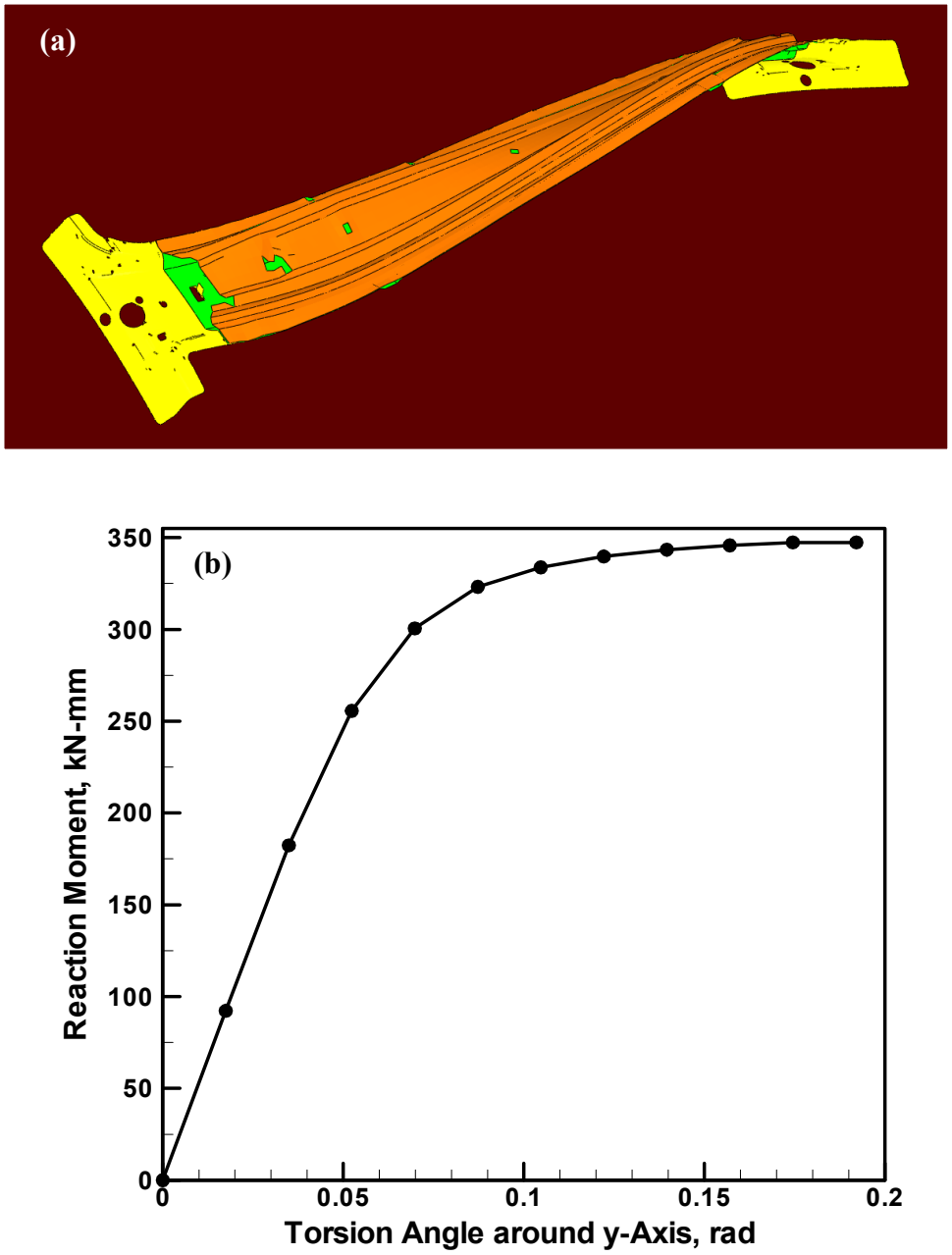

Figure 5-7: Typical Deformed Configuration Obtained in the Quasi-static Torsion Analysis; and (b) the Corresponding Mechanical Response Curve

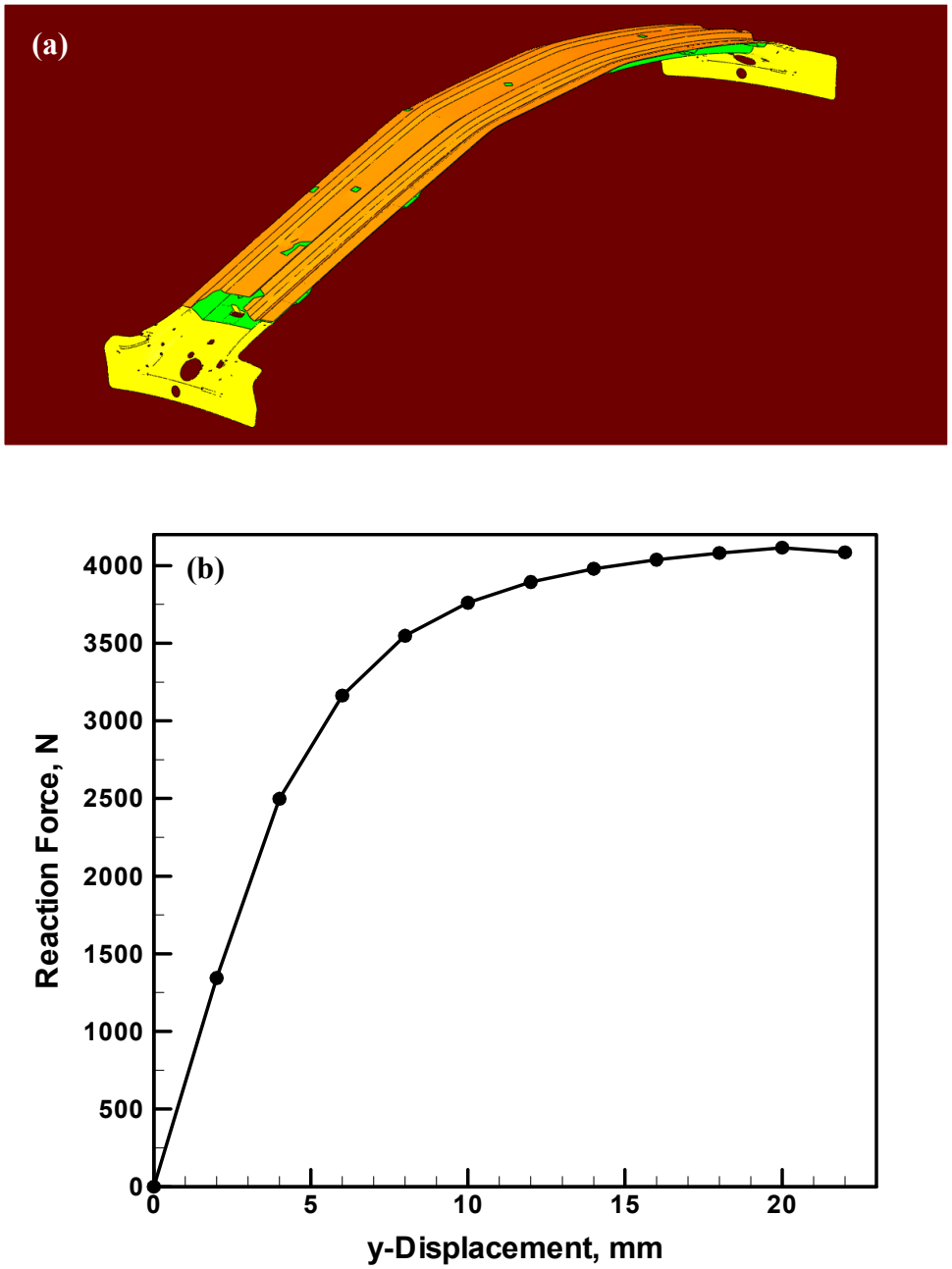

Figure 5-8: Typical Deformed Configuration Obtained in the Quasi-static Compression Analysis; and (b) the Corresponding Mechanical Response Curve

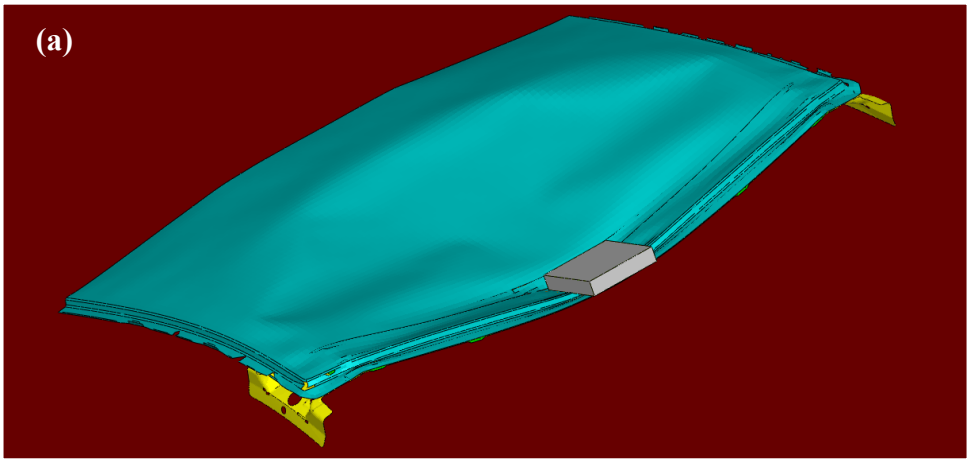

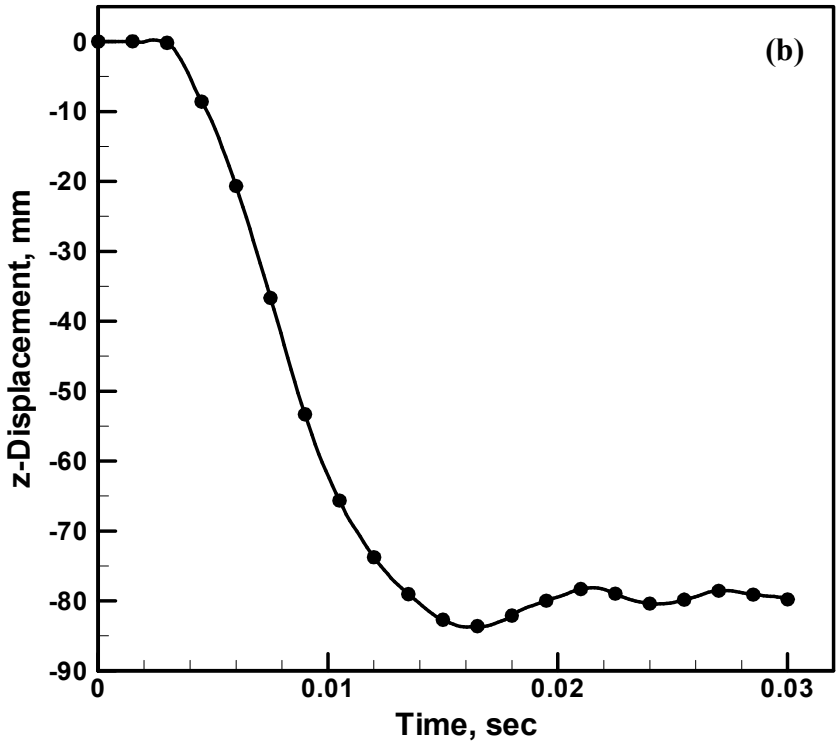

Figure 5-9: Typical Deformed Configuration Obtained in the Dynamic-impact Analysis and (b) the Corresponding Temporal Evolution of the Displacement at One of the Nodes of the Lower Shell

Typical results obtained using the dynamic-impact analyses are displayed in Figures 5-9(a)-(b). The deformation of the rear cross-roof assembly resulting from its impact by the 500kg steel plate propelled at a velocity of 40km/h in the negative vertical direction is displayed in Figure 5-9(a) while the corresponding temporal evolution of the vertical displacement of a node (located at the lower shell halfway both in the length and the width directions) is displayed in Figure 5-9(b). The maximum value of this displacement is used to quantify the dynamic material strength (i.e. the lower is this displacement, the higher is the component's dynamic strength).

As discussed earlier, the results presented in Figures 5-6(b), 5-7(b), 5-8(b) and 5-9(b) are used to define the quasi-static and dynamic structural requirements which must be met by the PMH rendition of the rear cross-roof beam, at a significantly lower component weight to warrant the associated increased manufacturing/material cost. It should be also noted that in all the calculations carried out in this section, it was assumed that the rear cross-roof beam (and the surrounding components) are made of a Cold Rolled, Drawing Quality (CRDQ) steel with a yield strength of 186MPa and the ultimate tensile strength of 315MPa.

5.4.3. Twin-shell to Single-shell Conversion and High–strength Steel Introduction

The results of the conversion from the twin-shell design to a single-shell design and of the substitution of the CRDQ steel with one of the high-strength steel grades for the all-metal rendition of the rear cross-roof beam are displayed in Figure 5-10. In the plot displayed in Figure 5-10, the initial yield strength of the steel grade used is plotted along the horizontal axis while the corresponding minimum lower-shell sheet-metal thickness needed to meet the dynamic-strength requirement of the component is shown along the y-axis. As expected, as the yield strength of the steel increases, the minimal required lower-shell sheet-metal thickness is reduced. The thickness decrease is monotonic but not linear (i.e. somewhat larger sheet-metal thickness reductions are encountered at lower steel yield-strength levels).

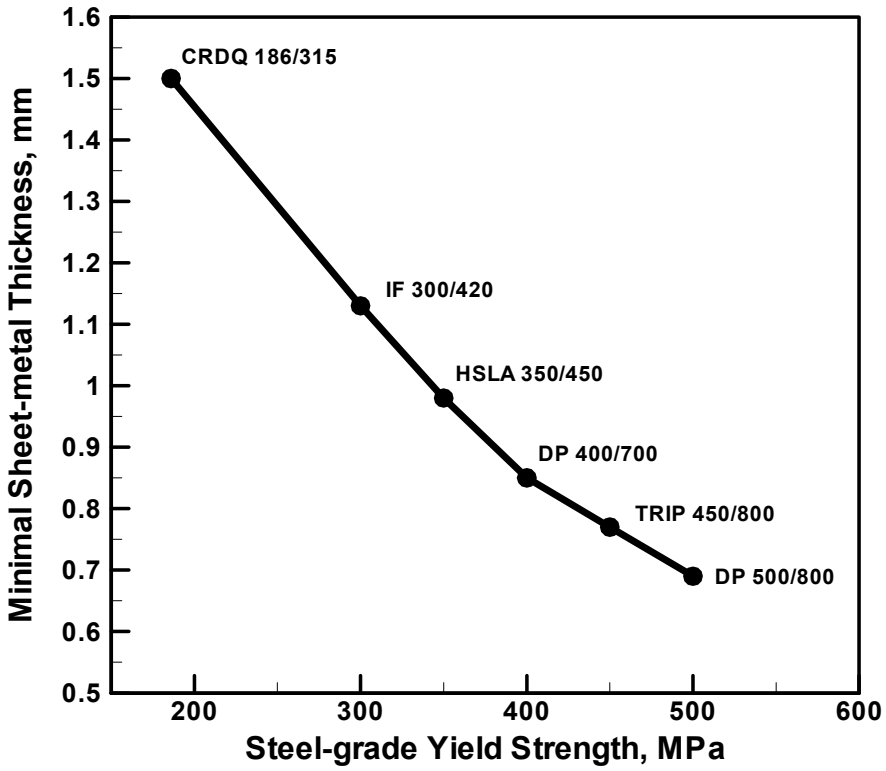

Figure 5-10: Variation of the Minimal Lower-shell Sheet-metal Thickness Needed to Ensure the Required Level of the Dynamic Strength of the Component as a Function of the Steel-grade Initial Yield Strength. Nomenclature: CRDQ - Cold Rolled, Drawing Quality; IF - Interstitial Free; HSLA - High Strength Low Alloy; DP - Dual Phase; TRIP - TRansformation Induced Plasticity; and e.g. 186/315 - Initial Yield Strength/Ultimate Tensile Strength

As indicated in Figure 5-10, a number of high-strength steel grades were investigated in the present work. A comprehensive summary of the mechanical and sheet-metal properties of these steel grades is provided in Table 5-1. The data listed in Table 5-1 were collected using variety of public-domain sources [5.13,5.17,5.18].

Table 5-1: Mechanical and Sheet-metal Properties of the Steel Grades Used in the Present Work

Property	Steel Grade					
	CRDQ 186/315	IF 300/420	HSLA 350/450	DP 400/700	TRIP 450/800	DP 500/800
E, Young's Modulus, (GPa)	210	210	210	210	210	210
ν, Poisson's Ratio	0.3	0.3	0.3	0.3	0.3	0.3
R_0, 0^o Thinning Resistance	1.6	1.6	1.1	1	0.9	1
R_{45}, 45^o Thinning Resistance	1.6	1.6	1.1	1	0.9	1
R_{90}, 90^o Thinning Resistance	1.6	1.6	1.1	1	0.9	1
n, Strain Hardening Exponent	0.22	0.2	0.14	0.14	0.24	0.14
σ_y, Initial Yield Strength, (MPa)	186.16	300	350	400	450	500
K, Strain Hardening Parameter, (MPa)	549.03	759	807	1028	1690	1303
σ_{UTS}, Tensile Strength, (MPa)	315.780	420	450	700	800	800
ε_0, Pre-strain	0.007	0.028	0.010	0.005	0.014	0.005

CRDQ - Cold Rolled, Drawing Quality;

IF - Interstitial Free;

HSLA - High Strength Low Alloy;

DP - Dual Phase;

TRIP - Transformation Induced Plasticity; and

e.g. 186/315 – initial yield strength/ultimate tensile strength.

5.4.4. Stamping-process Manufacturability Analysis

As discussed earlier, as steel-grades with higher yield-strength (and thus with lower ductility and smaller sheet-metal thickness) are used; manufacturability of the lower shell by stamping may become questionable. In fact, it was found that when the initial yield strength of the steel is increased above ~500MPa, the lower shell can not be safely stamped without potential formation of cracks/splits. This finding is displayed in Figures 5-11 and 5-12.

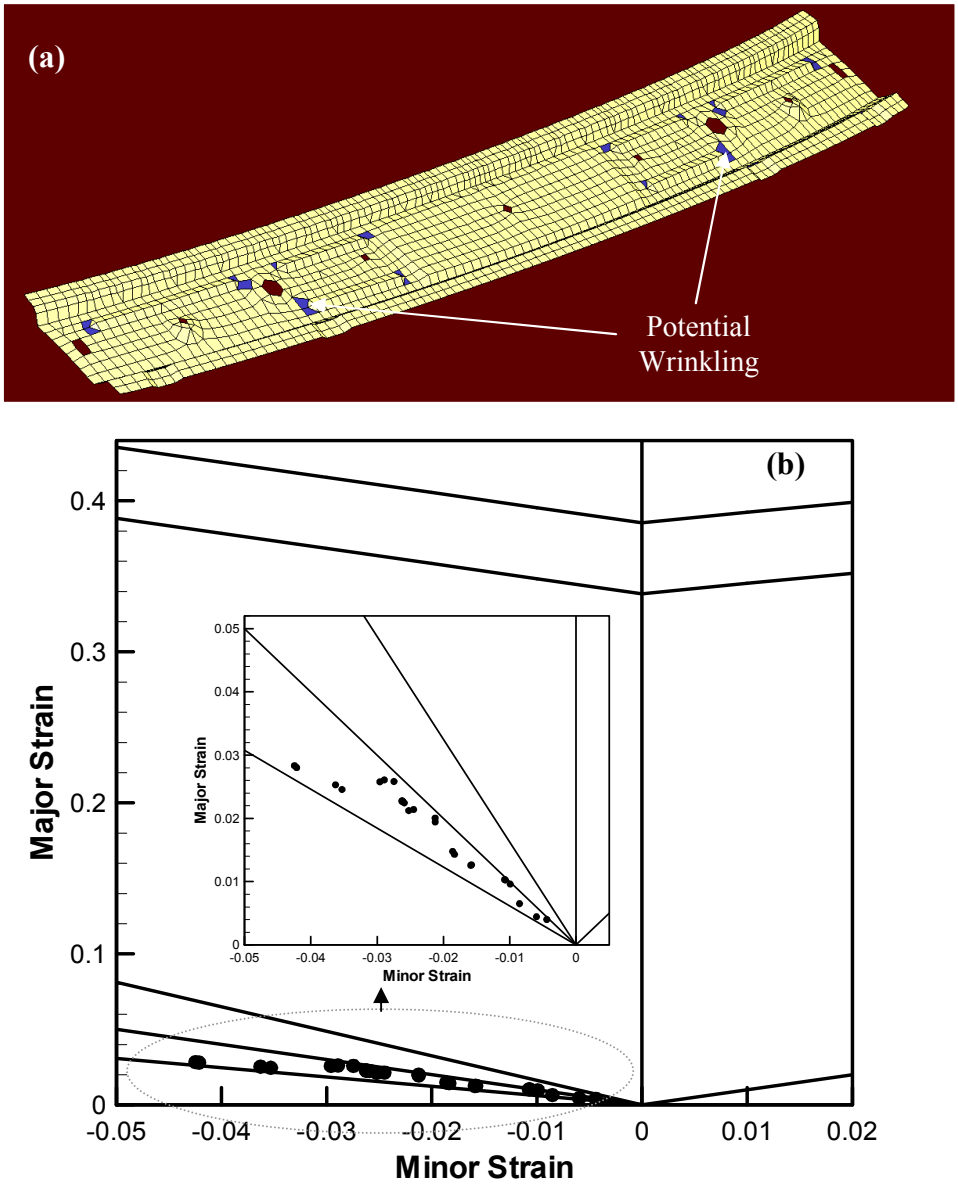

Figure 5-11: Manufacturability by Stamping of the Lower-shell Made of a 1.5mm-thick CRDQ-186/315 Steel Sheet: (a) The Location of Potentially Critical Elements; and (b) the Corresponding Portion of the Formability Limit Diagram (FLD)

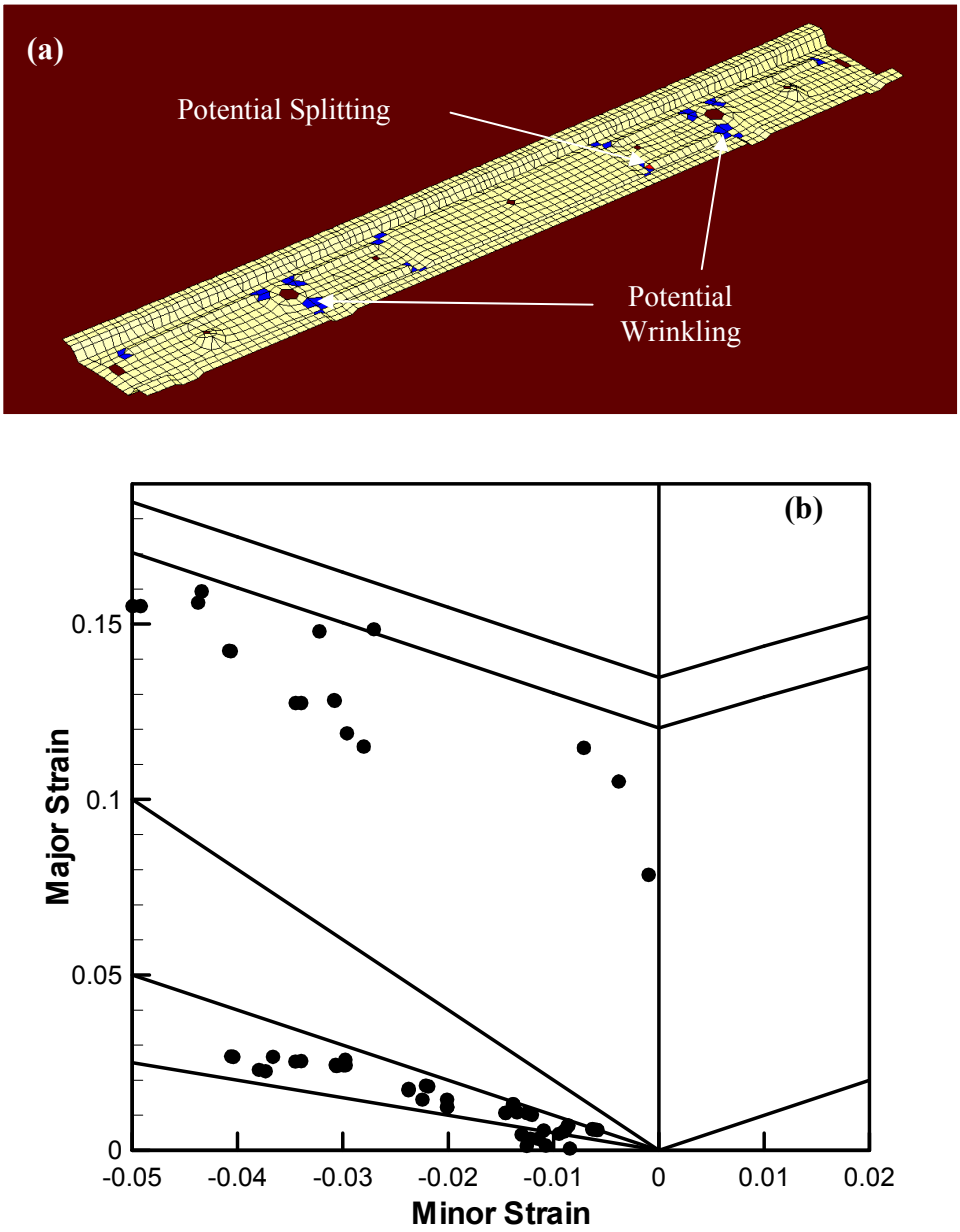

Figure 5-12: Manufacturability by Stamping of the Lower-shell Made of a 0.7mm-thick DP-500/800 Steel Sheet: (a) The Location of Potentially Critical Elements; and (b) the Corresponding Portion of the Formability Limit Diagram (FLD)

In Figure 5-11(a), the elements most likely to cause stamping defects in the case of the Cold Rolled Drawing Quality (CRDQ) steel with a 186MPa yield strength and a 315MPa ultimate tensile strength are identified and labeled accordingly. The corresponding FLD and the major-strain/minor-strain points for these elements are displayed in Figure 5-11(b). It is seen that only few elements have marginal tendency to wrinkle and no elements have tendency to split. The situation is quite different in Figures 5-12(a)-(b) which identify the corresponding elements and their FLD data in the case of Dual Phase (DP) steel with 500MPa yield strength and an 800MPa ultimate tensile strength. A number of elements are prone to wrinkling and marginal wrinkling and one of the elements shows the tendency for marginal splitting. Thus, in the case of the latter steel grade, manufacturability of the defect-free lower shell can not be guaranteed. Based on the results obtained in this section, the maximum yield strength of the steel used is limited to ~500MPa. Furthermore, based on the results displayed in Figure 5-9, the corresponding minimal sheet-metal thickness needed to ensure the required dynamic-strength level in the component is ~0.7mm.

5.4.5. Hybridization of Single-shell Component

The next step in the computational procedure used in the present work was to hybridize the lower shell with a rib-like plastic substructure which is injection molded against the lower shell and adheres to it via the operation of a number of direct-adhesion phenomena (e.g. micron-scale mechanical inter-locking, surface polarization and bonding, etc.). As mentioned earlier design concept-level (topology) and detail-level (size and shape) optimization of the injection-molded rib-like plastic substructure was not carried out in the present work. Rather the results of such analyses carried out in our prior work [5.6] pertaining to the number and the location of the ribs were used. In addition, the thickness of the ribs is increased in small increments until the (bending, torsion and compression) stiffness and buckling-resistance requirements are satisfied.

An example of the results obtained in this section which pertains to the case of the PMH-rendition of the rear cross-roof beam is displayed in Figure 5-13(a)-(b). A deformed configuration is shown in Figure 5-13(a) while the corresponding total-bending-force vs. total bending displacement of the corresponding reference node is depicted in Figure 5-13(b). A comparison of the results shown in Figure 5-6(b) and 5-13(b) shows that both the bending stiffness (quantified by the slope of the initial (linear portion) of the force/displacement curve) and the bending buckling-resistance (defined by the maximum bending force) are at the level or higher than their counterparts in the twin-shell all-metal rendition of the same component. Unfortunately, the weight of the component displayed in Figure 5-13(a) is only 2.1% lower than its twin-shell all-metal counterpart. Meeting the bending (stiffness and buckling-resistance) requirements, as will be discussed in more detail later, turned out to be the most challenging task. In other words all other quasi-static requirements could be satisfied at a substantially higher level of weight reduction in the PMH-rendition of the rear cross-roof beam.

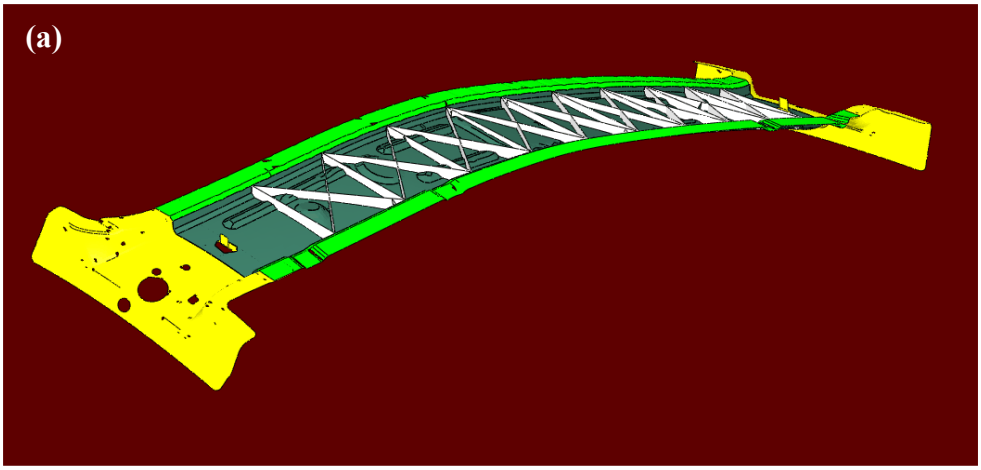

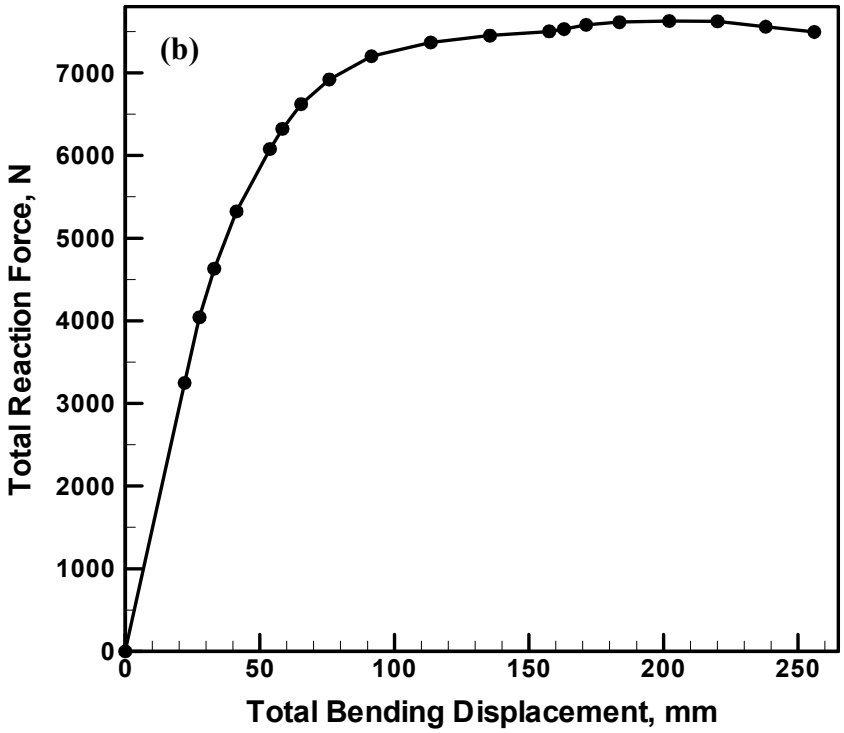

Figure 5-13: (a) Typical Deformed Configuration Obtained in the Quasi-static Bending Analysis of the PMH-rendition of the Rear Cross-roof Beam; and (b) the Corresponding Mechanical Response Curve

5.4.6. Manufacturability of the PMH Component by Injection Molding

Once the injection-molded plastic substructure is designed, its manufacturability by injection molding process is investigated. Due to the fact that the height of the ribs is relatively small, no serious problems were expected to accompany the injection molding process. Nevertheless, considering the fact that the stiffness of the lower shell was significantly reduced (due to the reduction in its wall thickness), and since this may lead to potential warping of the PMH component upon ejection of the mold, a compressive mold-filling, material packing, cooling, and in-mold stress development analysis was carried out using Mold Flow Plastics Insight [5.12]. In addition, a post-ejection component shrinkage and warping analysis was carried out using ABAQUS/Standard.

An example of the results obtained in this portion of the work is displayed in Figure 5-14(a)-(d). The fill-time contour plot displayed in Figure 5-14(a) reveals that the flow is balanced (a critical condition for preventing excessive component distortions upon ejection) and that total fill time is quite short (~2.5-3s).

The orientation of glass fibers used as reinforcements in the polymeric (nylon 6) material is displayed as a contour plot in Figure 5-14(b). The fiber-orientation plot depicted in Figure 5-14(b) reveals the probability for the fiber axis to be aligned with the local 1^{st} principal direction (defined by a line connecting the first and the second node of a finite element at hand). The orientation distribution of fibers affects the extent of orthogonality of the reinforced-plastic material (i.e. a random orientation of the fibers gives rise to an isotropic material while perfectly aligned fibers yield an orthotropic material). As mentioned earlier, the fiber orientation results are combined with a micro-mechanics based homogenization analysis (implemented in Moldflow), to determine the local effective mechanical and thermal properties of the two-phase (polymer +

glass fibers) material. These properties are exported into ABAQUS /Standard and used to carry out post-ejection warping analysis of the part.

A contour plot for the magnitude of the first principal (in-mold) stress component is displayed in Figure 5-14(c). Also displayed in Figure 5-14(c) are the locations of air traps and weld lines. The number of air traps and weld lines and their locations suggests that these defects will not seriously jeopardize the structural integrity of the PMH component.

The in-mold stresses and the corresponding temperature distributions are exported to ABAQUS/Standard and used in a thermo-mechanical analysis of post-ejection warping of the component. Likewise, the effective spatially-dependent mechanical and thermal properties of the injection-molded glass-reinforced nylon as determined using Moldflow are exported to ABAQUS/Standard and used in the same post-ejection warping analysis. An example of the warping-analysis results obtained is displayed in Figure 5-14(d) where the total nodal displacements for the entire PMH component are shown. Since the maximum nodal displacement of the PMH-component nodes is only 0.1678mm, one may conclude that post-ejection warping is not likely to be a serious problem.

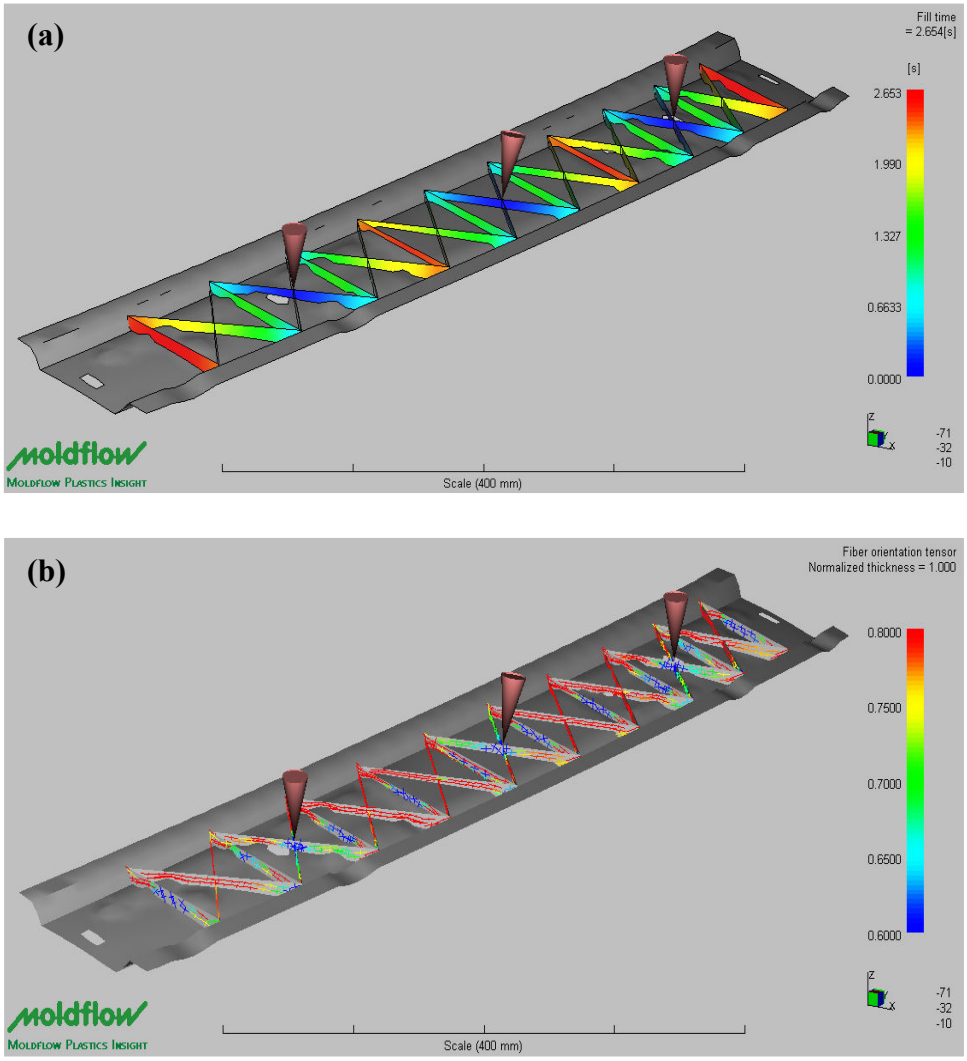

Figure 5-14: A Injection-molding Process Simulation Results: (a) Fill Time; (b) Fiber Orientation Tensor; (c) In-mold First Principal Stress; and (d) Post-ejection Total Warping Displacements

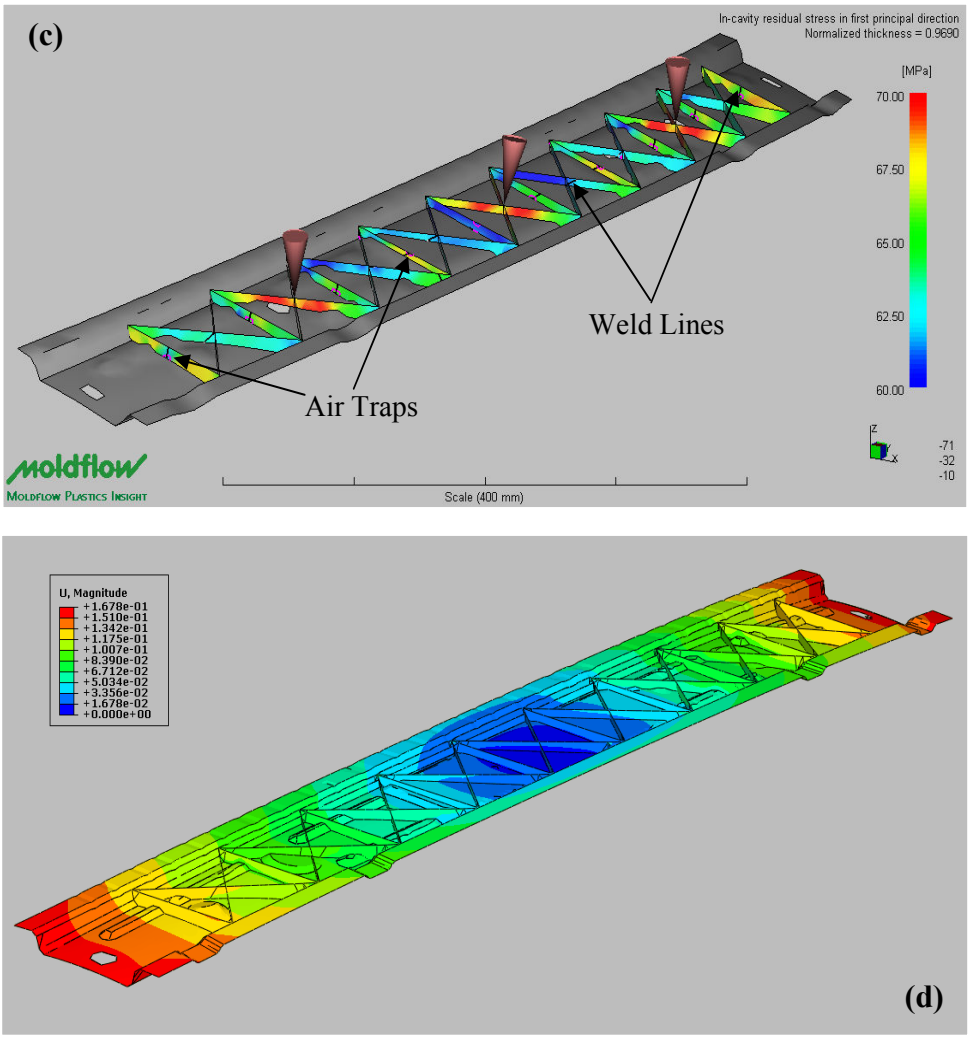

Figure 5-14: Continued…

5.4.7. A Brief Discussion

In the previous section, a comprehensive set of computational results pertaining to the performance and manufacturability of a prototypical PMH load-bearing BIW component was presented. In this section, a brief discussion of these results will be given. Overall, the results presented in Sections 5.4.1-5.4.6 are encouraging suggesting that the direct-adhesion PMH technology combined with the use of high-strength steels has a potential for reducing the component's weight relative to that of the twin-shell all-metal rendition of the same component. This finding is particularly the case if the bending stiffness of the component in question is not the main functional constraint for that component. In other words, the results obtained revealed that the most challenging constraints to be met were the bending stiffness (and bending-induced local buckling). This point is further iterated in Table 5-2 in which a summary of the predicted weight savings in the PMH-rendition of the rear cross-roof beam are listed for different cases of the design-controlling functional requirements. The results displayed in Table 5-2 indicate that, in the case of a design controlled by the bending-stiffness requirements, only a 2.1% weight saving is predicted. In sharp contrast, weight savings up to 7% are anticipated in the case of a torsional-stiffness controlled design. While the identification of the main design-controlling functional requirement typically requires the extension of the structural analysis to the entire vehicle (or at least to the entire subassembly containing the component in question and to the surrounding assemblies), the rear cross-roof beam is mainly required to provide lateral support for the C-pillars. Hence, its compression stiffness and compression buckling resistance appear to be the most likely candidates for the quasi-static structural design-controlling functional requirements. If this is the case, then the use of the direct-adhesion PMH technology and high-strength steel grades can yield weight reductions in a range between 4.5 and 4.9%. Such weight reductions are significant and can justify the associated high cost of the component hybridization.

Table 5-2: Projected Weight Savings for Different Cases of Design-controlling Functional Requirements

Potential Design-controlling Functional Requirements	The Resulting Weight Reduction in the PMH Component, %
Bending Stiffness	<= 2.1%
Bending Buckling Resistance	<= 2.6%
Torsion Stiffness	<= 6.5%
Torsion Buckling Resistance	<= 7.1%
Compression Stiffness	<= 4.5%
Compression Buckling Resistance	<= 4.9%

Another point worth mentioning is that the simple analyses of the stamping and the injection-molding processes suggest that (as long as steel grades with a yield-strength level lower than 500MPa are used and standard injection-molding practices are employed), no serious manufacturability issues should be encountered.

In our future work, the potential of the direct polymer-to-metal adhesion technology for use in race-cars and niche-segment automotive components will be investigated. Also the issues regarding the assembly of the direct-adhesion PMH components into the BIW will be addressed. Our preliminary analyses established that the PMH components in question, as long as they are based on steel stampings, will be integrated into the BIW using spot, seam, laser welding or a combination of these processes. Also, issues related to the end of the life of the vehicle (e.g. disassembly, recycling, etc.) will be investigated.

As correctly pointed out by one of the reviewers of this manuscript, endurance in long term durability of the direct-adhesion PMH components must also be addressed in our future work. It should be pointed out, however, that in our previous work (5.5), a preliminary investigation of reliability and durability of these components was presented. It was shown that

these aspects of long-term performance of the direct-adhesion PMH components are mainly controlled by water/moisture-induced irreversible changes in the injection-molded polymer and at the polymer/metal interfaces. Such irreversible changes include: a) hydrolysis, b) polymer oxidation and c) microstructural damage induced by the formation of micro-cavities etc.

The second reviewer of this manuscript suggested that the authors draw out some more general conclusions regarding the viability of the direct polymer-to-metal adhesion technology in load-bearing BIW automotive applications. Based on the results obtained from the present work and the results obtained from the previous studies (5.1,5.5-5.9). It appears that this technology has a great potential for reducing the weight of the main structural components of the BIW provided the following key aspects of the technology can be successfully handled: a) a low-cost, robust and reproducible process can be developed for attaining polymer-to-metal adhesion strengths in a range between 5 and 10MPa; b) the indicated level of the polymer-to-metal adhesion strength is not seriously compromised by various mechanical, thermal and chemical agents during fabrication, pre-treatment and painting of the BIW; and c) mechanical integrity of the polymer/metal interface is retained after a prolong in-service exposures to varying levels of moisture, road-salt concentrations and temperature.

5.5. Summary and Conclusions

Based on the results presented in this work the following summary and conclusions can be drawn:

1. A comprehensive set of quasi-static and dynamic structural mechanics and sheet-metal forming/ thermoplastic injection-molding process simulation analysis is carried out in order to assess suitability /feasibility of a direct-adhesion polymer-metal-hybrid technology in which metal stampings are made of high-strength low-ductility steels and a typical (5MPa) level of polymer-to-metal adhesion strength is present.

2. The results suggest that the most challenging requirement presented to the direct-adhesion PMH technology is the attainment of the component's bending stiffness. In other words, if the bending stiffness is to be maintained at the level presented in the original twin-shell all-metal component design, very small (if any) component weight reduction can be attained using this PMH technology.

3. If bending stiffness is not the main constraint associated with the hybridization of a load-bearing BIW component, then more significant reductions in the component weight can be attained using the direct-adhesion PMH technology.

5.6. References

5.1 M. Grujicic, V. Sellappan, G. Arakere, N. Seyr and M. Erdmann, "*Computational Feasibility Analysis of Direct-Adhesion Polymer-To-Metal Hybrid Technology for Load-Bearing Body-In-White Structural Components*," Journal of Materials Processing Technology, 195, 2008, 282-298.

5.2 O. J. Zoellner and J. A. Evans, "*Plastic-Metal Hybrid. A New Development in the Injection Molding Technology,*" ANTEC 2002 Annual Technical Conference, San Francisco, CA, 2002, 1-4.

5.3 *Plastic-Metal Hybrid Material*, http://www.hbmedia.net/polymotive/polymotive/2003/01/articles/frontend1.shtml

5.4 D. Recktenwald, "*Advanced Adhesives Foster Hybrid Structures*," Machine Design, 77, 21, November 2005, 124-126.

5.5 M. Grujicic, V. Sellappan, M. A. Omar. N. Seyr and M. Erdmann, "*An Overview of the Polymer-to-Metal Direct-Adhesion Hybrid Technologies for Load-Bearing Automotive Components*," Materials Processing Technology, 197, 2008, 263-273.

5.6 M. Grujicic, G. Arakere, P. Pisu, B. Ayalew, N. Seyr and M. Erdmann, "*Application of Topology, Size and Shape Optimization Methods in Polymer Metal Hybrid Structural Lightweight Engineering*," Multidiscipline Modeling in Materials and Structures, accepted for publication, September 2007.

5.7 M. Grujicic, V. Sellappan, L. Mears, X. Xuan, N. Seyr, M. Erdmann and J. Holzleitner, "*Selection of the Spraying Technologies for Over-Coating of Metal-Stampings with Thermo-Plastics for Use In Direct-Adhesion Polymer Metal Hybrid Load-Bearing Component*," 198, 2008, 300-312.

5.8 M. Grujicic, B. Pandurangan, W. C. Bell, M. Daqaq, L. Ma, N. Seyr, M. Erdmann and J. Holzleitner, "*A Computational Analysis and Suitability Assessment of Cold-Gas Spraying of Glass-Fiber Reinforced Poly-Amide 6 for Use in Direct-Adhesion Polymer Metal Hybrid Automotive Components,*" Applied Surface Science, 254, 2008, 2136-2145.

5.9 M. Grujicic, V. Sellappan, B. Pandurangan, G. Li, M. Erdmann and J. Holzleitner, *"Computational Analysis of Injection-Molding Residual-Stress Development in Direct-Adhesion Polymer-To-Metal Hybrid Body-In-White Components,"* Journal of Materials Processing Technology, accepted for publication, October 2007.

5.10 S. Keeler, "*Determination of Forming Limits in Automotive Stampings,*" Sheet Metal Industries, 42, 1968, 683-691.

5.11 T. Pepelnjak and K. Kuzman, "*Numerical Determination of the Forming Limit Diagrams,*" Achievements in Materials and Manufacturing Engineering, accepted for publication, 20, January-February 2007, 1-2.

5.12 Moldflow Plastics Insight, *Version 6.1*, *User Documentation*, Moldflow Corporation, Framingham, MA, 2006.

5.13 Manufacturing Solutions: HyperForm, Altair Engineering Inc., www.altair.com

5.14 ABAQUS, *Version 6.7*, *User Documentation*, Dassault Systems, www.3ds.com

5.15 MATLAB, *The Language of Technical Computing*, 7th Edition, 2006 (The Math Works Inc., MA.

5.16 A. Needleman, *"A Continuum Model for Void Nucleation by Inclusion Debonding,"* J. Appl. Mech., 54, 1987, 525-531.

5.17 *Cambridge Engineering Selector*, http://www.grantadesign.com/

5.18 *World Auto Steel*, http://www.ulsab-avc.org/

CHAPTER 6

CONCLUSIONS AND FUTURE WORK

6.1 General Discussion and Concluding Remarks

As stated in Chapter 1, the main objective of the present investigation was to establish using various computational analyses, the suitability of the direct adhesion PMH technology for use in load-bearing BIW components. In addition, the compatibility of this technology with a current BIW manufacturing process chain had to be investigated. Towards that end, several computational analyses were undertaken whose brief description and the main finding are summarized below:

First, a comprehensive multi-disciplinary computational analysis is developed to assess the potential use of a direct-adhesion polymer metal hybrid (PMH) technology in load-bearing body-in-white (BIW) automotive structural components. The analysis encompassed: (a) injection-molding process simulation and component manufacturability assess unit; (b) Determination of processing-induced residual stresses in the component, cooling and solidification induced shrinkage and warping, (c) Determination of the spatial distribution and the extent of material anisotropy; (d) Assessment of the ability of the PMH component to endure a typical E-coat curing treatment; and (e) the extent of polymer-to-metal adhesion needed to attain a significant component-weight reduction. Using a generic automotive BIW component, as a test structure, the analyses showed that the direct-adhesion PMH technology may have a future in load-bearing BIW structural components provided a durable polymer-to-metal adhesion with a strength exceeding 10MPa can be achieved.

Next, a comprehensive review is provided of the public-domain literature dealing with various polymer-to-metal direct-adhesion efforts. The efforts and their results were critically assessed with respect to their potential use in the BIW load-bearing applications. The analysis

included both the consideration of the functionality and durability of the BIW load-bearing components and the compatibility of various PMH technologies within the BIW manufacturing process chain. The overview of the literature revealed that while considerable amount of research has been done in the PMH direct-adhesion area, many aspects of these technologies which are critical from the standpoint of their use in the BIW structural applications have not been addressed (or addressed properly). Among the PMH technologies identified, the one based on micro-scale mechanical inter locking between the injection-molded thermoplastic polymer and stamped-metal structural rib component was found to be most promising. To fully utilize this approach, however, it was found that a polymer spraying technology may need to be employed. This would enable the deposition of a thin highly-adherent polymer-coat over the selected portion of the metal stamping. During the subsequent injection molding process, the plastic reinforcing substructure would be injection molded against the polymer over-coated stamping ensuring a good polymer-to-polymer adhesion.

Then, a comprehensive review is provided of the public-domain literature dealing with various powder-coating processes suitable for the fabrication of a polymer-coat/overlay within a U-shape BIW metal-stamping structural component which will be subsequently hybridized using the polymer-to-metal direct-adhesion injection-molding process. After the product (overlay coating) requirements and the capabilities/attributes of the various processes were identified, a set of engineering-design tools (e.g. the quality functional deployment, decision matrix, etc.) were used to identify the screen-out non-suitable processes and to rank the remaining ones. A detailed cost analysis is carried out while assessing the criteria used for ranking the candidate powder-coating processes. Cold-gas dynamic-spray process was identified as a prime candidate for the BIW structural-component hybridization application at hand. While no public domain data exist

regarding the ability of the cold-gas dynamic-spray process to deposit nylon a transient non-linear computational analysis carried out in a companion work suggested that such a process is feasible.

Lastly, a comprehensive set of quasi-static and dynamic structural mechanics and sheet-metal forming/thermoplastic injection-molding process simulation analyses are carried out in order to assess suitability/feasibility of a direct-adhesion polymer-metal-hybrid technology in which metal stampings are made of high-strength low-ductility steels and the a typical (5MPa) level of polymer-to-metal adhesion strength is present. The results suggest that the most challenging requirement presented to the direct-adhesion PMH technology is the attainment of the component's bending stiffness. In other words, if the bending stiffness is to be maintained at the level presented in the original twin-shell all-metal component design very small (if any) component weight reduction can be attained using this PMH technology. If bending stiffness is not the main constraint associated with the hybridization of a load-bearing BIW component, then more significant reductions in the component weight can be attained using the direct-adhesion PMH technology.

6.2 Suggestion for Future Work

In the present work, a fairly comprehensive multi-disciplinary computational investigation was carried out of various materials, processing, performance and durability issues related to the direct-adhesion PMH technologies while additional computational work could be carried out related to the component/process optimization, the end-of-life of the vehicle, etc. It appears more critical that the future work pertaining to the assessment of the suitability of the direct-adhesion PMH technologies in the load-bearing BIW components should be done experimentally. Among the specific experimental investigations which should be carried out, the following appear to meet more immediate attention:

(a) Experimental investigation of the polymer-to-metal adhesion strength which can be attained using the micro-scale mechanical interlocking direct-adhesion approach;

(b) Experimental investigation of the durability of polymer-to-metal bond which can be attained using the micro-scale mechanical interlocking direct-adhesion approach; and

(c) Experimental investigation of the ability of the cold-gas dynamic spray technology to deposit a nylon-based coating onto the stamped steel sub-component while ensuring the necessary level of the polymer-to-metal adhesion strength and its long-term durability.